12-1-2012

Synthesis and characterizations of pyridinium salts including poly(pyridinium salt)s and their applications

Tae Soo Jo
University of Nevada, Las Vegas, jot@unlv.nevada.edu

SYNTHESIS AND CHARACTERIZATIONS OF PYRIDINIUM SALTS INCLUDING POLY(PYRIDINIUM SALT)S AND THEIR APPLICATIONS

By

Tae Soo Jo

Bachelor of Chemical Engineering
Kwangwoon University
2004

Master of Chemical Engineering
Yonsei University
2006

A dissertation submitted in partial fulfillment
of the requirements for the

Doctor of Philosophy in Chemistry

Department of Chemistry

College of Sciences

Graduate College

University of Nevada, Las Vegas

December 2012

THE GRADUATE COLLEGE

We recommend the dissertation prepared under our supervision by

Tae Soo Jo

entitled

Synthesis and Characterizations of Pyridinium Salts Including Poly(Pyridinium Salt)s and their Applications

be accepted in partial fulfillment of the requirements for the degree of

Doctor of Philosophy in Chemistry
Department of Chemistry

Pradip Bhowmik, Ph.D., Committee Chair

Kathleen Robins, Ph.D., Committee Member

Vernon Hodge, Ph.D., Committee Member

Laxmi Gewali, Ph.D., Graduate College Representative

Tom Piechota, Ph.D., Interim Vice President for Research &
Dean of the Graduate College

December 2012

ABSTRACT

Synthesis and Characterizations of Pyridinium Salts Including Poly(pyridinium salt)s and Their Applications

by

Tae Soo Jo

Dr. Pradip K. Bhowmik, Examination Committee Chair
Department of Chemistry
University of Nevada La Vegas

Pyridinium salts, both molecular and polymeric, are an interesting class of multifunctional materials that exhibit liquid-crystalline and light-emitting properties. Moreover, their properties can be easily tuned by introducing new types of anions or by modifying their chemical structures. This dissertation describes synthesis and characterization of poly(pyridinium salt)s containing macrocounterions and fluorene moieties in their backbones, synthesis and characterization of nanocomposites of poly(pyridinium salt)s with single-walled carbon nanotubes via non-covalent interactions, and synthesis and characterizations of pyridinium salts having different aliphatic linkages and their application in organic acid sensing.

First, all of these ionic polymers were prepared by either ring-transmutation or by metathesis reaction. Their chemical structures were established by FTIR, ^{1}H spectroscopy and elemental analysis. Some polymers containing macrocounterions had relatively low melting transitions above which they formed thermotropic liquid-crystalline phase; and other polymers were amorphous as determined by VTXRD studies. Ionic polymers containing fluorene moieties in their backbones exhibited lyotropic properties in both polar protic and aprotic solvents at various critical concentrations. Light emission properties of this class of polymers in common organic solvents as well as in water and in solid states were also studied. To explore the application of poly(pyridinium salt)s, we developed a method of preparation of nano-composites with a number of poly(pyridinium salt)s and single-walled carbon nanotubes. The single-walled carbon nanotubes were effectively dispersed with various poly(pyridinium salt)s resulting in nanocomposites. The optical and solution properties of these composites were examined by a number of experimental techniques. Finally, some of the synthesized dicationic salts exhibited ionic liquid properties, but all exhibited fluorescent properties in solution and solid states. Due to the presence of methyl orange counterions, pyridinium salts could serves as a pH sensor in organic solvents.

ACKNOWLEDGMENTS

Instead of saying too many words, I want to say that thank you everybody (Dr. Bhowmik, Dr. Han, my family, my friends, and my wife) for their endless love, help, and support.

TABLE OF CONTENTS

LIST OF TABLES

LIST OF FIGURES

LIST OF SCHEMES

CHAPTER 1

SYNTHESIS AND CHARACTERIZATIONS OF POLY(PYRIDINIUM SALT)S

1.1. Abstract

Several poly(pyridinium salt)s containing various aromatic diamine moieties and organic counterions were prepared by the ring-transmutation polymerization reaction of bis(pyrylium tosylate) with aromatic diamines in dimethyl sulfoxide at 130−135 °C for 48 h. Their tosylate counterions were exchanged with other anions such as triflimide, methyl orange, dioctyl sulfosuccinate, dodecylbenzene sulfonate, and macro counterions by the metathesis reaction in an organic solvent. Their chemical structures were established by FTIR, ^{1}H, ^{19}F, and ^{13}C NMR spectroscopic techniques. Number-average molecular weights (M_n) of some polymers were in the range of 97−108 kg/mol, and polydispersity index (PDI) in the range of 1.12−1.88 as determined by gel permeation chromatography (GPC). All the polymers showed excellent thermal stabilities in nitrogen. They exhibited lyotropic or thermotropic liquid-crystalline phase in polar aprotic and protic organic solvents above their critical concentrations or at room temperature depending on their microstructures and counterions. Their optical properties were examined by using UV−Vis and photoluminescent spectroscopy, which revealed that some polymers emitted UV light, some emitted blue light, and some emitted green light (both in solutions and solid states) depending on the chemical structures, organic counterions, and solvent polarity of the organic solvents.

1.2. Introduction

Since the discovery of their conducting properties in 1977, conjugated polymers have drawn much attention over the past decade.[1–5] This important discovery led to the 2000 Nobel prize in Chemistry awarded to Shirakawa, MacDiarmid, and Heeger for their pioneering development of electrically conductive polymers.[6] The conjugated polymers are organic molecules consisting of a backbone chain with alternating single and double bonds. The interactions between the molecular orbitals along the backbone chain result in an extended system of delocalized π electrons. The representative examples are shown in scheme 1.1.

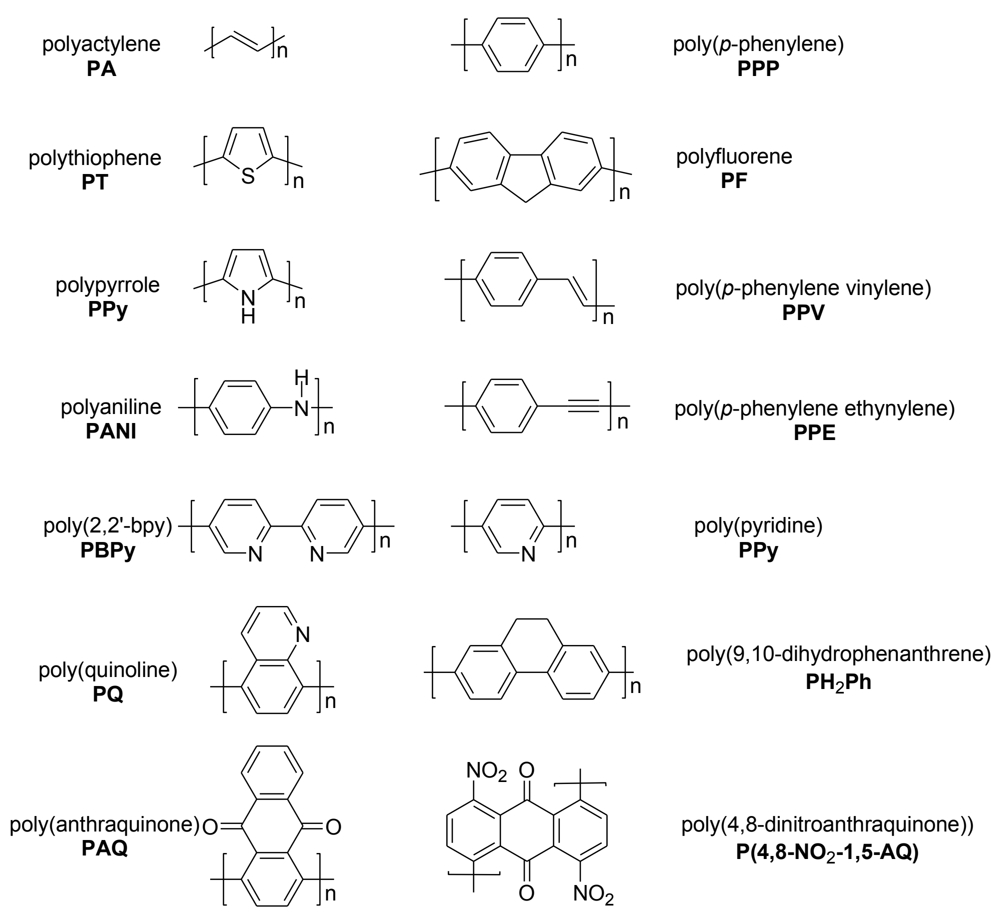

Scheme 1.1. Chemical structures of representative conjugated polymers.

Conjugated polymers possess a unique combination of properties that sets them apart from other materials. First, they have the mechanical and processing advantages of polymers due to their solubility in organic solvents or water. Owing to their photophysical properties, flexibility and easy processing, they can be good alternatives to inorganic semiconductors. Furthermore, the organic conjugated polymers can be easily tuned by chemical modification of the monomeric building blocks, allowing for structural improvement and tailoring of the properties of the final materials. The diverse properties of conjugated polymers make them useful in a variety of applications including optoelectronic devices,[7] solar cells,[8] photodetectors,[9] chemical and biological sensors.[10]

In a molecule containing an isolated double bond, a π electron can be promoted from the highest occupied molecular orbital (HOMO) to the lowest unoccupied molecular orbital (LUMO) by the absorption of a photon with energy greater than the energy gap, E_g, between the frontier orbitals. When a sufficient energetic photon (hv) is absorbed by a semiconducting material, an electron can be promoted from the valence band to the conduction band, producing what is called as an "exciton". The exciton is an excited-state quasiparticle composing of an electrostatically bound to electron pair.[11] The excited-state species can migrate from one location to another until it relaxes by some deactivation process resulting in luminescence. The schematic diagram of HOMO an LUMO is shown in Figure 1.1.

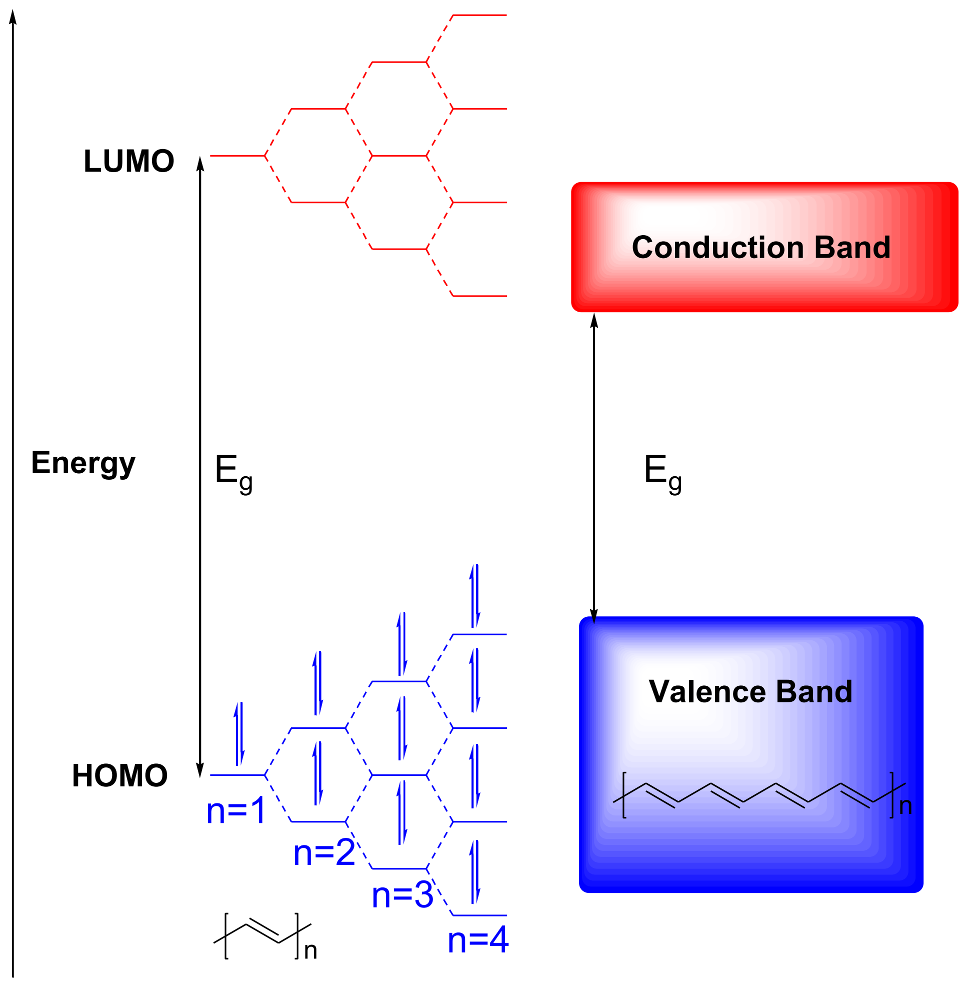

Figure 1.1. Schematic representation of the interacting HOMO and LUMO in a conjugated system the valence band and conduction band of a semiconducting polymer, and the corresponding energy gaps, E_g.

Luminescence can be classified into two categories, fluorescence and phosphorescence, depending on the spins of the electrons involved in the radiative transition (Figure 1.2). If the excited electron has the same spin as the electron in the corresponding ground-state orbital, the emission of light is called phosphorescence. If the excited electron has the opposite spin as the electron in the corresponding ground-state orbital, the emission of light is called fluorescence. Phosphorescence involved an electronic transition from a triplet excited state to a single ground state. Since this transition is formally forbidden by quantum-mechanical selection rules, it occurs at a much slower rate than fluorescence, which involves an allowed transition between a singled excited state to a singlet ground state.[12] In general, electronic transitions between the singlet states and the triplet states typically occur at negligible rates in conjugated polymers.

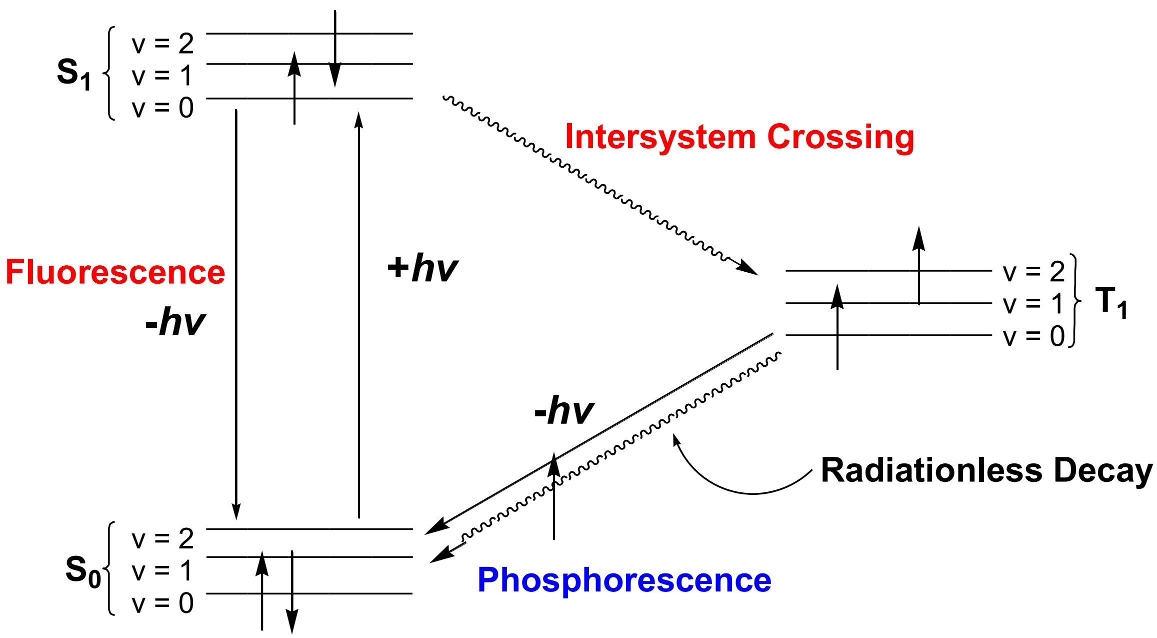

Figure 1.2. State energy diagram of photophysical processes in a typical fluorescent molecule. The singlet ground electronic state is denoted as S_0, and the first singled excited state is denoted as S_1, respectively. The first triplet excited state is denoted as T_1. Each of these electronic energy levels contains its own vibrational energy levels, v = 0, 1, 2, etc.

Absorption of an energetic photon typically excites an electron from the lowest energy state (S_0, v = 0) to S_1. In general, excited electrons rapidly relax by internal conversion to the lowest vibrational level of S_1. At this excited state (S_1, v = 0), the singlet exciton exists long enough to migrate over significant distances in a conjugated polymer. Therefore, the excited electron returns to its ground state by a deactivation process, such as fluorescence. Fluorescence involves electronic transitions from the lowest vibrational level (v = 0) of S_1 to the vibrational levels (v = 0, 1, 2, etc.) of the electronic ground state (S_0). Besides fluorescence, the excited state can also be deactivated by electron transfer or energy transfer processes involving a fluorescence-quenching defect.

Tuning the band structure of materials is one of the most important issues for developing high performance materials. Designing high-performance organic molecules with appropriate band structure (band gap and frontier molecular orbitals) is crucial for device efficiency and device life-time.[13] Theoretical and experimental studies indicate that the band gap of a conjugated polymer basically is determined by six factors: molecular weight (E_{Mw}), bond length alternation (E_{BLA}), planarity (E_{θ}), aromatic resonance energy (E_{Res}), substituents (E_{sub}) and intermolecular interactions (E_{inter}).[14] The band gap of conjugated polymers can be expressed by using the equation: $E_g = E_{\mathrm{Mw}} + E_{\mathrm{BLA}} + E_{\theta} + E_{\mathrm{Res}} + E_{\mathrm{sub}} + E_{\mathrm{inter}}$, which provides a tool for tailoring the band gap of conjugated polymers (Figure 1.3). However, the exact control of individual HOMO and LUMO energy levels is a complicated process because all of the factors (*vide supra*) have an influence on the band gap resulting in alteration of chemical, mechanical, and physical properties. Even though the use of alkyl or alkoxy chain can increase the solubility of conjugated polymers, this factor has an effect on the tendency for supramolecular arrangement (E_{inter}) and the increment of the torsion angle (E_{θ}). Therefore, any external stimulus will modify the planarity of the backbone and the degree of π−orbital overlap, resulting in the change of E_g.[15]

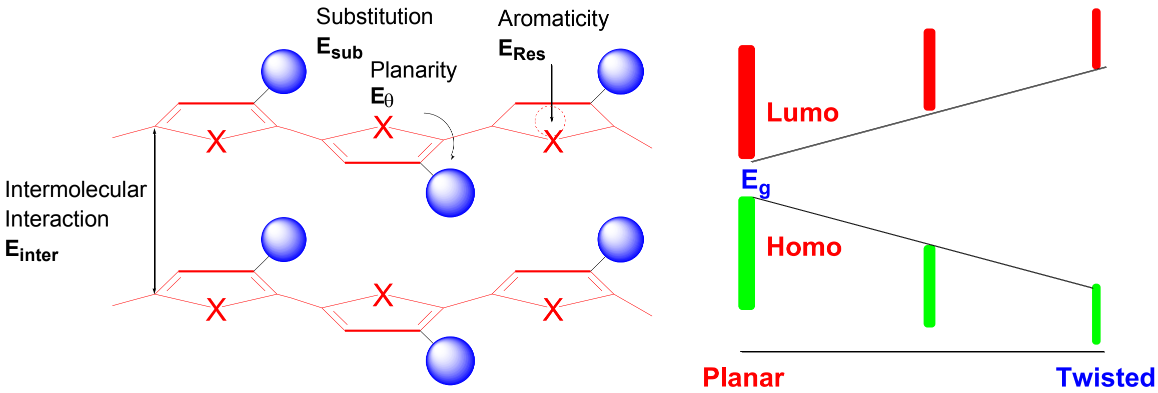

Figure 1.3. Schematic representation of the structural factors affecting the band gap of π−conjugated polymers.

The π−conjugated polymers containing aromatic moieties in the backbones are an attractive class of materials due to their potential use in organic electronic materials and devices such as field effect transistor (FETs), organic light-emitting diodes (OLEDs), and photovoltaic cells. These polymers have generally been synthesized by polycondensation reactions.[16] The versatility of functionalized π−conjugated polymers has led to tunable physical properties such as color, or emission efficiency by modifying their structure or improving purity.[17] The functionalization of conjugated polymers can occur via copolymerization with a functionalized comonomer for tuning the properties of these materials.[18] One of the well-known approach for synthesis of π−conjugated polymers is chain-growth coupling polymerization with an organometallic catalyst. This approach includes Kumada-Tamao coupling polymerization with a Ni catalyst and Suzuki-Miyaura coupling polymerization with a Pd catalyst. For example, poly(alkylthiophene) has been synthesized based on these coupling polymerization reactions over the past decade. The polymerization of Grignard thiophene monomer with $Ni(dppp)Cl_2$ (dppp = 1,3-bis(diphenylphosphino)propane) is well known as a regioregulated synthetic method for poly(alkylthiophene)s developed by McCullough and co-workers (Scheme 1.2).[19] Unfortunately, the polymers obtained possess broad molecular weight distribution.

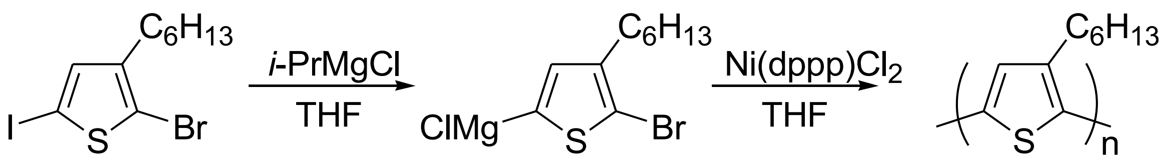

Scheme 1.2. Synthesis of poly(thiophene)s via Kumada-Tamao coupling polymerization reaction.

Other substituted thiophene monomers instead of hexyl groups also have been reported previously. The polymerization of butylthiophene, aryl-substituted thiophene, alkoxy-substituted thiophene, or ester containing thiophene monomers in Scheme 1.3 were used for the synthesis of conjugated poly(thiophene)s, however, the polymerization reaction usually results in low-molecular-weight polymers due to the low solubility of these polymers during the reactions.[20]

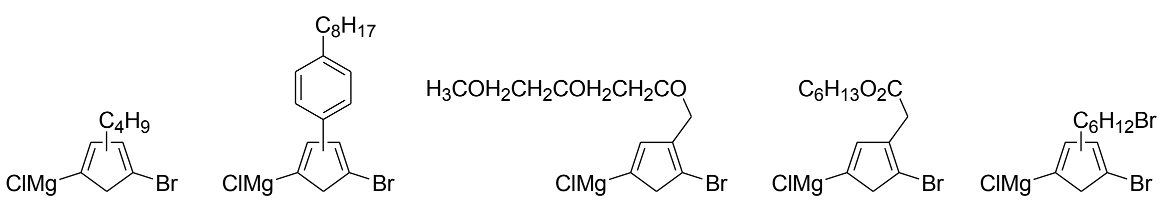

Scheme 1.3. Various monomers for poly(thiophene)s.

Various conjugated polymers except poly(thiophene)s also have been studied through Kumada-Tamao coupling polymerizations such as poly(p-phenylene), polypyrroles, polyfluorenes and polycarbazoles with Ni(dppp)Cl_2, Ni(dppe)Cl_2 or Ni(dppf)Cl_2 (Scheme 1.4).

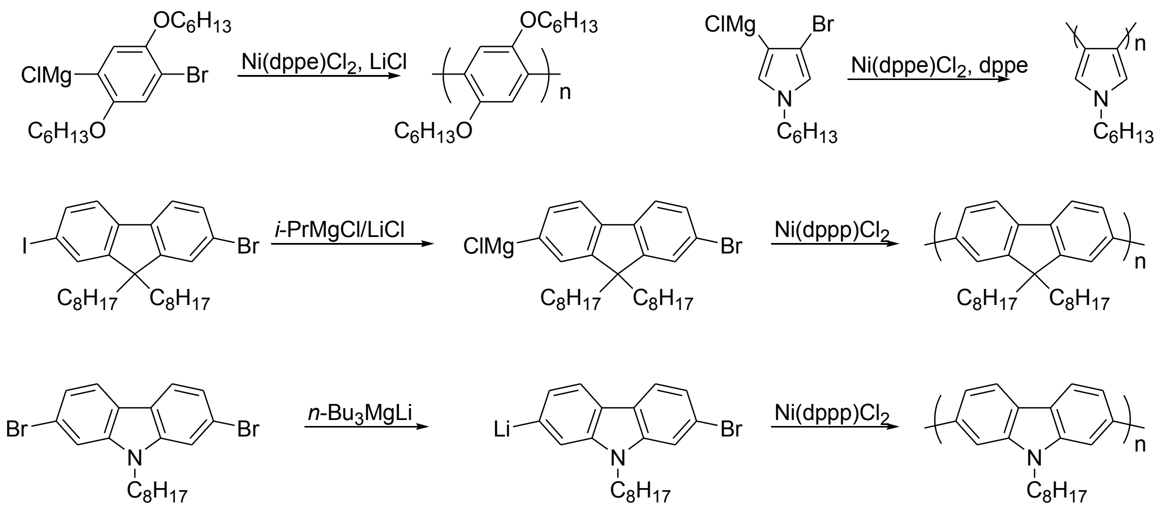

Scheme 1.4. Various conjugated polymers through Kumada-Tamao polymerization reaction.

In this approach, although many desired functional groups could be introduced into polymer main chain, the reduced reactivity of the comonomer during polymerization generally resulted in low-molecular-weight polymers.[21] Furthermore, steric effects introduced by the side-group functionality can reduce planarity of the backbone causing the interruption of conjugation length.[22]

Reinitzer and Lehman first discovered liquid crystals (LCs) in 1888,[23] and they have been under investigation and used in practical applications for more than 100 years. They exhibit properties of two states of matter, liquids and solids, hence the name liquid crystals. In crystals, molecules typically have orientational and positional order, whereas, molecules in liquids have neither. Liquid crystals are unique in that the molecules possess some orientational order, while maintaining fluidic properties. The driving forces for the formation of a LC phase (mesophase) are interactions between the anisometric molecules (dipole−dipole interactions, van der Waals interactions, π−π stacking, and etc.). In general, liquid crystals can be divided into two main types; thermotropic LCs and lyotropic LCs. Thermotropic LCs show mesophases depending on temperature and pressure. Their basic building units are usually individual molecules, which have pronounced shape anisotropy, such as rods, disk, etc. Thermotropic LCs have been successfully used in display devices. The schematic representations of LC phases are shown in Figures 1.4 and 1.5.

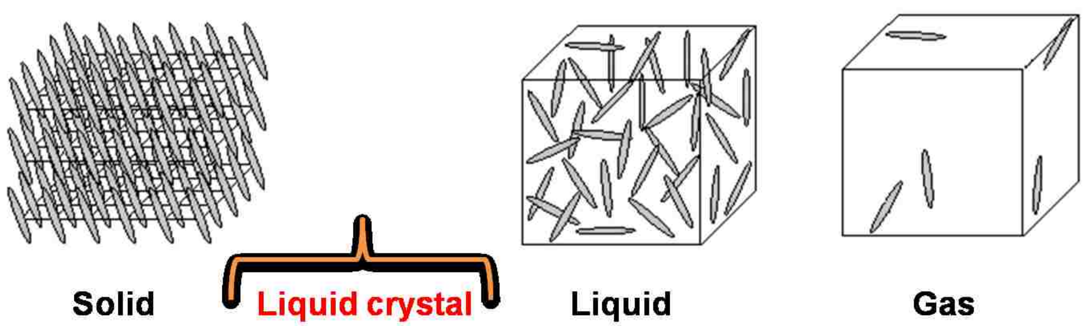

Figure 1.4. Schematic representation of liquid crystalline phase.

Lyotropic LCs are formed on the dissolution of lyotropic LC molecules in a solvent. A feature of lyotropic LCs that distinguishes them from thermotropic LCs is the self-assembly of molecules into supermolecular structures that represent the basic unit of these mesophases.[24] The most common lyotropic LC system are those formed by water and surfactants (amphiphiles), such as soaps, synthetic detergents, and lipids. Surfactant molecules are formed by a hydrophilic part chemically bound to a hydrophobic part.

Mixtures of these surfactant molecules with a solvent under certain conditions of temperature and concentration produce several different types of mesophases.

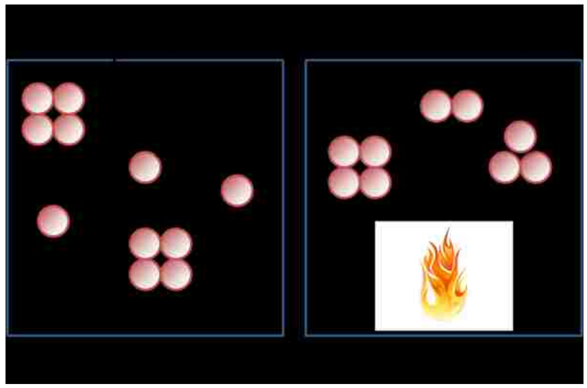

Figure 1.5. Schematic representation of lyotropic LC and thermotropic LC.

LCs display a variety of mesophases based on their chemical structures. Among many types of LC phases, the least ordered mesophase is called the nematic phase exhibiting rod-like molecules. The nematic phase can give an orientational order of the molecules, but without long-range positional ordering. In this phase, the rod-like molecules tend to align themselves parallel to each other with their long molecular axis on average parallel to a preferential direction (Figure 1.6a). This preferential direction is called the "director" of the phase (ñ). The rod-like molecules are free to rotate around the long molecular axis, and to some degree, rotation around their short molecular axis can also occur.

In the smectic mesophases, the mesogenic molecules have an orientational order like the nematic phase, but molecules also exhibit positional order. The molecules in the smectic A phase are arranged in layers and have on average their long molecular axis perpendicular to the layer planes. Or, in other words, the long molecular axis is on average parallel to the normal to the layer planes (Figure 1.6b). The smectic C phase is very close to the smectic A phase, however, the molecules are now not perpendicular to the layer planes, but are tilted (Figure 1.6c). The tilt angle is the angle between the long molecular axis and the axis normal to the layer planes. Moreover, when a molecule has both orientational and positional orders in their mesophase, it is called the smectic B phase (Figure 1.6d).

The columnar phases are another class of mesophases that molecules can assemble into cylindrical structures to play a role as mesogens due to their rich aromaticity through π–π stacking. These LCs are called discotic liquid crystals because they tend to stack up in one dimension. In the columnar nematic phase, short columns are ordered in a nematic way (Figure 1.6e). This phase is also called nematic columnar phase. In the columnar phases, the mesogens are stacked one of top of another to form columns. The columns themselves can be arranged in different two-dimensional lattices. In the hexagonal columnar phase, the molecules are stacked into columns that are further arranged into a hexagonal lattice (Figure 1.6g).

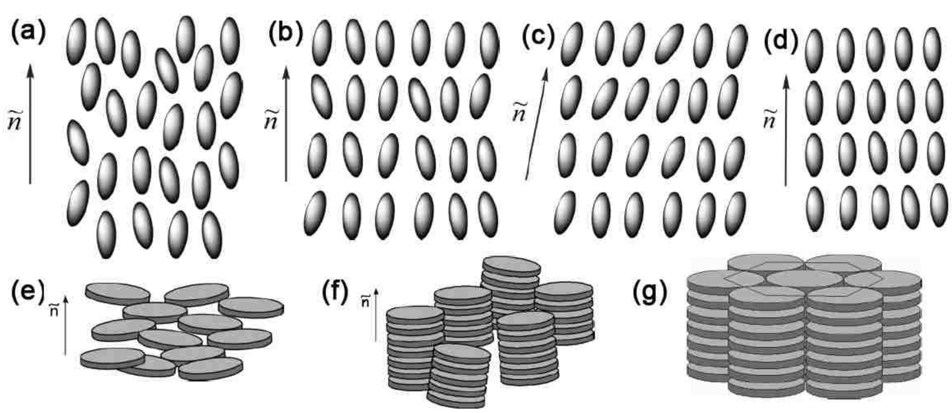

Figure 1.6. Schematic representation of (a) the nematic phase, (b) the smectic A phase, (c) the smectic C phase, (d) the smectic B phase, (e) the discotic nematic phase, (f) the columnar nematic phase and (g) the hexagonal columnar phase.

Polymeric quaternary ammonium compounds represent a class of polyelectrolytes that mainly derive unique properties from the density and distribution of positive charges along a macromolecular backbone. The typical properties of the quaternary polymer are independent of the electrostatic forces. The flexibility of the polymer chain as well as the formation of H-bonds, hydrophobic interactions or charge transfer interactions also play an important role in practical applications. Due to manifold application in industrial processes and daily life, the quaternary ammonium polymers have been researched for many years like other polyelectrolytes, and still continue to be an active area of research in diverse fields such as chemistry, physics, biology, environmental science, medicine, material science, and nanotechnology.

Cationic charged organic compounds have a few structural varieties due to a limited number of functional groups. The majoritiy of reported syntheses and applications are based on the presence of quaternary nitrogen centers in their chemical structures since they are synthetically accessible, and have good hydrophilicity for aqueous applications and high thermal stability. Macromolecular chemical structures can be transformed into polycationic structures by two different synthetic routes: the chain- or step-growth polymerization reaction of suitable monomers and the cationic functionalization of reactive precursor polymers (Scheme 1.5 and 1.6).

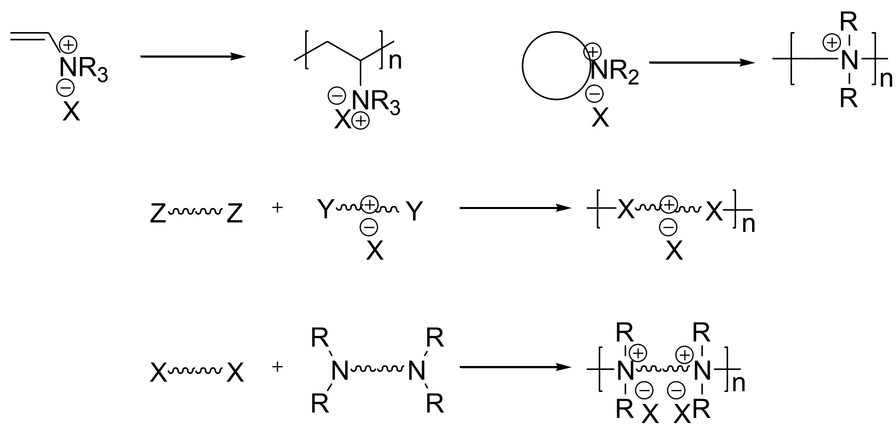

Scheme 1.5. Representative polymerization reactions to prepare cationic polymers.

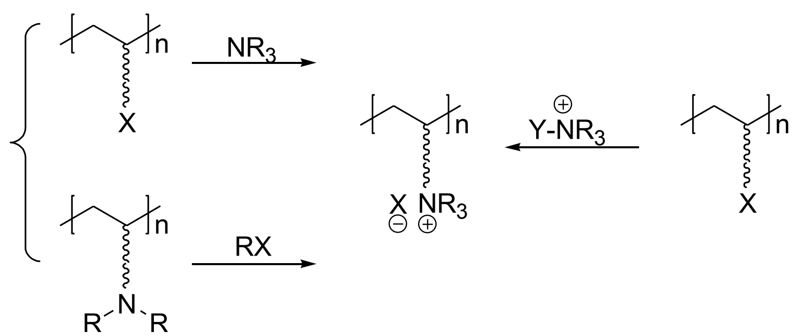

Scheme 1.6. Representative cationic functionalization of reactive precursor polymers.

The first approach can lead to polymer with full functionality, but the molecular weight of the polyelectrolytes is often difficult due to the sensitivity of their conformation in aqueous media or reduced reactivity of the monomers. Most well-known cationic quaternary polyelectrolytes are synthesized via free radical polymerization in aqueous media. The reaction in aqueous system can have a low chain transfer to the solvent and a protection of the propagating polymer radical by a strongly bound hydration shell, thus hindering the termination reaction. Furthermore, the formation of hydrogen bonds between the monomer and water may increase the reactivity of the monomers.[25] To obtain well-defined molecular architectures with predictable and narrow polydispersity index, controlled free radical polymerizations (CRPs) such as atom transfer radical polymerization (ATRP) and the reversible addition fragmentation transfer (RAFT) have been successfully extended to the synthesis of cationic homo- and block-copolymers.[26] The narrow molecular weight distributions of the polymers via CRPs improve the precision of any physicochemical or physical measurements supporting their applications in structure-property relationships.

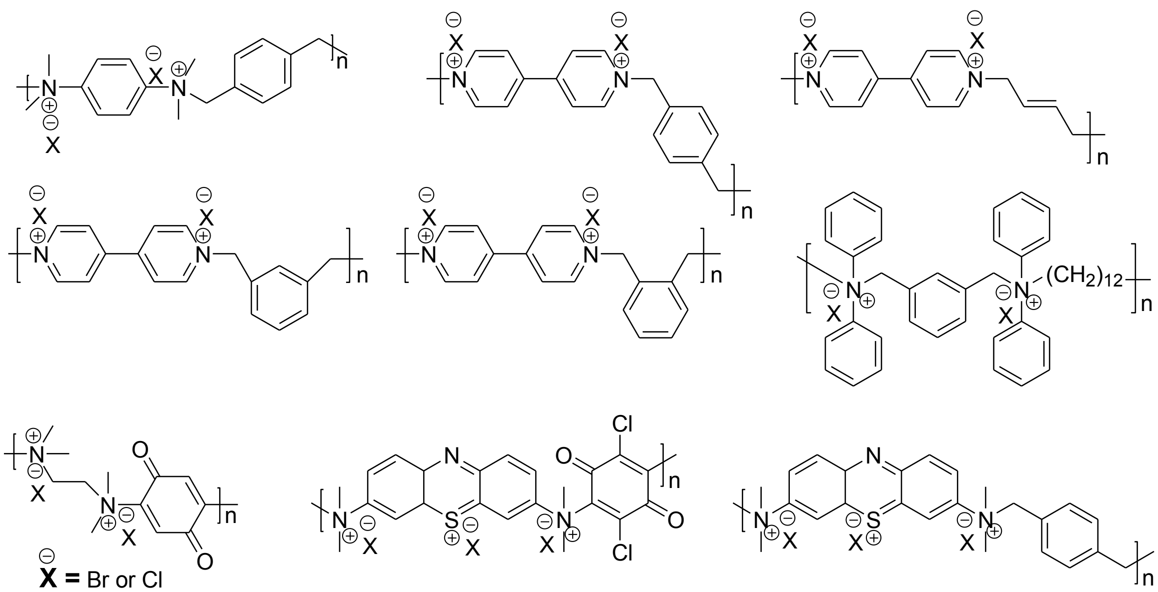

Scheme 1.7. Chemical structures of main-chin cationic polymers.

Many cationic polyelectrolytes can be obtained by functionalization of reactive precursor polymers. Because the neighboring effect may involve complex reaction kinetics during the chemical modification, the reaction sometimes cannot be carried out to 100% conversion. Furthermore, the solubility of the polymer can be modified during the polymer-analogous reaction resulting in a hindrance of the accessibility of the functional groups. There are several well-known ways to introduce quaternary nitrogen in the polymer: First, the quaternization of a halogen containing polymer with a tertiary amine; Second, the quaternization of a polymeric tertiary amine with an alkyl or aryl halide; and Third, the quaternization of polymer containing OH-groups by appropriate agents like 2,3-epoxypropyltrimethyl ammonium chloride. In general, the quaternization reaction needs high dielectric-constant solvents to dissolve all components of the initial polymer, alkylating agent and modified polymer.[27] The representative cationic polymers are shown in Scheme 1.8.

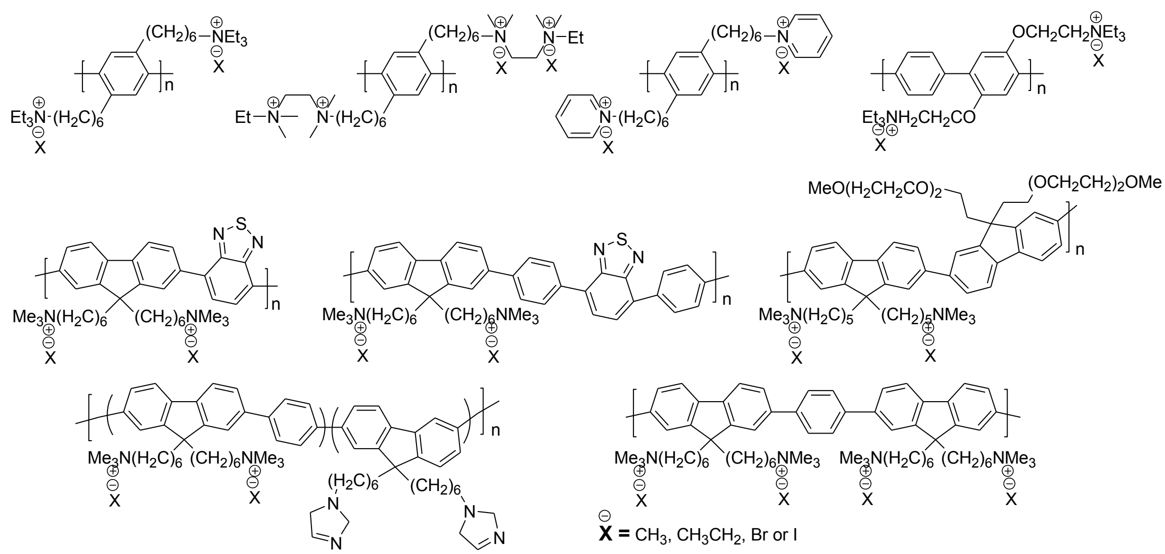

Scheme 1.8. Chemical structure of side-chain cationic polymers.

Conjugated polymers also can be used for biosensors via fluorescence quenching experiments in both solution and solid thin films. Typically these sensors rely on a signal amplification that occurs when excitation of the conjugated polymer is transferred to a reporting dye, or via binding-induced changes in the emission of the conjugated polymer itself.[28] Solubility in aqueous media of conjugated polymers is essential for interfacing with biomacromolecules that are only soluble in aqueous solution. In general, ionic

π–conjugated organic polymers can be water-soluble by introducing charged functional groups in the polymer main or side chain.[29] Therefore, water-soluble conjugated polymers usually contain two parts: one is the π–conjugated backbone guaranteeing their good optical properties, the other is the charged functionalities ensuring for the solubility in water. The combination of conjugated polymer and ionic functionality can further extend their applications in new materials that can be used for microelectronic or photovoltaic devices.[30] For example, polythiophenes,[31] polyfluorene,[32] and poly(phenylenevinylene)[33] can have solubility in water with amino acid, ammonium or charged imidazole moiety and these substituted polymers can have specific metal ion recognition which can be used in drug delivery and cell imaging.

Poly(pyridinium salt)s could be classified as one of the polyviologens, which has 4,4′-bipyridinium salt moiety in their polymer backbones.[34] These polymers can be obtained from 4,4′-bipyridine and dihaloalkanes or dihaloarylalkanes through the Menschutkin reaction. Due to the lowest cathodic redox, viologens can easily be reduced to highly colored cation salts.[35] Katriztky et al. first reported the poly(pyridinium salt)s via a ring-transmutation polymerization reaction. However, polymers synthesized by this method usually have low molecular weights (M_n ~ 10,000 g/mol) resulting in poor mechanical properties in most applications. A new class of poly(pyridinium salt)s with two *N*-aryl pyridinium salts separated by 1,4-phenylene unit was developed and studied by Harris et al.[36] This reaction involved a ring-transmutation reaction in *N*,*N*-dimethylformamide (DMF) or dimethyl sulfoxide (DMSO) at elevated temperature. Even though this method provided high enough molecular weights supported by inherent viscosity, the synthesized polymers showed limited solubility to only high boiling polar organic solvents. The solubility and thermal stability were significantly improved by exchanging the inorganic counterions to organic counterions such as tosylate, triflimide, or dodecylbenzene sulfonate.[37] Bhowmik et al. have continuously explored the behavior and properties with various aromatic and aliphatic moieties in these classes of ionic polymers.[38] The interesting properties of poly(pyridinium salt)s are their photoluminescence properties in solution and solid states. They can emit light from UV to green based on their chemical structures. Moreover, the polymers can have high thermal transition and stability. Most poly(pyridinium salt)s display high glass transition (T_g) > 150 ^{o}C, which is a desirable characteristic for many applications, and thermal stability (T_d) > 200 ^{o}C.[37,38] Furthermore, it has been reported that poly(pyridinium salt)s can have liquid crystalline properties such as thermotropic (in melt) or lyotropic (in solution). These interesting physical, optical and solution behaviors make the poly(pyridinium salt)s high-performance materials that are desirable for various opto- and micro-electronic applications. Due to their excellent solubility in organic solvents and polycationic property, poly(pyridinium salt)s have potential for use in multi-layered polyelectrolyte assemblies via layer-by-layer (LBL) approach based on electrostatic interactions. The representative poly(pyridinium salt)s are shown in Scheme 1.9.

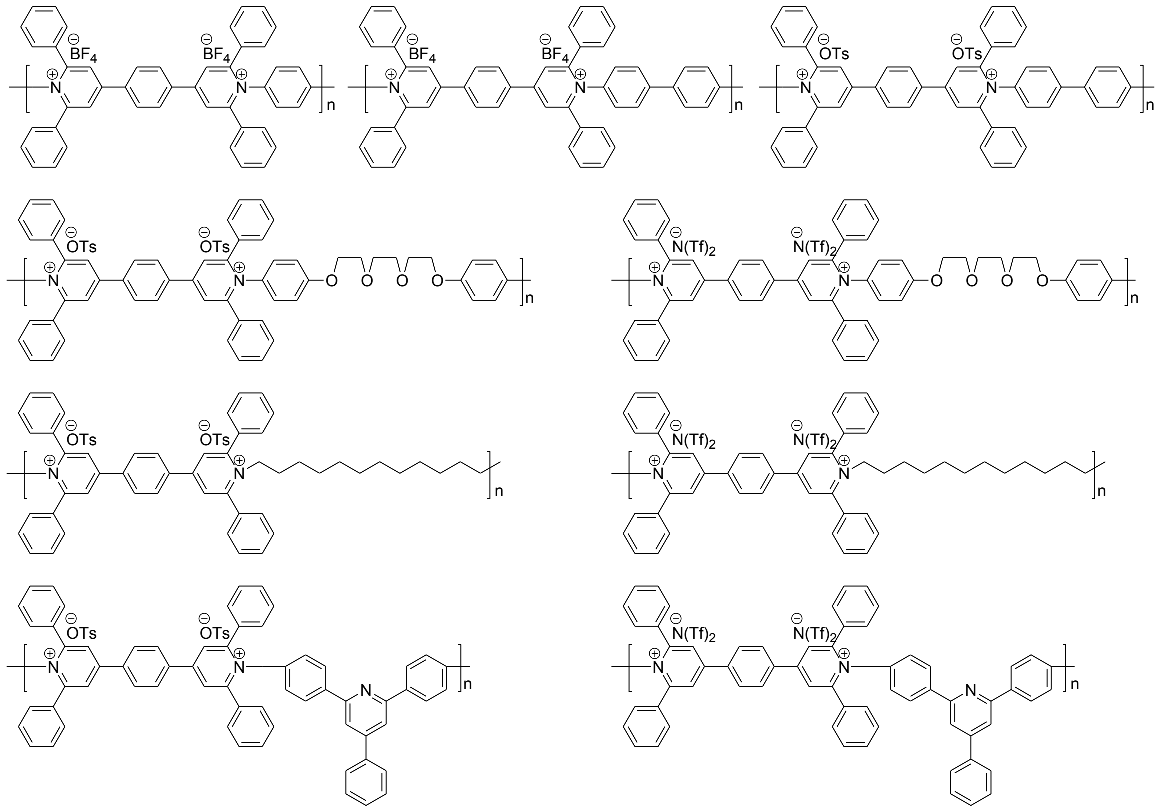

Scheme 1.9. Chemical structures of poly(pyridinium salt)s with organic counterions.

1.3. Objective

In this chapter, we report the synthesis of ionic polymers, poly(pyridinium salt)s with various rigid aromatic moieties and organic counterions in dimethyl sulfoxide (DMSO) through ring-transmutation polymerization reaction. Their chemical structures, thermal, solution, and optical properties are characterized by several experimental techniques. We found that poly(pyridinium salt)s containing a 9,9-dioctyl-9*H*-fluorene segment in the repeating units, and they can have lyotropic liquid-crystalline property. Introduction of macrocounterions into poly(pyridinium salt)s can make them soluble in water. Due to the π conjugation in polymers, the synthesized polymers can have light emission characteristics in solution and solid states. We believe that this series of materials is the cornerstone that could open a new field in the area of materials science.

1.4. Results and Discussion

1.4.1. Poly(pyridinium salt)s derived from 9,9-dioctyl-9*H*-fluorene-2,7-diamine

Polymer **1** was synthesized with a reaction between bispylium salt, **M**, and 9,9-dioctyl-9*H*-fluorene-2,7-diamine in DMSO at 130−135 °C for 48 h in nitrogen. To increase the reactivity of the reaction, a small amount of toluene was added to the solution to remove the generated water during the reaction by using a Dean-Stark trap set-up. Polymers **2−5** were made by a metathesis reaction in MeOH by changing the tosylate counterion to various organic counterions as outlined in Scheme 1.10.

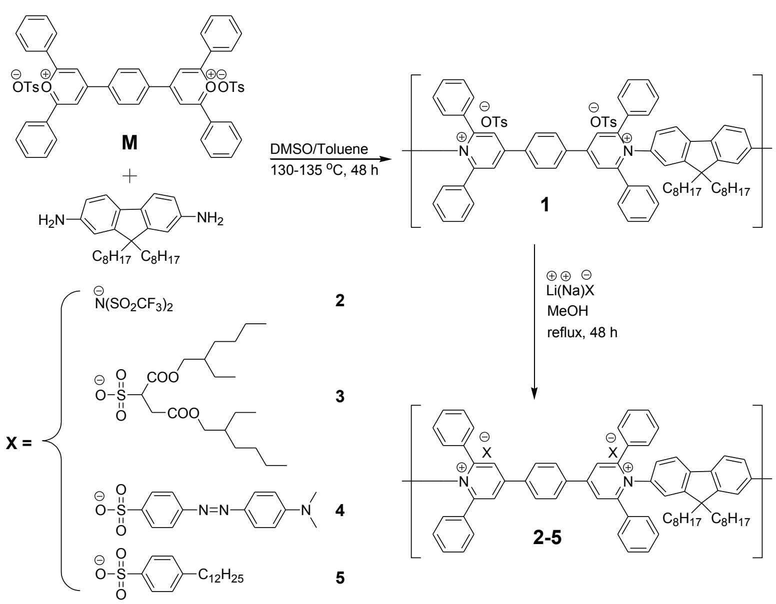

Scheme 1.10. Synthesis of poly(pyridinium salt)s−fluorene polymers.

Their chemical structures were confirmed by FTIR, ^{1}H, and ^{19}F NMR spectroscopy and elemental analysis. The signals of carbon nuclei of polymers could not be obtained even at elevated temperatures because of viscous solutions of these polymers in DMSO. Moreover, the relatively high viscosity of each of these copolymers and the broadness of their proton spectra were suggestive of the high molecular weight polymers. The FTIR spectra showed the representative characteristic peaks for polymer **1**: 1620−1448 (C=C and C=N aromatic ring stretching), 1196 ($C{-}N^+$), 1119 (S=O asymmetric stretching) and 1033−1010 (S=O symmetric stretching). After exchange of tosylate to triflimide, an additional C−F stretching vibration peak at ν = 1350 cm^{-1} in polymer **2** was recorded indicating the presence of triflimide counterion. Moreover, polymers **3** and **4** displayed unique additional peaks at ν_{max} = 1736 cm^{-1} (C=O stretching) from dioctyl sulfosuccinate counterion and 1458 and 1365 cm^{-1} (N=N and C−N stretching) from methyl orange, respectively. The expanded ^{1}H NMR spectra of polymer **1** showed characteristic broad peaks at δ = 8.82 and 8.62 ppm for the protons of the aromatic moieties of poly(pyridinium salt) and a set of resonances at δ = 7.45, 7.08 and 2.27 ppm for the protons of the aromatic moiety and methyl group in the tosylate counterion (Figure 1.7). A broad triplet at δ = 0.88 revealed the presence of dioctyl fluorene moiety in the repeating units (not shown). Exchange of the counterion from tosylate to triflimide was confirmed by the disappearance of tosylate resonances and appearance of a new signal at δ = −78.7 ppm in the ^{19}F NMR spectrum, signifying in the completion of the reaction. For polymer **3**, new additional peaks from the dioctyl sulfosuccinate counterion appeared in the range of the aliphatic region, and their ^{1}H integral ratios were in good agreement with each other. After changing the counterion from tosylate to methyl orange, a new set of signals was observed at δ = 7.79, 7.70, 6.8 (aromatic protons) and 3.06 ($-N(CH_3)_2$) in the ^{1}H NMR spectrum. These results indicated the metathesis reaction went to completion without causing any side reactions. The polymer **5**, which had dodecylbenzene sulfonate as the counterion, showed the expected proton signals in its NMR spectrum.

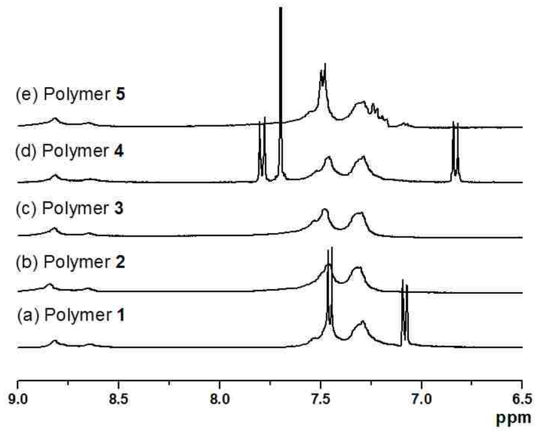

Figure 1.7. Expanded ^{1}H NMR spectra (delay time = 1 s, number of scans = 16 scans) of polymers **1**−**5** (10 mg/mL in d_6-DMSO at 25 °C).

Molecular weight properties (M_n and PDI) of the polymers were investigated using GPC with the interdetector signals such as refractometer, viscometer and low- and right-angle light scattering detectors. To minimize the polyelectrolyte interaction between polymers, a small amount of LiBr was used to suppress the ionic interactions between the polymer chains and those with GPC column packing material.[26] The data including radii of gyration and hydrodynamic radii for the synthesized polymers are compiled in Table 1.1 and their GPC chromatographs are displayed in Figure 1.8. For polymers **1**−**5**, number-average molecular weights (M_n) were in the range of 96.5−107.8 kg/mol and PDI values were between 1.12 and 1.88. As expected, the molecular weights and PDI indices of these polymers are essentially in a similar range, since polymers **2**−**5** were synthesized by the metathesis reactions of polymer **1** with the corresponding salts in an organic solvent. It is reasonable to assume that all of these ionic polymers had sufficiently high enough molecular weights for a meaningful comparison of their lyotropic liquid-crystalline properties. In other words, thermal, solution, optical, and physical properties can be studied without concern for the secondary effects that might occur from polymers with radically different molecular weights.

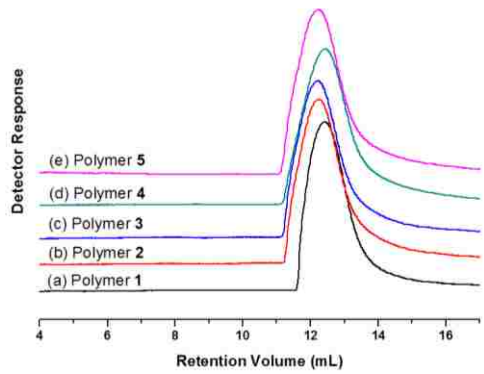

Figure 1.8. Gel permeation chromatography (2 mg/mL in DMSO with 0.01 M LiBr) of polymers **1**−**5**. M_n is relative to pullulan standard of P-50.

Table 1.1. Molecular weights of poly(pyridinium salt)s−fluorene polymers

Polymer	M_n [a]	M_w [b]	PDI [c]	*dn/dc* (mL/g)	R_h (nm) [d]	R_g (nm) [e]
1	96.5	181.8	1.88	0.1417	13.3	50.0
2	103.6	155.8	1.50	0.0878	12.7	24.4
3	107.8	130.0	1.21	0.0885	12.4	24.2
4	96.6	108.1	1.12	0.1089	11.8	33.0
5	103.9	124.1	1.19	0.0945	12.2	28.8

[a] Number-average molecular weight in kg/mol.
[b] Weight-average molecular weight in kg/mol.
[c] Polydispersity index (M_w/M_n).
[d] Hydrodynamic radius.
[e] Radius of gyration

In general, highly π−conjugated polymers have some limitations when it comes to processing them into thin films or fibers due to their poor solubility in common organic solvents. To increase the solubility of the polymers, long alkyl chains or flexible linkages were introduced to enhance the interaction between polymer and solvents. As reported earlier, poly(pyridinium salt)s with various linkages in the main chain or with organic counterions showed good solubility in organic solvents while maintaining sufficiently high molecular weights.[39] The synthesized poly(pyridinium salt)s−fluorene polymers displayed good solubility in DMSO, CH_3CN, and MeOH that motivated us to study the lyotropic LC properties of the synthesized polymers in these solvents. It has been reported that many poly(pyridinium salt)s exhibit lyotropic LC properties in both aprotic polar solvents and protic polar solvents at various critical concentrations (C^*) depending on the rigidity of backbones of the polymer structures.[40] Polymer **1** containing tosylate as a counterion formed an isotropic solution in the range of 0−10 wt %, a biphasic phase at 20 wt % and a lyotropic phase at 30 wt % in DMSO. Furthermore, such lyotropic properties of polymer **1** were observed at 20 wt % in acetonitrile and methanol, respectively. Similarly, polymer **2** with triflimide counterions displayed lyotropic properties at 30 and 20 wt % in DMSO and CH_3CN. However, there was no development of a LC phase in CH_3OH because of its poor solubility resulting in the phase separation of polymer and solvent. In contrast to polymers **1** and **2**, polymer **3** formed the lyotropic LC phases at relatively high concentrations (40 wt % in DMSO and 30 wt % in CH_3CN and CH_3OH) in these solvents because of the bulky and long alkyl chain counterions which caused its increased solubility in these solvents. In general, there are several key factors that determine the formation of lyotropic properties in a polymer such as rod-like structures with an extended chain character to facilitate the alignment of the polymer chain along a particular direction or sufficient solubility to exceed the C^*.[41] The solubility and chain stiffness of a polymer are dependent on the microstructure, molecular weight, polymer−polymer and polymer−solvent interactions, and temperature.[40] Therefore, the presence of bulky−flexible organic counterions in the poly(pyridinium salt)s might enhance these interactions, resulting in increased solubility and formation of a lyotropic phase at high concentrations. However, in case of polymer **4**, the formation of LC was not observed in CH_3CN and CH_3OH but in DMSO. This is because the solubility of polymer **4** was poor in CH_3CN and CH_3OH resulting in less interaction between polymer and solvents. However, due to its high solubility in DMSO, a fully-grown LC texture was observed at a high concentration (50 wt %) in this solvent. Polymer **5** was highly soluble in DMSO and CH_3OH, but not in CH_3CN. Its isotropic or biphasic solutions were observed over a broad range of concentrations (0−50 wt %) in these solvents. This phenomenon may arise from the increased solubility of polymer **5** due to long aliphatic chain in the counterions. Therefore, the lyotropic properties of polymer **5** were found to be at relatively high concentrations (35 wt % in DMSO and 40 wt % in CH_3OH) in these solvents. Table 1.2 summarizes the solution properties of polymers **1-5** in various organic solvents and Figure 1.9 shows the representative photomicrographs of lyotropic phases of some of these ionic polymers.

Table 1.2. Solution properties of poly(pyridinium salt)s−fluorene polymers

Polymer	**1**	**2**	**3**	**4**	**5**
DMSO (ε = 48.9)	0−10% I[a] 20% B[a] 30% L[a]	20% B 30% L	0−30% I 40% L	0−40% I 50% L	0−30% I 35% L
CH_3CN (ε = 37.5)	10% B 20% L	20% L	0−20% I 30% L	–	–

CH_3OH (ε = 32.6)	10% B 20% L	–	20% B 30% L	–	30% B 40% L

[a] I = Isotropic; B = Biphasic (anisotropic + isotropic); and L = Lyotropic.

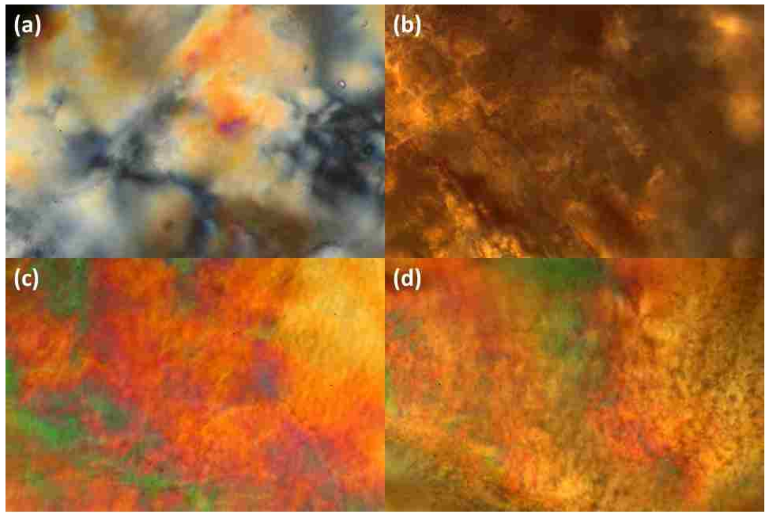

Figure 1.9. Photomicrographs of (a) polymer **1** at 30 wt % in DMSO , (b) polymer **2** at 20 wt % in CH_3CN, (c) polymer **3** at 30 wt % in CH_3CN, and (d) polymer **5** at 40 wt % in MeOH under crossed polarizers exhibiting lyotropic LC phase, respectively (magnification 400x).

For fabrication and processing of polymers, amorphous materials are a particularly interesting class of materials for various optoelectric applications.[42] Therefore, thermal properties of the synthesized ionic polymers were evaluated by differential scanning calorimetry (DSC) and thermogravimetric analysis (TGA) analysis and summarized in Table 1.3. Polymer **1** displayed T_g at 148 °C and one endotherm at 190 °C (not shown) that is attributed to the loss of entrapped solvent molecules. This finding is supported by TGA analysis (*vide supra*). Change of the counterion form tosylate to triflimide significantly lowered the glass transition temperature by 41 °C. This decrease in T_g was presumably related to the fact that the bulky size of triflimide counterion may provide a mechanism for the decrease in electrostatic interactions between this anion and pyridinium moiety. This phenomenon is in excellent agreement with the analogous poly(pyridinium salt)s as well as ionic liquids.[43] Unlike those of polymer **2,** DSC thermograms of polymers **3** and **4** did not provide any meaningful information with regard to their glass transition temperatures. However, it is worth noting that T_g of the polymer decreased steadily with the size of counterion that is associated with the respective ionic polymer, from 148 °C for polymer **1** to 67 °C for polymer **5**. This result indicated that the large size of counterions resulted in the significant increase of the segmental mobility of the polymer chain at relatively low temperature (Table 1.3 and Figure 1.10).

High thermal stability is generally required for polymers used at high operating temperatures. Although highly π−conjugated aromatic materials can increase the thermal stability of materials, poor solubility often is associated with their rigid structures. In this study, poly(pyridinium salt)s−fluorene polymers with various organic counterions were found to have excellent T_ds in the range of 302−423 °C (Figure 1.11). Moreover, polymer **2** displayed the highest T_d among the polymers in this series. This characteristic trend may be attributed to the high T_d of lithium triflimide and non-nucleophilic character of triflimide counterion.[38,39]

Table 1.3. Thermal properties of poly(pyridinium salt)s−fluorene polymers

Polymer	**1**	**2**	**3**	**4**	**5**
T_g^a (°C)	148	107	−	−	67
T_d^b (°C)	352	423	305	302	362

[a] Glass transition was recorded from a heating rate of 10 °C/min in nitrogen.
[b] Thermal decomposition was recorded at 5 wt % weight loss in nitrogen.

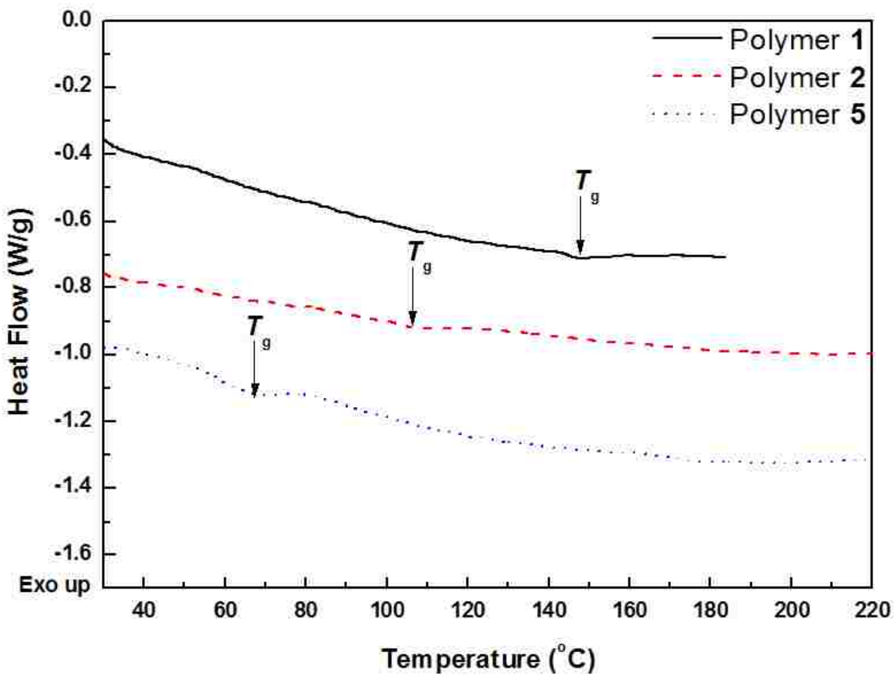

Figure 1.10. DSC thermograms of the polymers **1**, **2**, and **5** obtained at a heating rate of 10 °C/min in nitrogen.

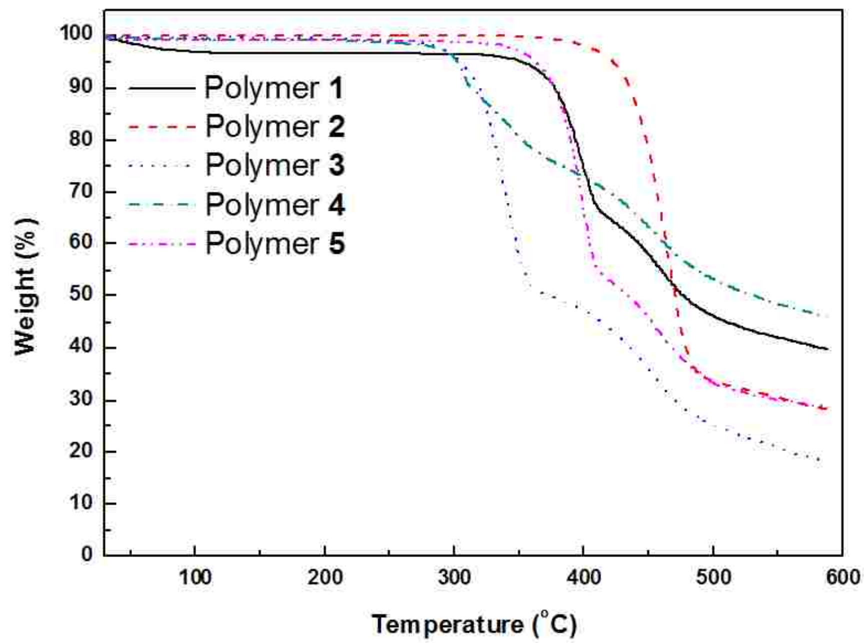

Figure 1.11. TGA thermograms of the polymers **1−5** obtained at a heating rate of 10 °C/min in nitrogen.

One of the interesting characteristics of π-conjugated polymers is their optical property in solution and solid states. The poly(pyridinium salt)s−fluorene polymers synthesized in this study exhibited good solubility in common organic solvents (*vide supra*). Therefore, the optical properties of the polymers were examined by UV−Vis and photoluminescene spectroscopy (PL) in various organic solvents. The absorption spectra of fluorene homopolymer are at λ_{max} 373 nm in chloroform and 381 nm in THF, respectively.[44] This absorption peak was not observed in any of these UV−Vis absorption spectra of polymers **1−5** in the identical solvents. Moreover, polymers **1−5** showed essentially identical λ_{max} in the range of 340−351 nm various organic solvents such as DMSO, acetonitrile, methanol, tetrahydrofuran (THF) or chloroform as detected in their absorption spectra. These results suggested that the absorption spectra of these polymers are a composite of π–π^* transitions of both phenylated bispyridinium and 9,9-dioctyl-fluorene moieties. In other words, the interactions between various organic solvents and the chromophores of polymers did not cause any significant changes in the energies of their ground states. The optical band gaps ($E_g s$) of the polymers as determined from the onset of wavelength (low energy region) in the UV−Vis absorption spectra are summarized in Table 1.4.

Table 1.4. Optical properties of poly(pyridinium salt)s−fluorene polymers

Polymer	**1**	**2**	**3**	**4**	**5**
UV abs (nm)[a]	347	347	347	351(429)	347
Band gap (eV)	3.04	3.04	3.04	2.99	3.04
PL λ_{em} DMSO (nm)	534	534	533	538	533
PL λ_{em} CH_3CN (nm)	535	532	534	−	531
PL λ_{em} CH_3OH(nm)	529	528	527	527	528
PL λ_{em} THF (nm)	−	517	493	−	497
PL λ_{em} $CHCl_3$ (nm)	−	524	524	−	518
PL λ_{em} film (nm)	570[b]	528[c]	483[b]	−	495[b]

[a] Recorded in DMSO.
[b] Thin film cast from CH_3OH.
[c] Thin film cast from CH_3CN.

The light emission spectra of the polymers were recorded in various organic solvents and displayed in Figure 1.12. In DMSO, there was a minor change in the emission peak maxima for each of these polymers **1**−**5** which suggests that fluorescence was not affected by the nature of counterions. In contrast, a hypsochromic effect was observed on changing the polarity of the solvents from DMSO to THF. Polymer **2** exhibited λ_{em} = 534 nm at excitation wavelength of 383 nm in DMSO; whereas λ_{em} = 517 nm at excitation wavelength of 341 nm in THF. Like polymer **2**, polymer **3** exhibited λ_{em} = 533 nm at excitation wavelength of 347 nm and λ_{em} = 493 nm at excitation wavelength of 344 nm in DMSO and THF, respectively. However, the emission spectra of polymer **4** were recorded in DMSO and MeOH that exhibited λ_{em} peaks at 538 and 527 nm (excitation wavelengths at 357 and 344 nm, respectively. Unlike other polymers in the series, its emission spectra could not be measured in other solvents because of its poor solubility. These data implied a positive solvatochromism phenomenon that is the λ_{em} peaks were shifted to the longer wavelengths with the increasing solvent polarity. Polymer **5** followed a similar trend in the PL study. From the results of the optical studies, the fluorescence in the solution state was dependent on the polarity of the solvents not on chemical structures of the counterions.

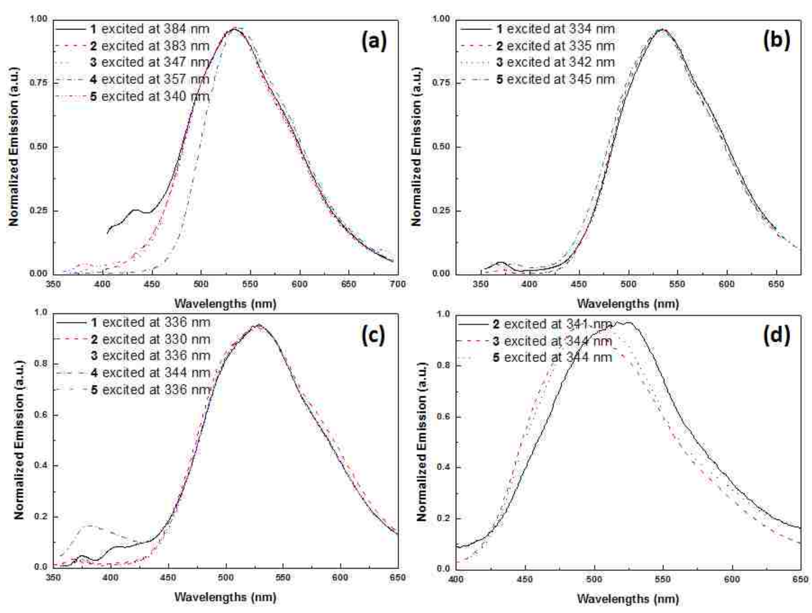

Figure 1.12. Emission spectra of (a) polymers **1-5** in DMSO, (b) of polymers **1-3** and **5** in acetonitrile, (c) of polymers **1-5** in methanol, and (d) of polymers **2,3,** and **5** in THF at various excitation wavelengths.

To evaluate the optoelectronic applications, the light-emitting properties of the polymers in their solid states were studied. Polymer **1** emitted λ_{em} peak at 570 nm (green) with an excitation wavelength at 392 nm. Compared to that of the solution spectrum, a bathochromic shift of 41 nm was observed. This emission property may be attributed to fact that the more ordered structures were built up during the film formation resulting in the more $\pi-\pi$ stacking in the solid state. By exchanging the counterion to triflimide, **2**, which has bulkier counterions than tosylate, a blue shift was found compared to that of polymer **1** which means the size of counterions may hinder the formation of ordered structures. Furthermore, the polymer **3** containing the largest counterion in size exhibited the most blue-shifted (λ_{em} = 483 nm at excitation wavelength of 330 nm) emission peak (Figure 1.13). The overall shape of the fluorescence spectra in their solid states was dependent on the size of counterions, but that of the fluorescence spectra in solutions was independent of the size of counterions. Although further study is needed, these data imply that these polymers emit blue and green light in the solid states, and these emissions are affected by the size of the counterions. Furthermore, the full-width at half-maximum (FWHM) values of PL spectra in the solution and solid states of these ionic polymers were greater than 100 nm suggesting that their light-emission stemmed from a number of chromophoric species.

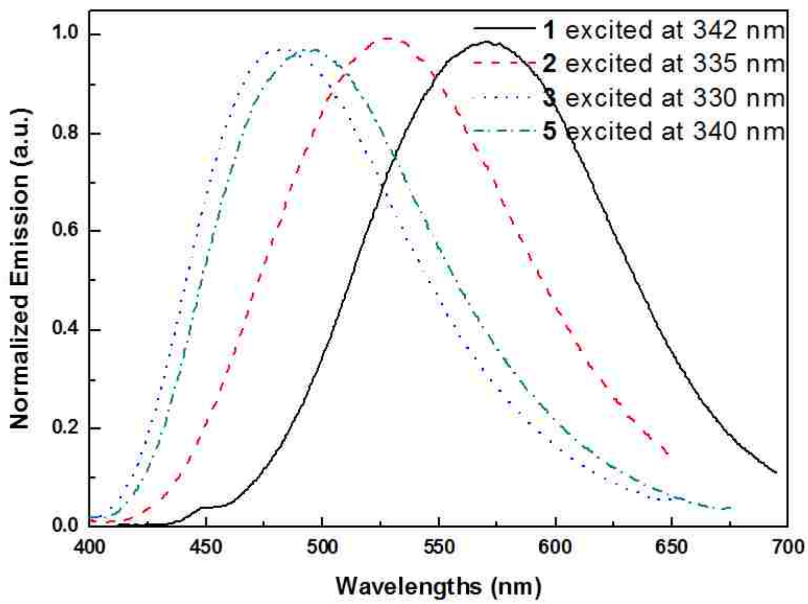

Figure 1.13. Emission spectra of polymers **1-3** and **5** in thin films cast from CH_3OH or CH_3CN at various excitation wavelengths.

1.4.2. Water-soluble poly(pyridinium salt)s containing macrocounterions

The synthetic route for the preparation of water-soluble poly(pyridinium salt)s is presented in Scheme 1.11. As reported elsewhere,[39a,45] polymers **I-1–I-5** were synthesized through the ring-transmutation polymerization reaction with the bis(pyrylium) salt, **M**, and various diamines in DMSO. Water generated during the reaction was removed by an azeotropic distillation to enhance the degree of polymerization. To make water-soluble poly(pyridinium salt)s, the tosylate counterions were exchanged to macrocounterion via the metathesis reaction. Initially, the reaction was carried out in DMSO at elevated temperature because of the polymer's high solubility in this solvent. However, a complete exchange reaction was not obtained and therefore the solvent was changed from DMSO to methanol for its completion. After the reaction was heated to reflux in methanol for 48 h, the solvent was completely removed by a rotary evaporator and excess diethyl ether was added into gel-like polymer to remove any remained macrocounterion salts and precipitate out the desired polymer. To characterize the chemical structures of the polymers, FTIR, ^{1}H, and ^{13}C NMR analysis were conducted.

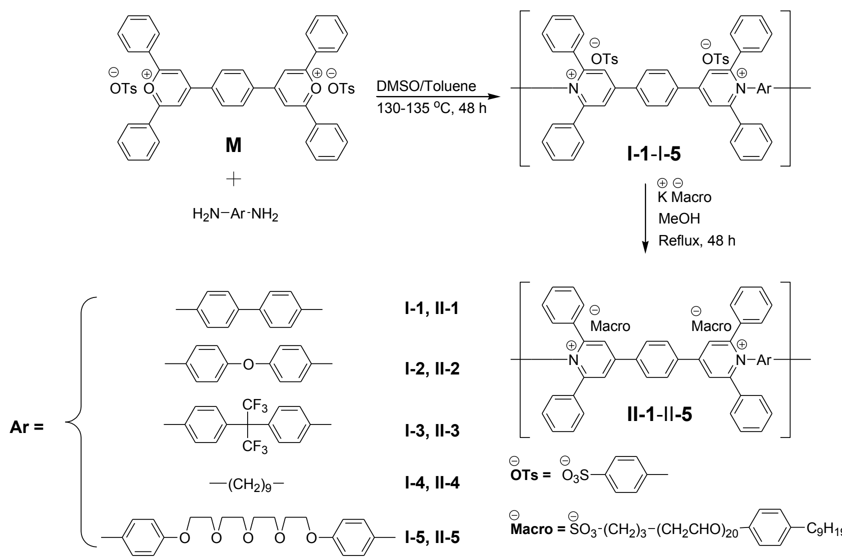

Scheme 1.11. Synthesis of water-soluble poly(pyridinium salt)s with macrocounterions.

In FTIR result, polymers **II-1−II-5** contained the representative characteristic peaks: 1620 (C=C aromatic ring stretching), 1458 (C−H aliphatic bending), 1200−1111 (C−N^{+} and S=O asymmetric stretching) and 1033 (S=O symmetric stretching). As shown in Figure 1.14, the ^{1}H NMR spectrum of polymer **I-2** showed unique resonances at δ = 8.87 and 8.67 ppm for the hydrogens of the poly(pyridinium salt)'s aromatic group and a set of resonances at δ = 7.10 and 2.27 ppm for the hydrogens of the aromatic and methyl hydrogens in the tosylate counterions. Their hydrogen integration ratios matched with each other, meaning the desired poly(pyridinium salt)s were successfully synthesized. Exchange of counterions from tosylate to macrocounterions was confirmed by the disappearance of doublet peaks of aromatic tosylate counterions at 7.10 ppm and a methyl peak at 2.27 ppm and appearance of new peaks at 7.10−7.50 and 6.84 ppm for aromatic hydrogens from macrocounterions. Moreover, their chemical structures were further confirmed by ^{13}C NMR analysis. The unique methyl peak in tosylate at 21.2 ppm disappeared in ^{13}C NMR spectra after the metathesis reaction. These results suggested that the tosylate counterions were completely converted to the macrocounterions. The other polymers, which had different linkages in their repeating units, showed the identical trends in their NMR spectra.

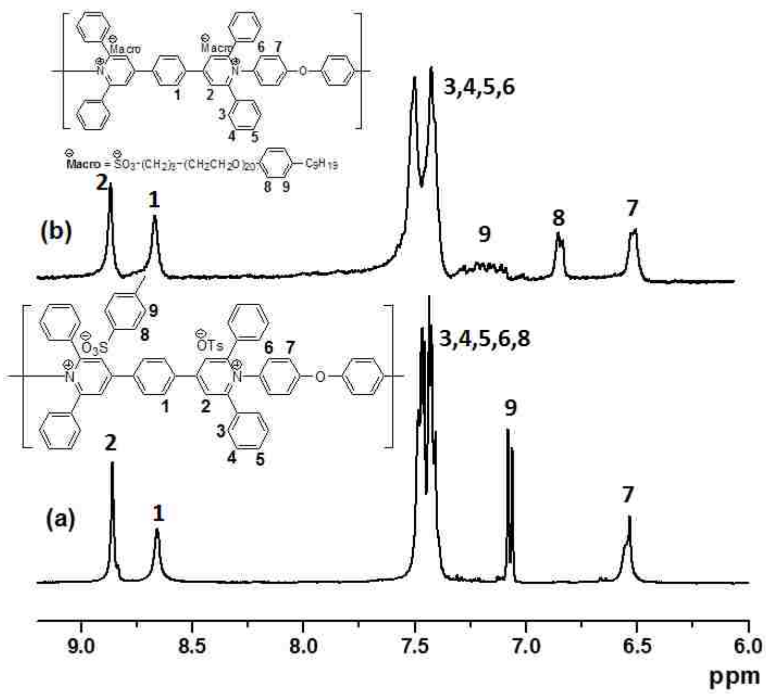

Figure 1.14. Expanded ^{1}H NMR spectra of polymers (a) **I-2** and (b) **II-2** (10 mg/mL in d_6-DMSO).

Good solubility of polymers in organic solvents and H_2O can be of significant interest for their diverse applications because of their easy processing in thin film states. The solubility of polymers **II-1−II-5** was examined in various organic solvents and H_2O. As summarized in Table 1.5, the enhanced solubility of these polymers was observed when compared to those of polymers **I-1−I-5**. The change of solubility might be caused by the introduction of flexible, bulky macrocounterions. These macroions resulted in the decrease of molecular packing between polymer chains and also provided a favorable mechanism for the interactions of oligooxyethylene groups and various polar solvents including water.

Table 1.5. Solubility of polymers **II-1−II-5**[a]

Polymer	**II-1**	**II-2**	**II-3**	**II-4**	**II-5**
H_2O	+[b]	+	+	+	+
DMSO	+	+	+	+	+
CH_3CN	+	+	+	+	+
CH_3OH	+	+	+	+	+
Acetone	±[b]	+	+	+	+
THF	±	+	+	+	+

[a] Solubility was measured in 10 mg/mL concentration.
[b] + represents soluble and ± represents partially soluble.

The thermal properties of the polymers **II-1−II-5** were evaluated by DSC and TGA measurements. Their DSC and TGA thermograms are shown in Figures **1.15** and **1.16**, respectively, and their thermal properties are summarized in Table 1.6. As reported earlier, some of poly(pyridinium salt)s (**I-4** and **I-5**) had thermotropic LC properties at elevated temperatures and their liquid crystal-to-isotropic liquid transition (T_i) were over 100 °C.[39] Polymers **I-1−I-3** had T_g over 200 °C from the previous results and their melting transitions (T_is) could not be measured because of their thermal decomposition prior to T_is. Even though glass transition temperatures (T_gs) were not detected in DSC thermograms, polymers **II-1** and **II-2** showed solid-to liquid crystal transitions (T_ms) at 34 and 32 ^oC, respectively. They also exhibited T_i values at 200 and 160 °C as determined by VTXRD (*vide infra*). In contrast, polymer **II-3–II-5** did not form LC phase, but transformed from solid-to-liquid phase (T_ms) at relatively low temperatures of 29-34 °C as supported by VTXRD studies (not shown). The reasons for their low T_ms were related to both the presence of flexible linkages in their backbones and the presence of flexible oligooxyethylene macrocounterion. In contrast, polymers **II-1** and **II-**2 exhibited thermotropic LC phase at relatively low temperatures (Table 1.6) that persisted up to their T_is of 200 and 160 °C, respectively, because of the presence of rod-like structural moieties in their main chains.

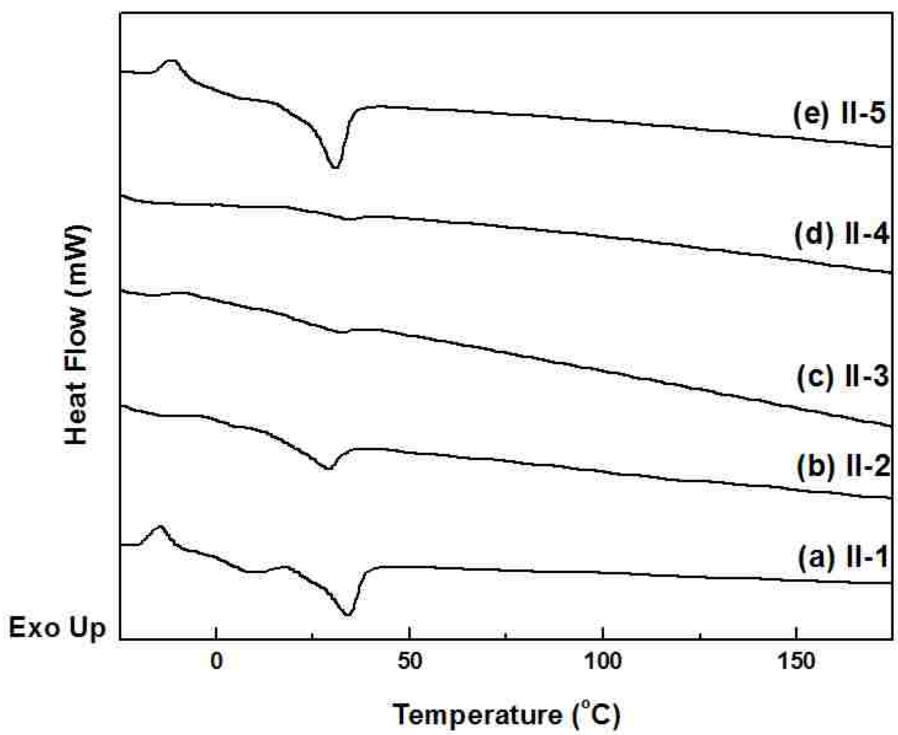

Figure 1.15. DSC thermograms of polymers **II-1−II-5** obtained from the second heating cycle at a heating rate of 10 °C/min.

TGA analyses suggested that polymers **I-1−I-5** exhibited two-step decomposition processes (not shown). The first decomposition started around 300 °C due to the cleavage of the C–S bond in tosylate counterion which is consistent with the previously reported results of other poly(pyridinium salt)s.[37–39] The second degradation was from the main chain decomposition of poly(pyridinium salt)s. The T_ds values of polymers **II-1−II-5** were slightly increased which were presumably related to the higher thermal stability of the macrocounterions when compared to tosylate counterions. Note here that decomposition of sodium tosylate occurs at 155 °C and that of macrocounterion salt occurs at high temperature of 235 °C. Therefore, the thermal stability of the salt (precursor) that is used for the preparation of an ionic polymer can affect its decomposition temperature. Polymer **II-4** showed the lowest thermal stability at 261 °C when compared with those of other polymers, which is related to low thermal stability of aliphatic linkage than aromatic linkages.

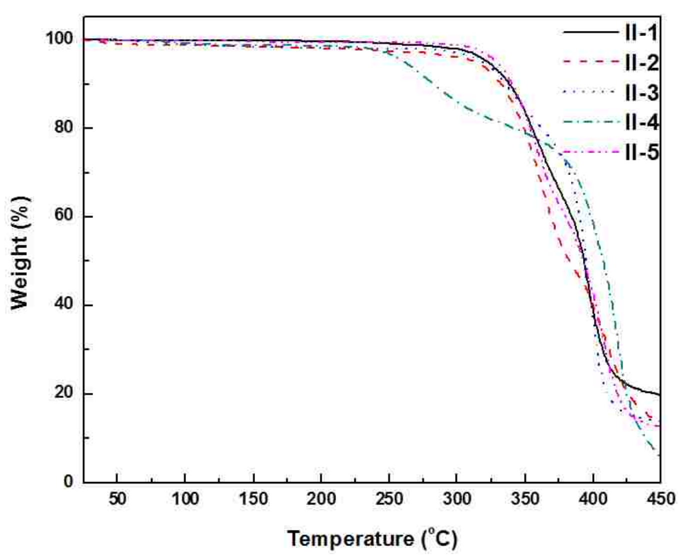

Figure 1.16. TGA thermograms of polymers **II-1−II-5** obtained at a heating rate of 10 °C/min.

Table 1.6. Thermal properties of polymers **II-1−II-5**

Polymer	**II-1**	**II-2**	**II-3**	**II-4**	**II-5**
T_m (°C)	34[a]	29[a]	–	–	–
T_i (°C)	200[b]	160[b]	32[c]	34[c]	31[c]
T_d[d] (°C)	322	313	318	261	329

[a] Solid to liquid crystal phase temperature determined by DSC.
[b] Liquid crystal to isotropic phase temperature determined by VTXRD.
[c] Solid to liquid phase temperature determined by DSC.
[d] Thermal decomposition was recorded at the temperature at which 5 wt % loss of polymer occurred in nitrogen.

To investigate the microstructures of polymers **II-1−II-5**, VTXRD analysis was performed. The polymers containing flexible linkages (**II-3−II-5**) showed amorphous characteristics at room temperature, and thermal treatment did not induce the formation of crystal structures. However, the polymers **II-1** and **II-2** exhibited some crystalline structures on 1st cooling and 2nd heating cycles, and the phases they formed on melting were identified as lamellar structures on the basis of VTXRD experiments. For **II-1**, an additional transition occurred around 150 °C on heating and 130 °C on cooling cycles. The isotropic liquid phase of **II-1** was almost reached at 200 °C. In both temperature ranges, the structure was identified as lamellar.

Even though polymer **II-2** presented an amorphous phase up to *ca*. 160 °C from the 1st heating cycle, the ordered lamellar structure occurred on 1st cooling cycle from the isotropic liquid phase. The lamellar phase became an amorphous phase below 40 °C. This thermal behaviour is fully reversible on further heating and cooling cycles. The X-ray patterns recorded on cooling cycle at 80 and 140 °C for **II-1**, and at T = 100 °C for **II-2**, chosen as representative examples, exhibited a set of eight (**II-1**) to four (**II-2**) sharp and small-angle reflections in the ratio 1:2:3:4:5:6:7:8, 1:2:3:5, and 1:2:3:4, respectively, in agreement with a lamellar arrangement, and the presence of a diffuse scattering at 4.5 Å corresponding to the molten lateral chains.

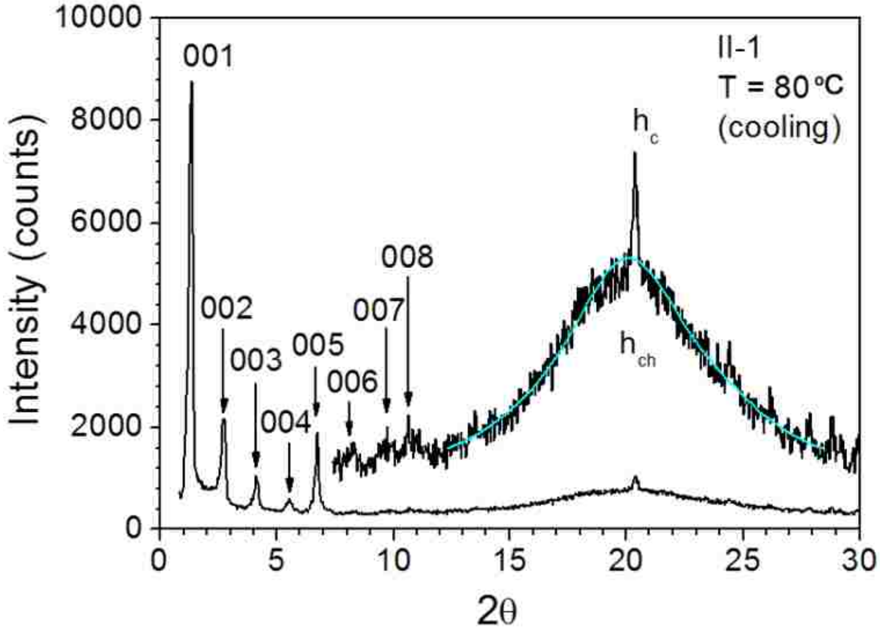

Figure 1.17. X-ray diffraction patterns for polymer **II-1** registered on 1st cooling at 80 °C.

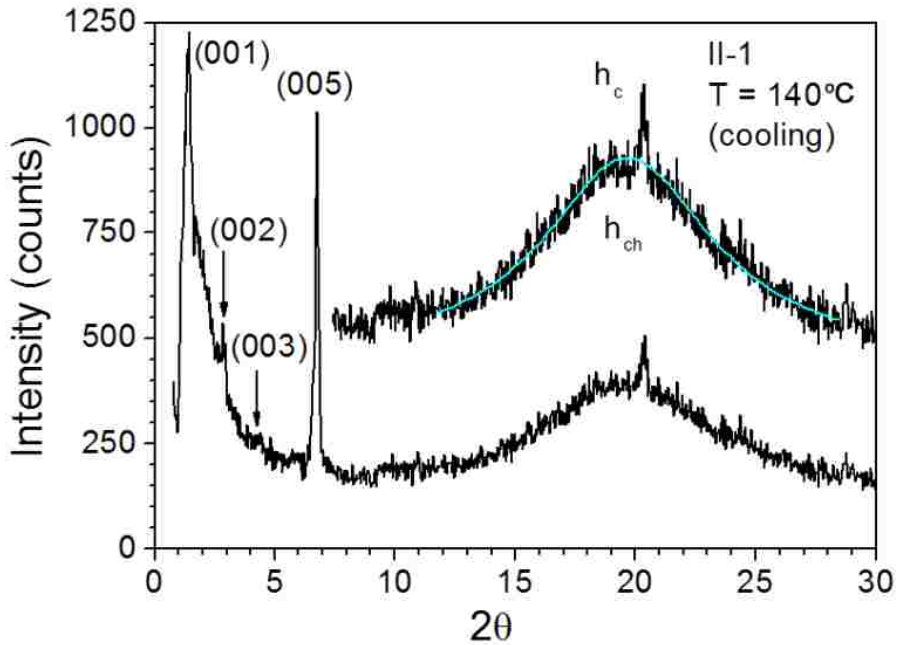

Figure 1.18. X-ray diffraction patterns for polymer **II-1** registered on 1st cooling at 140 ^{o}C.

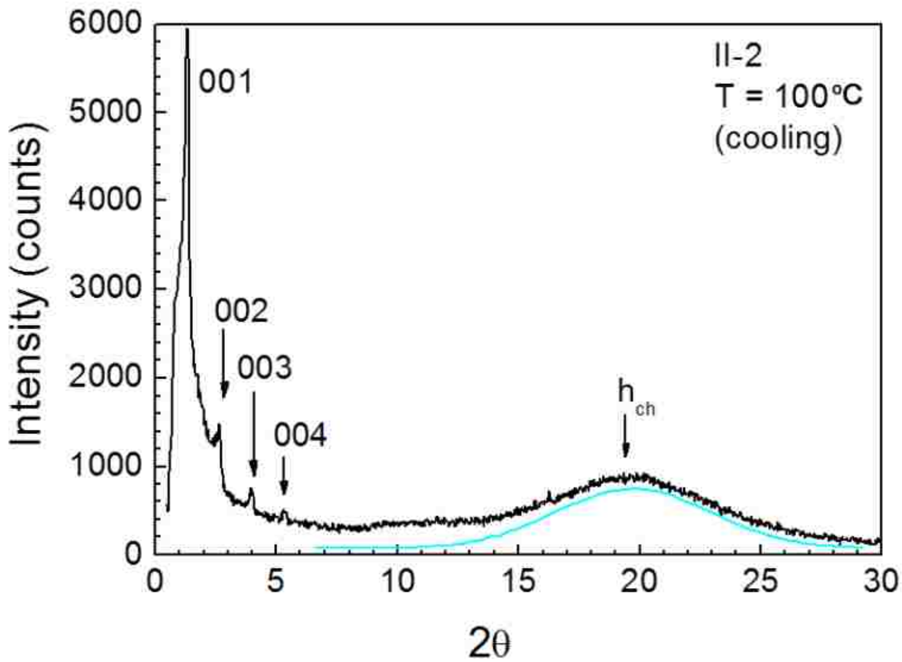

Figure 1.19. X-ray diffraction patterns for polymer **II-2** registered on 1st cooling at 100 °C.

As noted, **II-1** exhibited an additional phase, above the highly segregated mesophase (e.g., with very sharp peak), of the same nature. For **II-2**, the intensity of the reflections decreased with diffracting angles, whereas for **II-1**, the fifth reflection, (005), was highly intense (Figures 1.17−1.19 and Table 1.7). The large volume of the oligooxyethlene chain permits to wrap the rigid monomeric units of the polymers to yield highly segregated structures.

A possible representation of the lamellar ordering is shown in Figure 1.20. The polymers are a priori more or less correlated within the layers (laterally), but not between layers, where they can behave independently.

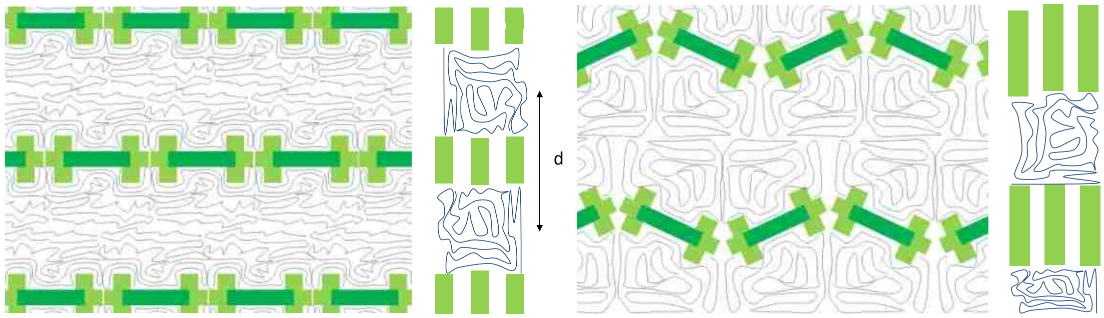

Figure 1.20. Schematic diagram of lamellar structures of polymers **II-1** and **II-2**.

Table 1.7. XRD data for polymers **II-1** and **II-2**

Polymer	Temperature	$d_{meas.}$ (Å)	I	distance	$d_{theor.}$ (Å)
II-1	80 °C	63.90	VS, sh	001	64.07
		31.96	S, sh	002	32.04
		21.16	M, sh	003	21.36
		15.85	M, sh	004	16.02
		13.1	S, sh	005	12.81
		10.7	W, sh	006	10.68
		9.15	W, sh	007	9.15
		8.02	W, sh	008	8.01
		4.5	VS, br	−	h_{ch}
		4.35	M, sh	−	h_c
	140 °C	64.0	VS (sh)	001	64.15
		32.0	W, sh	002	32.08
		21.15	S, sh	003	21.38
		13.03	VS, br	005	12.83
		4.5	M, sh	−	h_{ch}
		4.36		−	h_c
II-2	100 °C	67.0	VS, sh	001	66.95
		33.62	M, sh	002	33.47
		22.2	M, sh	003	22.31
		16.74	W, sh	004	16.73
		8.9	massif	−	−
		4.5	VS, br	−	h_{ch}

Even though poly(pyridinium salt)s with various organic counterions and aromatic linkages can have thermotropic LC properties, some polymers with $^{-}BF_4$ or triflate as a counterion do not have thermotropic LC properties due to their decomposition temperatures prior to their melting temperatures.[45,46] As we reported before, polymers **I-4** and **I-5** developed LC texture at 220 and 155 °C, respectively. These LC textures persisted up to their decomposition temperature or T_i. By transferring counterions from tosylate to triflimide, their T_g, T_m and T_i were decreased because the triflimide counterion provided reduced electrostatic interactions between negatively charged anions and positively charged bispyridinium ions. These reduced interactions appear to be associated with the increased ion mobility and reduced lattice energy in the crystalline state. In a similar vein, macrocounterion also provided the lamellar LC phase for polymer **II-1** and **II-2** at relatively lower temperatures. Figure 1.21 shows the crystalline phases of polymer **II-1** and **II-2** recorded at room temperature. Furthermore, when these two polymers were heated to above T_i and then cooled to room temperature, the birefringent LC textures of polymers related to lamellar LC phases were observed with the polarized light microscope under crossed polars. The observation of these textures in polymers with macrocounterions suggested their lamellar phase (Figure 1.22).[39a] These results suggested that the incorporation of the bulky macrocounterion was conducive to the thermotropic LC property of poly(pyridinium salt)s due to the significant reduction of strong ionic interactions between positive and negative charges, which are in excellent agreement with other thermotropic LC poly(pyridinium salt)s.[47]

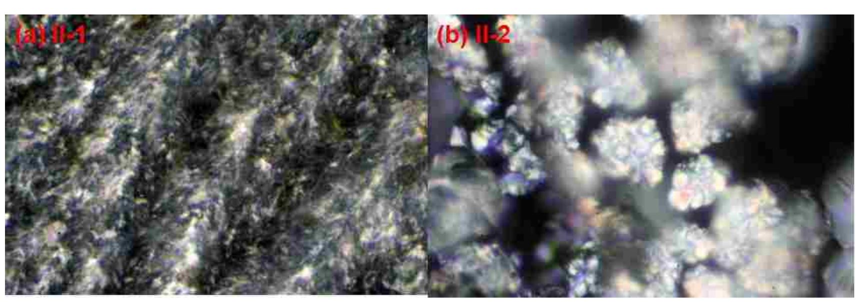

Figure 1.21. Photomicrographs of polymers **II-1** and **II-2** at room temperature under crossed polarizers exhibiting crystalline phases (magnification, 400x).

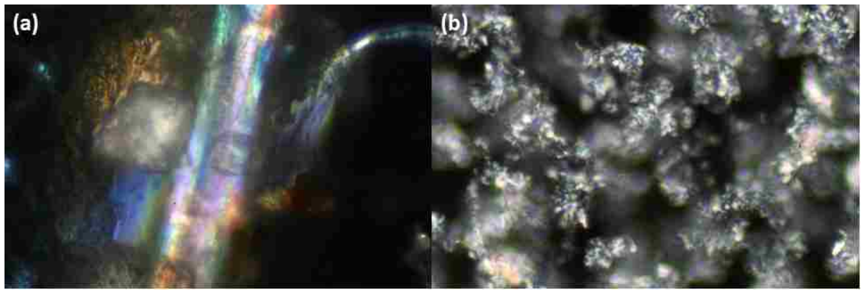

Figure 1.22. Photomicrograph of polymers (a) **II-1** and (b) **II-2** from their T_i under crossed polarizers exhibiting thermotropic LC phase (magnification, 400x).

Due to chromophores, 4,4′-(1,4-phenylene)bis(2,6-diphenylpyridiniun) ions, in polymer main chain, optical properties both in solution and solid state of polymers **II-1**−**II-5** were studied and their results were compiled in Table 1.8. They showed almost identical absorption maxima between 337 and 345 nm in H_2O as detected in their UV−Vis spectra. By changing the solvents (CH_3CN, CH_3OH, acetone, THF, and $CHCl_3$), no significant differences in their absorption spectra were observed, suggesting closely spaced π−π* transitions occurred in all of these polymers in various polar solvents. This phenomenon implies that the polarity of solvents and the interaction between solvents and backbone of polymers were less sensitive in energies of the ground states of chromophores for this class of ionic polymers. The optical band gaps (E_gs) of these polymers as determined from the onset of wavelength in the UV−Vis spectra in H_2O were between 3.00 and 3.21 eV. These band gaps were higher than those of other conjugated polymers such as poly(*p*-phenylene vinylene)s,[48] but comparable with other poly(pyridinium salt)s.[37−39] Furthermore, polymers **I-1**−**I-5** had essentially similar λ_{max}

peaks in their absorption spectra when compared with those of polymers **II-1−II-5** in the identical organic solvents. The results suggested that the UV−Vis spectra of all polymers were independent of the counterions and polarity of solvents.

Table 1.8. Optical properties of poly(pyridinium salt)s

Polymer	**II-1**	**II-2**	**II-3**	**II-4**	**II-5**
UV abs (nm)[a]	345	337	345	330	337
Band gap (eV)[a]	3.04	3.00	3.04	3.21	3.00
PL λ_{em} H_2O (nm)	492	496	447	445	533
PL λ_{em} CH_3CN (nm)	500	527	446	442	542
PL λ_{em} CH_3OH (nm)	497	522	451	443	542
PL λ_{em} Acetone (nm)	487	–	446	442	534
PL λ_{em} THF (nm)	492	482	413	439	527
PL λ_{em} $CHCl_3$ (nm)	463	–	421, 443	440	500, 520
PL λ_{em} film (nm)[b]	463	466	461	518	512

[a] Obtained from H_2O.
[b] Thin film cast from methanol.

The PL spectra of polymers **II-1−II-5** in H_2O are shown in Figure 1.23. In the case of polymer **II-1**, there was a major λ_{em} peak at 492 nm, along with a weak shoulder at the shorter and longer wavelength side, at an excitation wavelength of 330, 338 and 350 nm. In CH_3OH, it showed a major λ_{em} peak at 497 nm with a shoulder peak at 523 nm when excited at wavelengths of 325, 335 and 345 nm. Polymers **II-1** and **II-2** exhibited essentially identical emission spectra in water. However, when non-linear, bulky or flexible linkages were introduced in the polymer chain (**II-3, II-4 and II-5**), hypsochromic shifts in their photoluminescent peaks were obtained. For polymer **II-3**, a major λ_{em} peak at 447 nm, which is independent of the excitation wavelengths used, appeared in H_2O. In CH_3CN, CH_3OH, acetone, THF, and $CHCl_3$ solvents, similar blue shifted emission peaks were observed resulting in no effect on the polarity of solvents. For better comparison, the emission spectra of polymers **I-1**, **I-2** and **I-4** were examined in the identical solvents. Polymer **I-2** showed a maximum emission peak at 518 nm in methanol, which is similar to that of polymer **II-2**. In case of polymer **I-3** and **II-3**, they showed almost identical λ_{em} at 448 and 446 nm in CH_3CN, respectively. Furthermore, **I-4** displayed λ_{em} at 440 and 442 nm when excited at 310 and 305 nm wavelengths of light in methanol and acetonitrile, respectively, and its maximum emission peaks are close to polymer **II-4** in the identical solvents. By changing the counterion from tosylate to macrocounterion, PL spectra results were not different in the identical solutions suggestive of the fact that the structure of linkages in the polymer main chain has more effect on optical property than the structure of the counterion. Furthermore, the FWHM values of emission spectra for polymers **II-1**−**II-5** in various solutions were slightly narrow in relatively non-polar solvents such as THF and $CHCl_3$ that can be considered an indication of isolated emitting chromophores.[49]

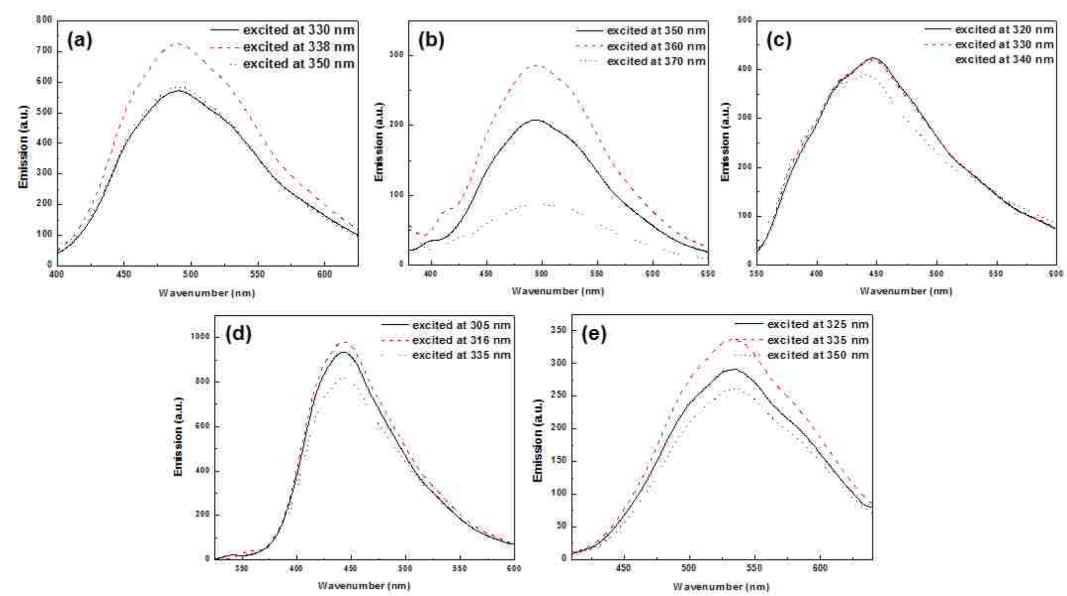

Figure 1.23. Emission spectra of polymers (a) **II-1**, (b) **II-2**, (c) **II-3**, (d) **II-4** and (e) **II-5** in H_2O at various excitation wavelengths.

The films of polymers **II-1**−**II-5** were prepared from casting in methanol on quartz plates. The solid state emission spectra of all polymers are shown in Figure 1.24, and their maximum emission peaks are compiled in Table 1.8. In thin films, polymer **II-1** showed a λ_{em} at 465 nm at excitation wavelength 325, 345 and 360 nm, respectively. In contrast to its solution emission spectra in methanol, its cast film of polymer **II-1** from methanol exhibited a single λ_{em} peak at low wavelegth when compared with those of its solution spectra. Similarly, the cast films of polymers **II-2** and **II-5** exhibited hypsochromic shifts of 56 and 30 nm in their λ_{em} values, when compared with those of their solutions spectra. Even though polymer **I-3** displayed a similar emission spectra in the solution and solid state, polymer **II-4** was red shifted by 75 nm in its λ_{em} value. This property may be attributed to the fact that the FWHM values of emission spectra in the thin film of polymer **II-4** (143 nm) were much wider when compared with those in methanol solutions (78 nm). These features strongly suggest that there are more ordered structures in the solid-state morphology of polymer **II-4**. In general, both intramolecular and intermolecular π−π interactions of chromophores of polymers are responsible for the formation of ordered structures, causing a red-shifted emission and low quantum yields of light-emitting polymers in the solid state.[50] Although further study is needed, we speculate that these π−π interactions of chromophores, polarity of solvents, and aromatic linkages in the polymer backbone can play an important role in the emission spectra of poly(pyridinium salt)s in the solid state.

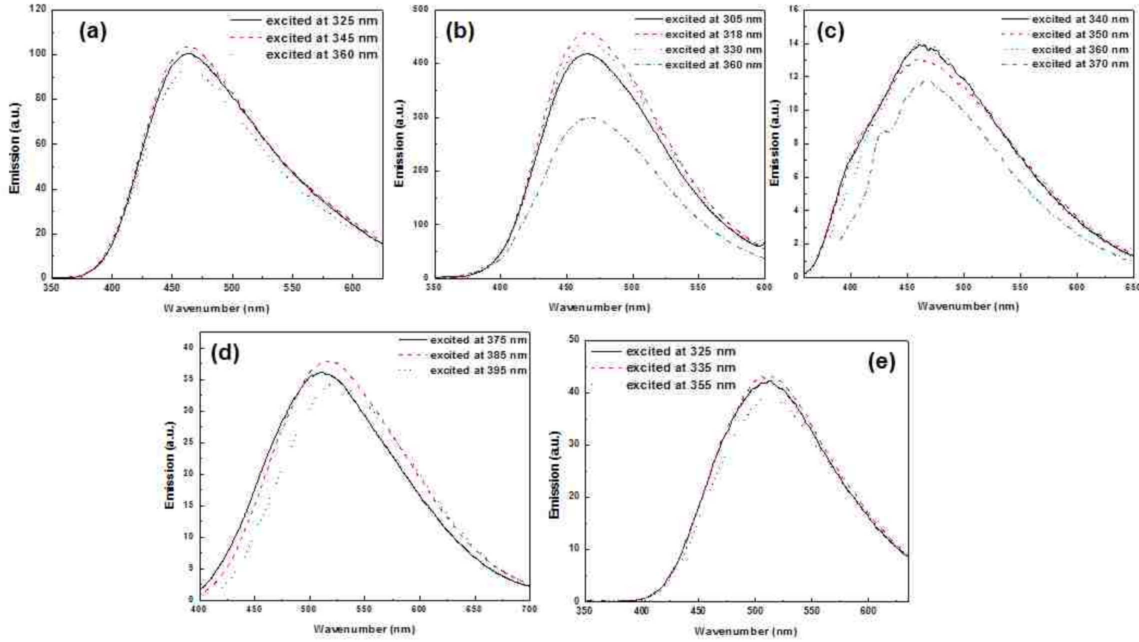

Figure 1.24. Emission spectra of polymers (a) **II-1**, (b) **II-2**, (c) **II-3**, (d) **II-4** and (e) **II-5** in thin films cast from methanol at various excitation wavelengths.

1.5. Experimental

1.5.1. General Comments

4,4′-Oxydianiline, benzidine, 2,2′-bis(4-aminophenyl)hexafluoropropane, nonane-1,9-diamine, methyl orange, dodecylbenzene sulfonic acid (sodium salt), dioctyl sulfosuccinate (sodium salt) and poly(ethylene glycol) 4-nonylphenyl 3-sulfopropyl ether potassium salt were purchased from commercial vendors (Sigma-Aldrich and TCI America) and 4,4′-oxydianiline was purified by sublimation before use. The bis(2-(2-(4-aminophenoxy)ethoxy)ethyl) ether, 9,9-dioctyl-9*H*-fluorene-2,7-diamine and the 4,4′-(1,4-phenylene)bis(2,6-diphenylpyrylium *p*-toluene sulfonates), **M**, were synthesized according to the reported procedures.[37–39]

^{1}H, ^{19}F and ^{13}C NMR spectra were obtained using a Varian NMR spectrometer (400 MHz for ^{1}H, 376 MHz for ^{19}F, and 100 MHz for ^{13}C) with three RF channels at room temperature, and chemical shifts were referenced to tetramethylsilane (TMS) for proton and carbon nuclei and $CFCl_3$ for fluorine nuclei. NMR samples were prepared by applying gentle heat to dissolve the polymer (10 mg for ^{1}H and ^{19}F and 30 mg for ^{13}C) in d_6-DMSO (1 mL). Differential scanning calorimetry (DSC) measurements of polymers were conducted using a TA module DSC Q200 series instrument in nitrogen at heating and cooling rates of 10 °C/min. The temperature axis of the DSC thermograms was calibrated before using the reference standard of high purity indium and tin. Thermogravimetric analyses (TGA) of polymers were performed using a TGA Q50 instrument in nitrogen. The TGA data were collected at temperatures between 30 and 600 °C at a heating rate of 10 °C/min. The UV−Vis absorption spectra of polymer solution in organic solvents were recorded at room temperature using Varian Cary 50 Bio UV−Visible spectrophotometer in quartz cuvettes. Photoluminescence spectra in solutions and thin films were recorded using a PerkinElmer LS 55 luminescence spectrometer with a xenon lamp light source. Thermotropic and lyotropic liquid crystal properties of the materials were obtained using a polarized optical microscopy (POM, Nikon, Model Labophot 2) equipped with crossed polarizer. The VTXRD measurements of two polymer **II-1** and **II-2** were carried out on both samples for both heating and cooling cycles, with temperature steps of 20 and 10 °C, respectively. Samples were exposed to an X-ray beam for about one hour at each temperature. The XRD patterns were obtained using the following setup. A linear monochromatic $CuK_{\alpha1}$ beam (λ = 1.5405 Å) was obtained using a sealed-tube generator (900 W) equipped with a bent quartz monochromator. The crude powder was filled in Lindemann capillaries of 1 mm diameter and 10 μm wall thickness. The diffraction pattern was recorded with a curved INEL CPS120 counter gas-filled detector linked to a data acquisition computer; periodicities up to 60 Å can be measured, and the sample temperature can be controlled to within ±0.05 °C from 20 to 200 °C. In each case, exposure times were varied from 1 to 24 h.

1.5.2. Synthesis of Polymer **1**

The bis(pyrylium) salt, **M**, (5.00 g, 5.65 mmol), 9,9-dioctyl-9*H*-fluorene-2,7-diamine (2.38 g, 5.65 mmol), and DMSO (120 mL) were placed in a 250 mL three-necked, round bottomed flask equipped with a magnetic stirrer. A small amount of toluene (6 mL) was added to remove the water generated during the reaction by azeotrope, which was facilitated by using Dean-Stark trap and water condenser. The solution was heated at 130−135 °C on stirring for 48 h in nitrogen. After the reaction was completed, the solution was concentrated by a rotary evaporator until the solution became viscous. It was then poured into water to precipitate the polymer. The precipitated solid was washed with water several more times to remove any residual salts and collected by vacuum filtration. The collected polymer was additionally washed a few times with boiling water and dried *in vacuo* at 110 °C for 48 h. Data for polymer **1**: Anal. Cacld for $C_{83}H_{82}N_2O_6S_2$ (1267.68): C, 78.64; H, 6.52; N, 2.21; S, 5.06. Found: C, 76.67; H, 6.62; N, 2.27; S, 4.79; FTIR (KBr film, ν_{max} cm^{-1}): 3047 (=C−H aromatic stretching), 1620−1448 (C=C and C=N aromatic ring stretching), 1196 (C−N$^+$), 1119 (S=O asymmetric stretching) and 1033−1010 (S=O symmetric stretching).

1.5.3. General Procedure for Synthesis of Polymers **2−5**

Polymers **2−5** were synthesized through a metathesis reaction from the respective polymer **1** with excess appropriate counterion salts. In general, polymer **1** (1.00 g, 0.789 mmol) was dissolved in MeOH (50 mL) and a solution of counterion salts (1.73 mmol, 2.2 equiv based on the polymer ratio) was added into the solution while keeping the temperature at 40 °C. The solution was heated to reflux on stirring for 48 h. After the reaction was completed, the solution was concentrated by a rotary evaporator until it became viscous. The concentrated solution was poured into water to precipitate out the polymer. The solid polymer was then suspended in water and stirred for 2 h to remove any residual salts and this procedure was repeated one or two more times until all tosylate counterions were completely exchanged to the target counterions. The complete exchange of counterions was confirmed by the analysis of ^{1}H NMR spectrum. The purified polymer was dried *in vacuo* at 80 °C for 24 h. Data for polymer **2**: Anal. Cacld for $C_{73}H_{68}F_{12}N_4O_8S_s$ (1485.58): C, 59.02; H, 4.61; N, 3.77; S, 8.63. Found: C, 59.29; H, 4.59; N, 3.86; S, 8.43; FTIR (KBr film, ν_{max} cm^{-1}): 3063 (=C−H aromatic stretching), 1620−1466 (C=C and C=N aromatic ring stretching), 1350 (C−F stretching), 1196 (C−N$^+$), 1119 (S=O asymmetric stretching) and 1057 (S=O symmetric stretching); for polymer **3**: Anal. Cacld for $C_{109}H_{142}N_2O_{14}S_2$ (1786.43): C, 74.03; H, 8.09; N, 1.58; S, 3.63. Found: C, 73.25; H, 7.90; N, 1.65; S, 3.48; FTIR (KBr film, ν_{max} cm^{-1}): 3055 (=C−H aromatic stretching), 1736 (C=O stretching), 1620−1458 (C=C and C=N aromatic ring stretching), 1242−1158 (C−N$^+$ and S=O asymmetric stretching) and 1034 (S=O symmetric stretching); for polymer **4**: Anal. Cacld for $C_{97}H_{96}N_8O_6S_2$ (1534.99): C, 75.95;

H, 6.31; N, 7.30; S, 4.18. Found: C, 74.01; H, 6.40; N, 6.96; S, 3.83; FTIR (KBr film, ν_{max} cm^{-1}): 3048 (=C−H aromatic stretching), 1620−1458 (C=C and C=N aromatic ring stretching), 1458 (N=N), 1365 (C−N stretching), 1196−1111 (C−N^{+} and S=O asymmetric stretching) and 1026 (S=O symmetric stretching); for polymer **5**: Anal. Cacld for $C_{105}H_{126}N_2O_6S_2$ (1576.26): C, 80.01; H, 8.06; N, 1.78; S, 4.07. Found: C, 78.37; H, 8.02; N, 1.87; S, 3.91; FTIR (KBr film, ν_{max} cm^{-1}): 3055 (=C−H aromatic stretching), 1620−1458 (C=C and C=N aromatic ring stretching), 1195−1134 (C−N^{+} and S=O asymmetric stretching) and 1034−1011 (S=O symmetric stretching).

1.5.4. General Procedure for Synthesis of Polymers **I-1**−**I-5**

The bis(pyrylium) salt, **M**, was reacted with an appropriate diamine by a ring-transmutation reaction to yield each of the target polymers. Equal mole ratio of monomers was placed in three-necked, round-bottomed flask equipped with a magnetic stirrer in DMSO. A small amount of toluene was added to remove the water generated during the reaction by azeotropic distillation, which was facilitated by using Dean-Stark trap and water condenser. The temperature was increased up to 130−135 °C and the solution was stirred for 48 h in nitrogen. After the polymerization reaction was completed, the solution was cooled to room temperature. Excess of DMSO was removed by a rotary evaporator until the solution became viscous. It was then poured into water to precipitate the polymer. The precipitated solid was washed with water several more times to remove any residual impurities and collected by vacuum filtration. The collected polymer was additionally washed a few times with boiling water and dried *in vacuo* at 110 °C for 48 h. Data for polymer **I-1**: Anal. Cacld for $C_{66}H_{50}N_2O_6S_2$ (1031.24): C, 76.87; H, 4.89; N, 2.72; S, 6.22. Found: C, 73.56; H, 5.10; N, 2.52; S, 7.50; for polymer **I-2**: Anal. Cacld for $C_{66}H_{50}N_2O_7S_2$ (1047.24): C, 75.70; H, 4.81; N, 2.67; S, 6.12. Found: C, 72.96; H, 4.78; N, 2.58; S, 6.00; for polymer **I-3**: Anal. Cacld for $C_{69}H_{50}N_2O_6F_6S_2$ (1181.27): C, 70.16; H, 4.27; N, 2.37; S, 5.43. Found: C, 66.87; H, 4.95; N, 2.50; S, 5.23; for polymer **I-4**: Anal. Cacld for $C_{63}H_{60}N_2O_6S_2$ (1005.29): C, 75.27; H, 6.02; N, 2.79; S, 6.38. Found: C, 74.96; H, 7.35; N, 2.89; S, 5.93; for polymer **I-5**: Anal. Cacld for $C_{74}H_{66}N_2O_{11}S_2$ (1223.48): C, 72.65; H, 5.44; N, 2.29; S, 5.24. Found: C, 70.58; H, 5.51; N, 2.58; S, 4.41.

1.5.5. General Procedure for Synthesis Polymers **II-1−II-5**

Polymers **II-1−II-5** were prepared by the metathesis reaction from the respective tosylate polymers with excess macroion salt. For example, polymer **I-1** (500 mg, 0.485 mmol) was dissolved in methanol (25 mL) and DMSO (a few drops) and macro counterion (1.02 mmol, 2.1 equiv based on polymer molar ratio) was added into the round-bottomed flask. The reaction was heated to reflux for 48 h on stirring. At the end of the metathesis reaction, excess methanol was removed by a rotary evaporator to form a viscous solution, and diethyl ether was poured to precipitate the polymer. This procedure was repeated one or two more times until all tosylate counter ions were completely exchanged to macroions, which was confirmed by ^{1}H NMR spectrum. Collected gel-like polymer was washed with diethyl ether until clean layer appeared to remove any remained excess macroions. The purified polymer **II-1** was dried *in vacuo* at 80 °C for 24 h.

1.6. Conclusions

A series of poly(pyridinium salt)s with various diamines and organic counterions was prepared via the ring-transmutation polymerization and metathesis reaction. The chemical structures of the synthesized polymers were fully characterized by using FTIR and NMR spectroscopic techniques. The poly(pyridinium salt)s having fluorene repeating units in the chemical backbone provided M_n values in the range of 96.5−108 kg/mol, and PDI values were between 1.12 and 1.88 determined by GPC analysis. All the polymers had excellent thermal stabilities, which were dependent on the chemical structures of polymers and organic counterions. The poly(pyridinium salt)s with macrocounterions were soluble in water, which is useful for processing these materials into thin films. The synthesized polymers displayed liquid-crystalline properties either lyotropic or thermotropic based on the chemical structures of their backbones. Because of the presence of chromophores, the light emission properties of poly(pyridinium salt)s were studied by UV−Vis and photoluminescence spectrometers, and they fluoresced light in the non-polar solvents, polar solvents and in the solid states. In the solutions, they usually emitted light ranging from blue to green and exhibited positive solvatochromism phenomenon. In some cases, light emissions were dependent on their size of counterions in the solid states.

CHAPTER 2

DISPERSION OF SINGLE-WALLED CARBON NANOTUBES WITH POLY(PYRIDINIUM SATL)S VIA A COGULATION METHOD

2.1. Abstract

The dispersion of single-walled carbon nanotubes (SWNTs) with poly(pyridinium salt)s having various aromatic moieties is accomplished via the non-covalent coagulation method in dimethyl sulfoxide (DMSO). The interactions between SWNTs and polymers were characterized by using various spectroscopic techniques. The concentration of incorporated SWNTs was tuned by adjusting the weight ratio of SWNTs to polymer. High concentration of the composites (>33 wt % of SWNTs) became viscous or aggregated due to strong van der Waals interactions.

The ^{1}H NMR results suggested that the strong interactions between polymers and SWNTs were observed because of their broadened and reduced intensity of proton signals. These results supported the strong π−π and cationic−π interactions through main-chain poly(pyridinium salt)s and SWNTs. The UV−Vis absorption spectra were independent on the incorporation of SWNTs resulting in no energy change on the ground state. The resulting composites displayed high quenching efficiency in the photoluminescent properties due to the efficient energy or electron transfer between the polymers and SWNTs. TEM revealed well-dispersed SWNTs in the polymer matrices. When compared with the effect of aromatic repeating units, more π conjugated poly(pyridinium salt)s provided better interaction with SWNTs. The enhanced thermal

stability of the composites was founded in TGA analysis and the fully-grown lyotropic LC properties of the poly(pyridinium salt)s were disrupted by the introduction of SWNTs into the polymer.

2.2. Introduction

Since the discovery of carbon filaments by Radushkevich and Lukyanovich[1a] in 1976, these materials are considered one of the most attractive in the field of nanotechnology due to their outstanding thermal, electrical, mechanical and optical properties.[1b,c] The discovery of carbon nanotubes (CNTs) by Ijima in 1991 has lead to a new class of engineered composite nanomaterials with superior properties.[2] CNTs are allotropes of carbon with a cylindrical nanostructure. Nanotubes have been constructed with length-to-diameter ratio of up to 132,000,000:1, significantly larger than for other material. These cylindrical carbon molecules have unusual properties, which are valuable for nanotechnology, electronics, optics and other fields of materials science and technology. Based on their extraordinary thermal conductivity and mechanical and electrical properties, carbon nanotubes find application as additives to various structural materials. There are two main types of carbon nanotubes that can have high structural perfection. Single-walled carbon nanotubes (SWNTs) consist of a single graphite sheet seamlessly wrapped into a cylindrical tube and multi-walled carbon nanotubes (MWNTs) comprise an array of such nanotubes that are concentrically nested like rings of a tree trunk (Figure 2.1).

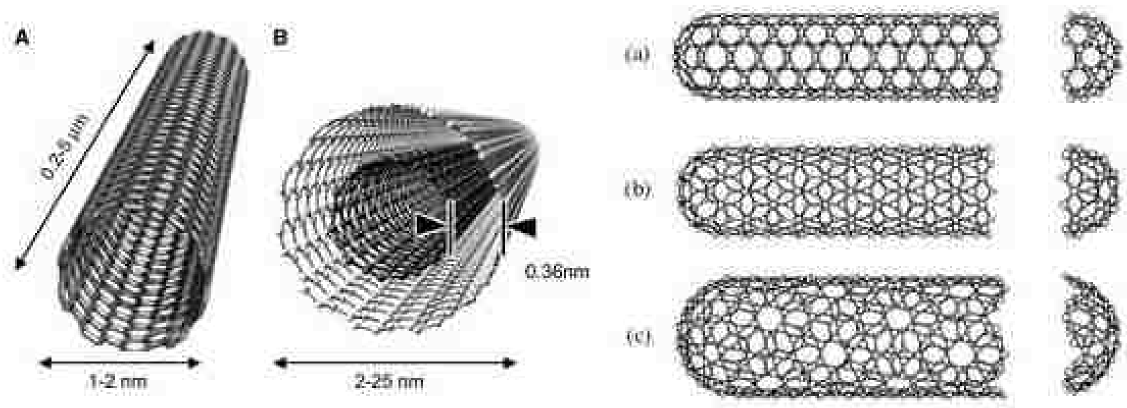

Figure 2.1. Schematic diagrams of (Left) single-walled carbon nanotubes and multi-walled carbon nanotubes and (Right) types of single-walled carbon nanotubes.

CNTs possess unique electrical properties. The diameter being in the nanometer range gives rise to quantum effects and the differences in the conducting properties are caused by the molecular structure. CNTs can either be conducting or semiconducting, depending on their chirality. They are metallic if the structure is armchair and all other structures are predicted to be semi-conducting. The geometry of the nanotubes determines band structure and thus the energy band gap. The energy band gap of semiconducting CNTs highly depends on the nanotube diameter. The conductivity and resistivity of SWNTs ropes can be measured by placing electrodes on different parts of the CNTs, and the resistivity is on the order of 10^{-4} Ω·cm at 27 °C. This means SWNT ropes are the most conductive carbon fibers known. The current density that is possible to achieve is 10^{7} A/cm^2, however in theory the SWNT ropes should be able to sustain much higher stable current densities, as high as 10^{13} A/cm^2. Furthermore, it has recently been reported that SWNTs can route electrical signals at high speeds (up to 10 GHz) when used as interconnects on semi-conducting devices.[3,4]

The CNTs are expected to have high stiffness and axial strength as a result of the carbon–carbon sp^2 bonding. The practical application of the nanotubes requires study on the elastic response, the inelastic behavior and buckling, yield strength and fracture. Experimental and theoretical investigations of these properties have been conducted. Nanotubes are the stiffest known fiber, with a measured Young's modulus of 1.4 TPa.[5] They have an expected elongation to failure of 20−30%, which combined with the stiffness, projects to a tensile strength well above 100 GPa, by far the highest known.[6] Mechanical properties of engineering fibers are summarized in Table 2.1.

Table 2.1. Mechanical properties of engineering fibers

Material	Specific Density	E (TPa)	Strength (GPa)	Strain at Break (%)
Carbon nanotubes	1.3−2.0	1.4	100 >	10
HS Steel	7.8	0.2	4.1	< 10
Carbon Fiber - PAN	1.7−2.0	0.2−0.6	1.7−5.0	0.3−2.4
E/S glass	2.5	0.07	2.4	4.8
Kevlar	1.4	0.13	3.6−4.1	2.8

Prior to CNTs, diamond was the best thermal conductor. CNTs have now been shown to have a thermal conductivity at least twice that of diamond. They have the unique property of feeling cold to the touch, like metal, on the sides with the tube ends exposed, but similar to wood on the other sides. The specific heat and thermal conductivity of carbon nanotube systems are determined primarily by phonons. The measurements yield linear specific heat and thermal conductivity above 1 K and below room temperature, while a behavior of the specific heat is observed below 1 K. The linear temperature dependence can be explained with the linear k-vector dependence of the frequency of the longitudinal and twist acoustic phonons. The behavior of the specific heat below 1 K can be attributed to the transverse acoustic phonons with quadratic k dependence. The measurements of the thermoelectric power (TEP) of nanotube systems give direct information for the type of carriers and conductivity mechanisms. These outstanding beneficial characteristics make CNTs useful for a wide range of applications in biomedical, nanocomposite, electronics, optics, and sensing.[7] Transport properties of conductive materials are summarized in Table 2.2.

Table 2.2. Transport properties of conductive materials

Material	Thermal conductivity (W/m.k)	Electrical conductivity (S/m)
Carbon nanotubes	> 3000	10^6−10^7
Copper	400	6 x 10^7
Carbon Fiber - Pitch	1000	2−8.5 x 10^6
Carbon Fiber - PAN	8−105	6.5−14 x 10^6

CNTs have attracted particular interest because they have remarkable mechanical and other physical properties. The combination of these properties such as stiffness, electrical conductivity, permeability, and thermal stability with polymers suggests that CNTs are ideal candidates for high performance polymer composites; in a sense they may be the next generation of carbon fibers. Although tens or hundreds of kilograms of CNTs are currently produced per day, the development of high-strength and high-stiffness polymer composites based on these carbon nanostructures has been hampered by the lack of of high quality nanotubes in large quantities. In addition, a number of fundamental challenges arise from the small size of CNTs. Although significant advances have been made in recent years to overcome difficulties with the manufacture of polymer nanocomposites, processing remains a key challenge in fully utilizing the properties of the nanoscale reinforcement. A primary difficulty is achieving a good dispersion of the

CNTs in a composite, independent of CNTs shape and aspect ratio. Without proper dispersion, aggregation of CNTs tends to act as defect sites which limit the mechanical performance; such agglomerates also adversely influence physical composite properties such as optical transmissivity. When dispersing CNTs in a low viscosity medium, diffusion processes and particle-particle and particle-matrix interactions play an increasingly important role as the diameter drops below 1 μm. It is not only the absolute size but rather the specific surface area of the CNTs, and the resulting interfacial volumes, which significantly influence the dispersion process. Therefore, the insolubility and improper orientation of CNTs limit their ultimate properties and performance. In order to maximize the improvement in material properties with CNTs, one must carefully control the dispersion of CNTs within the polymer matrix in common organic solvents. To overcome these conventional problems associated with the dispersion of CNTs, the functionalization and dispersion of CNTs have been studied over two decades and resulted in the development of a number of functionalization methods.[8]

Over the years, numerous effort has been aimed at finding appropriate media to solubilize CNTs. Various solvents have been examined in order to solubilize and/or disperse SWNTs. Non hydrogen-bonding Lewis bases, such as dimethylformamide (DMF), *N*-methylpyrrolidone (NMP) and hexamethylphosphoramide (HMPA), with high electron pair donicity and low hydrogen-bonding parameters have demonstrated the ability to readily form stable dispersions of SWNTs produced by different techniques.[9,10] However the high electron pair donicity alone has proven to be insufficient as dimethyl sulfoxide (DMSO) is not an effective solvent for SWNTs although it contains three lone pairs.[11] A systematic study of the efficiency of a series of amide solvents to disperse as-produced and purified laser-generated SWNTs suggests that the favorable interaction between SWNTs and alkyl amide solvents is attributed to the highly polar π system and optimal geometries of the solvent structures.[12] Ortho-dichlorobenzene (*o*-DCB) and monochlorobenzene (MCB) have also been demonstrated to be effective solvents for SWNTs. The high solubility of SWNTs in these solvents was attributed to π−π stacking due to the similarity of the aromatic solvent molecules and carbon nanotube side wall.[13] However, this concept is somehow undermined by the poor solubility of SWNTs in toluene,[11] since it also contains a phenyl ring. It was also reported that in *o*-DCB dispersions, sonication caused the decomposition and polymerization of *o*-DCB and the homopolymer coated on the tubes was proposed to contribute to the stabilization of SWNTs in *o*-DCB suspension.[14] A theoretical study indicated that the interaction between *o*-DCB and SWNTs surface was enhanced when there were defects on the side wall, which would suggest that the high solubility of SWNTs in *o*-DCB is probably due to the destruction of nanotube surface during sample preparation.[15] The solubility of SWNTs in various organic solvents are summarized in Table 2.3.

Table 2.3. Room temperature solubility of SWNTs in various organic solvents

Solvent	mg/L
1,2-Dichlorobenzene	95
Chloroform	31
1-Methylnaphthalene	25
1-Bromo-2-metylnaphthalene	23
N-Methylpyrrolidone	10
Dimethylformamide	7.2
Tetrahydrofuran	4.9
1,2-Dimethylbenzene	4.7
Pyridine	4.3
Carbon disulfide	2.6
1,3,5-Trimethylbenzene	2.3

The enhanced dispersion of CNTs can occur via covalent functionalizations, requiring treatment with strong oxidizing reagents, or non-covalent modification of CNTs. The covalent functionalization of CNTs with strong oxidizing reagents is a well-known method to disperse CNTs in organic solvents. This covalent modification can be obtained both by either modification of carboxylic acid groups on the SWNTs or direct addition of reagents to the sidewalls of SWNTs. Carboxylic acid groups are introduced at the defect sites of SWNTs by nitric acid oxidation, and long alkyl chains, polymers, and sugars have been attached by esterification and amidation reactions (Figure 2.2).[16] Fluorine,[17] aryl cations,[18] hydrogen,[19] nitrenes,[20] carbenes,[21] radicals,[22] and 1,3-dipoles[23] could be introduced along the side wall of SWNTs. These functionalizations can improve the processability and solubility of SWNTs but also alter the intrinsic properties of SWNTs.

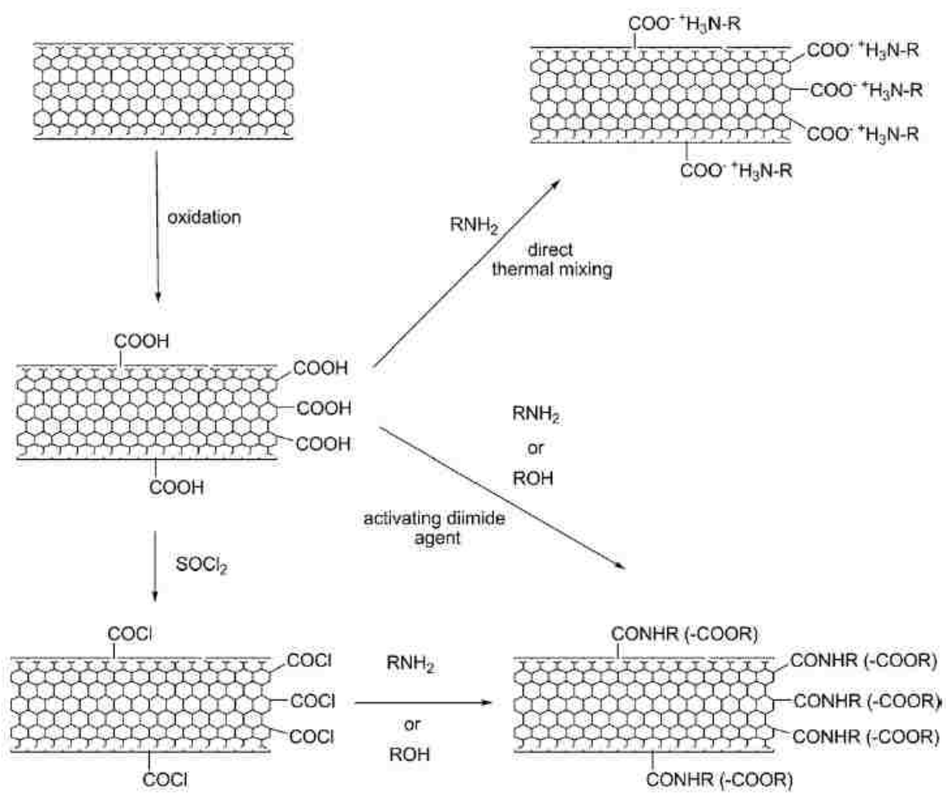

Figure 2.2. Oxidation of CNTs and derivatization reaction with amines or alcohols.

Furthermore, the covalent functionalization of SWNTs could be performed via atom transfer radical polymerization (ATRP) from initiator functionalized SWNTs. The chemically modified SWNTs with the presence of polymers will help the SWNTs to be dissolved in good solvents with a low degree of functionalization. The covalent modification can be approached from grafting "from" or "to" (Figure 2.3). The grafting "from" process is based on the initial immobilization of an initiator on the nanotube surface, followed by the *in situ* polymerization of appropriate monomers with the formation of the polymer molecules bound to the nanotubes. The grafting "to" approach is based on attachment of end-functionalized polymer molecules to a functional group on the nanotube surface via chemical reactions. Furthermore, this approach also can be obtained by a living radical mechanism such as 2,2,6,6-tetramethylpiperidine (TEMPO) group (Figure 2.4).[24]

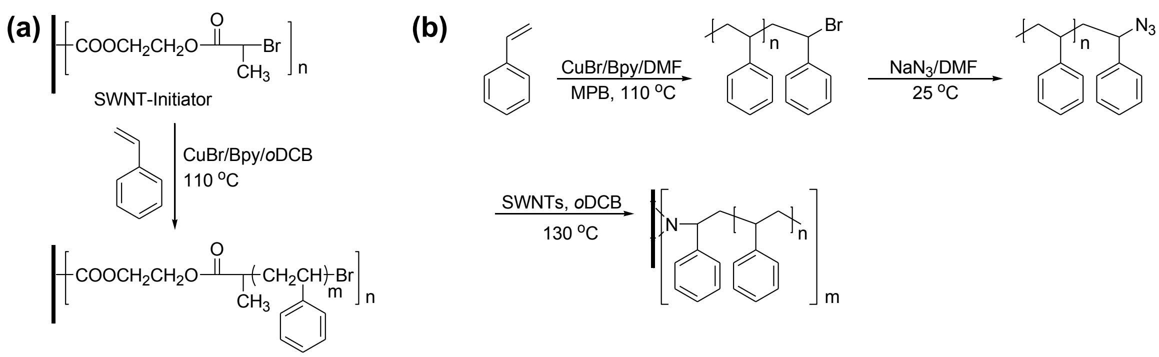

Figure 2.3. Covalent functionalizations of SWNTs via grafting (a) "from" and (b) "to" through the atom transfer radical polymerization.

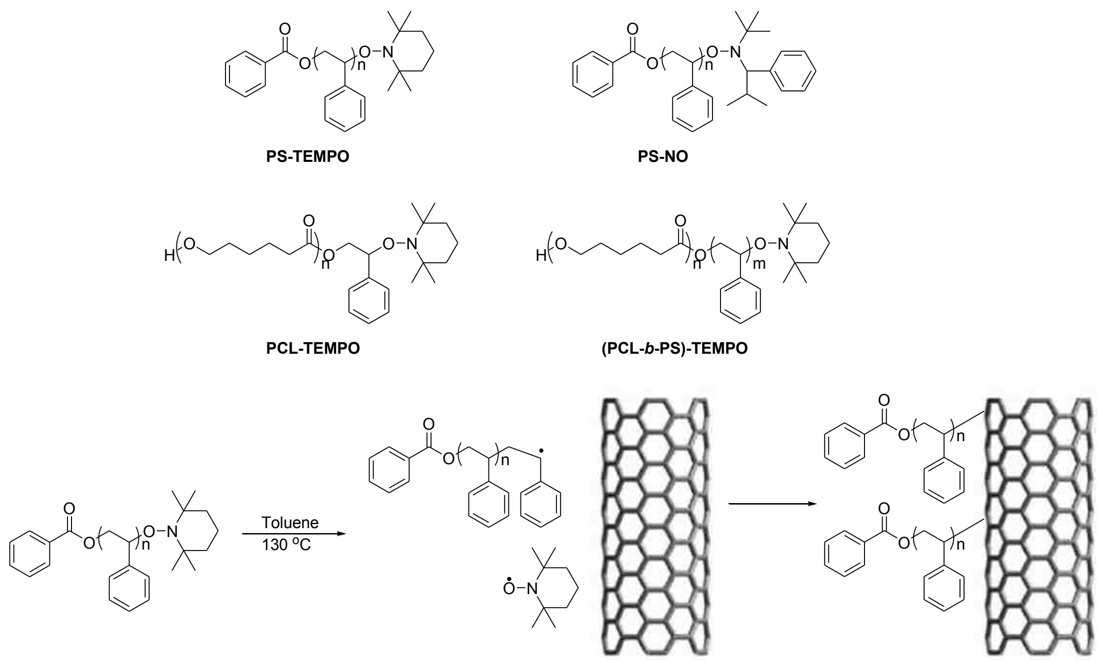

Figure 2.4. Covalent functionalization of SWNTs by TEMPO.

Even though the covalent functionalizations can expand the application of CNTs by tuning the chemical structures of initiators, they have drawbacks due to precise control of initiator and substrate concentrations. Furthermore, this approach inevitably disrupts long range π−conjugation lengths of CNTs resulting in the significant decrease of electrical conductivity, diminished mechanical strength and other undesired properties.[25] Therefore, non-covalent modification is an attractive approach because it can modify the material characteristics without altering the intrinsic properties of CNTs. For example, one of the most common methods for preparing the dispersion of CNTs is melt processing that is particularly useful for dealing with thermoplastic polymers. In this method, amorphous polymers can be processed above their T_g while semi-crystalline polymers need to be heated above their T_m to induce sufficient softening for process. In general, melt processing involves the blending of polymer with CNTs by application of intense shear forces and the merit of this technique is its simplicity and speed. However an optimized processing condition is required not only for different nanotube types, but also for the whole range of polymer-nanotube combinations.[26] Some representative examples of thermoplastic polymers are shown in Scheme 2.1.

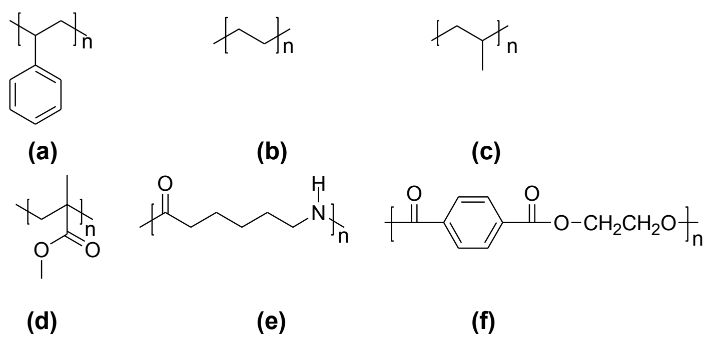

Scheme 2.1. Chemical structures of thermoplastic polymers for melting processing: (a) polystyrene, (b) polyethylene, (c) polypropylene, (d) poly(methyl methacrylate), (e) nylon 6, and (f) polyethyleneterephthalate.

The CNTs are expected to serve as mechanical reinforcements for lightweight composite systems with the further promise of multifunctionality and the use of CNTs as polymer composite reinforcements has been accomplished through epoxy resin. Because of the intrinsic van der Waals attraction of the CNTs to each other, which is associated with their high aspect ratio, CNTs are held together as bundles and ropes, having very low solubility in most solvents. The dispersion property becomes more important when CNTs are blended into the polymer. In principal, the polymer-CNTs composites can be cured when mixed with a catalyzing agent or hardener. In most cases, the nanotube dispersion is performed by using sonication before curing. Even though Ajayan and co-workers first reported the dispersion of MWNTs in epoxy resins, Raman response to tension and compression in cured epoxy composites showed poor load transfer behavior especially under tension.[27] A latter study reported the difficulty in breaking up the entanglements of the nanotubes although ultrasonication and the intense stirring process improved the dispersion of the nanotubes. Even on the millimeter scale the distribution of nanotubes was not uniform in the epoxy resins.[28]

Surfactants, biomolecules and polymers are widely used as dispersants and non-covalent modifier of CNTs.[29−32] Among them, the polymers can be a good candidate as efficient dispersants because of their long chain structure that can wrap themselves around CNTs by disrupting the van der Waals interactions between the walls of CNTs. Conjugated polymer-based functionalizations of CNTs are particularly interesting because of their extensive π conjugated backbones that can interact with the side walls of CNTs through π−π interactions. These approaches provide enhanced thermal-/photo-stability, high mechanical strength, and high electrical conductivity of CNTs as well as excellent optoelectronic properties of conjugated polymers. Even, they can be used in the purification and extraction of a specific type SWNTs from various types of nanotubes.[33] It has been reported that the conjugated polymers assist the dispersion of CNTs in organic solvents by helical wrapping or non-helical adsorption through π stacking depending on the flexibility of the polymer backbone.

Poly(phenylenevinylene) derivatives (Scheme 2.2) showed potential characteristics for use as a polymeric dispersion agent for CNTs. The polymer chin tends to form a helical structure due to the dihedral angle caused by the *m*-phenylene linkages in the polymer backbone and the eightfold increases in electrical conductivity was observed from the composite materials of CNTs.[34] Furthermore, it was shown using spectroscopic techniques such as UV−Vis absorption and Raman as well as electron microscopy that the purification of CNTs from carbonaceous impurities was possible using poly(*m*-phenylene-*co*-2,5-dioctoxy-*p*-phenylenevinylene) as an extracting agent.[33]

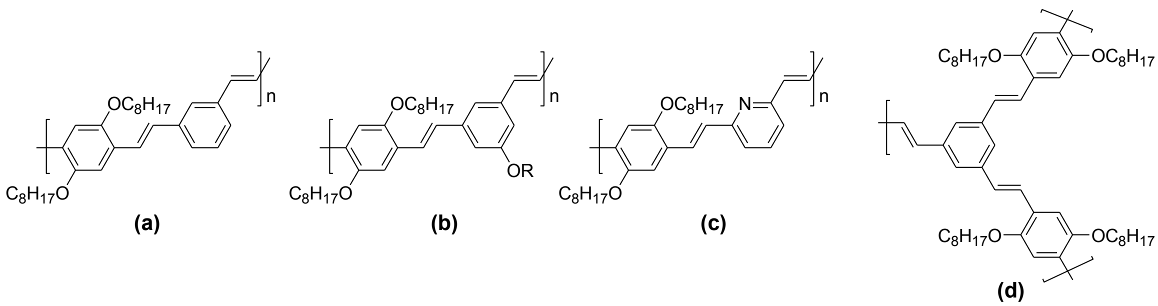

Scheme 2.2. Chemical structures of poly(phenylenevinylene) derivatives (a) poly(*m*-phenylene-*co*-2,5-dioctoxy-*p*-phenylenevinylene), (b) poly(5-alkoxy-*m*-phenylene)-*co*-(2,5-dioctoxy-*p*-phenylene)-vinylene), (c) poly(2,6-pyridinylenevinylene)-*co*-(2,5-dioctoxy-*p*-phenylene)vinylene, and (d) stilbene-like dendrimer.

A group of pyrene containing poly(phenyacetylene)s also showed the efficient dispersion of MWNTs in chloroform or THF solutions with a maximum concentration of about 0.64 mg/mL. The thermal properties of the composites were stable up to 338 ^{o}C and they emitted blue-green light more efficiently when the conjugation length of the backbone is longer.[35] The representative of pyrene containing polymers are shown in Scheme 2.3.

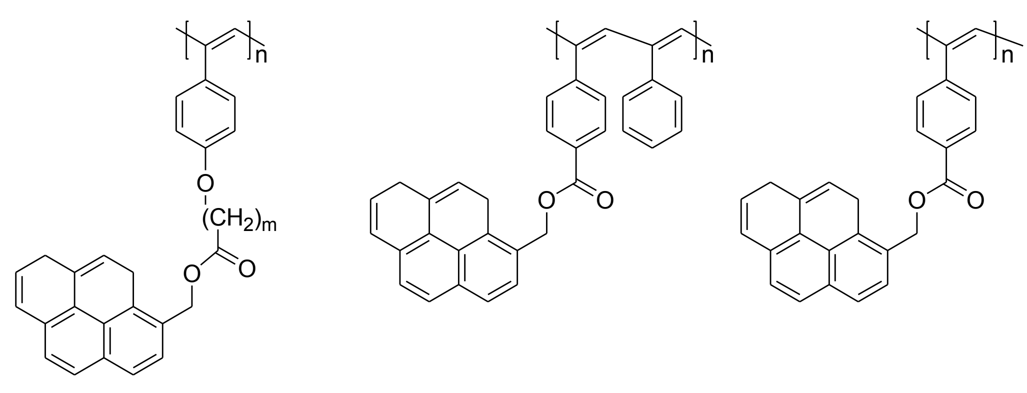

Scheme 2.3. Chemical structures of a group of pyrene containing poly(phenylacetylene)s.

Poly(phenylenevinylene)s having a rigid backbone could also be used to disperse SWNTs in various organic solvents and the maximum dispersion was observed to be 2.2 mg/mL in chloform.[36] Because they cannot wrap around the SWNTs owing to its rigid backbone, the major interaction between polymer backbone and nanotube surface is most likely through π−π interactions. Like other conjugated polymers, stable supramolecular assemblies in chloroform with SWNTs were observed with longer π−extended repeating units. Furthermore, fluorene based conjugated polymers posses the potential use as a dispersant due to their π stacking property. In both cases, the strong emission-quenching of fluorescence was monitored because of photoinduced charge transfer from polymers (donor) to SWNTs (acceptors).[37] The examples of poly(phenyleneethynylene)s and polyfluorenes are shown in Scheme 2.4.

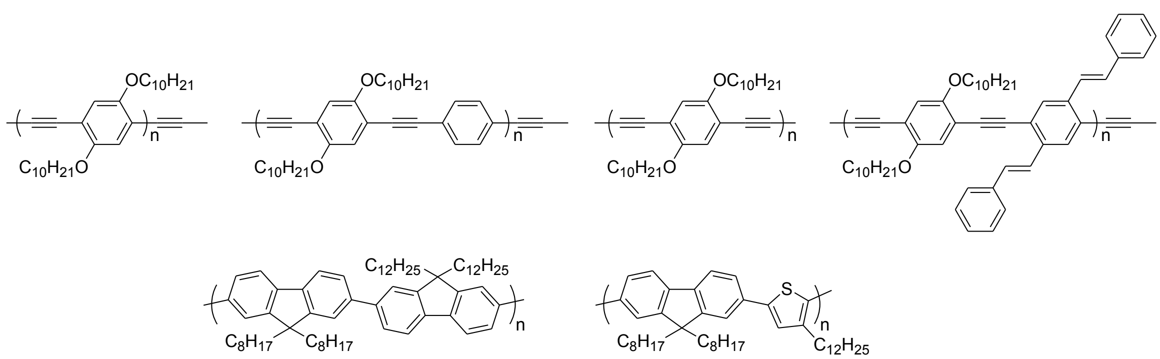

Scheme 2.4. Chemical structures of linear conjugated poly(phenyleneethynylene)s and conjugated polyfluorenes.

Dispersing CNTs in aqueous media is an important issue because of the following reasons: water solubility of polymer/CNTs composites enables their processing under environmentally friendly conditions, layer-by-layer assembly through electrostatic interactions can be possible and the water dispersible composites can be important materials for biomedical, chemo- and bio-sensor applications.[38−40] Conjugated polyelectrolytes have been found to strongly interact with CNTs through π−π and cationic−π interactions resulting in their dissolution in common organic solvents and water.[41] For example, sulfonated polystyrene,[42a] poly(*N*-cetyl-4-vinylpyridinium bromide-*co*-*N*-ethyl-4-vinylpyridinium bromide-*co*-4-vinylpyridine),[42b] and polycationic poly(diallyldimethylammonium) chloride[42c] provided enhanced dispersion of CNTs with varying degree of success. Furthermore, sulfonated poly(phenylene) and poly(phenyleneethynylene) were incorporated with single-walled carbon nanotubes (SWNTs) through non-covalent functionalization and they displayed the formation of stable complex in aqueous solution.[43] The introduction of SWNTs with sulfonated polyaramide, poly(1,4-phenylene-benzobisoxazole) or sulfonated poly[bis(benzimidazobenzisoquinolinones)] in Scheme 2.5 displayed lyotropic LC properties or potential use in a fuel cell membrane for the development of high-performance SWNTs-composite materials.[44] Recently, amphiphilic linear conjugated polymers has been utilized to dissolve SWNTs in aqueous media and almost 20% of the solubilized tubes were found to be individualized through helical wrapping mechanism. The hydrophobic conjugated polymers and water-soluble conjugated polyelectrolytes in the presence of a phase transfer catalyst could be used to disperse SWNTs in numerous organic solvents and aqueous media.[38−40]

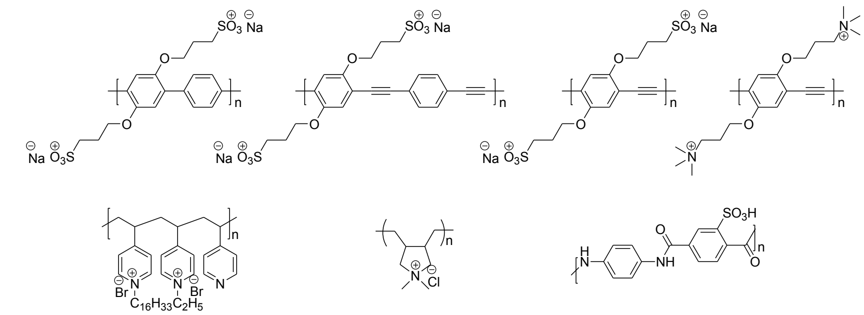

Scheme 2.5. Chemical structures of non-conjugated and conjugated polyelectrolytes.

The alignment of CNTs can be achieved by using liquid crystalline properties.[45] It has been reported that the self-organization of the hosts induces alignment of dispersed SWNTs and the alignment can be controlled by applying an external electric or magnetic field when SWNTs are dispersed into the thermotropic liquid-crystalline hosts. By dynamically changing the orientation of SWNTs, the alignment control of SWNTs can tune the electronic conductivity. Liquid-crystalline (LC) phases of acid-functionalized CNTs in water and protonated CNTs in superacids also have been reported in the literature.[46] The construction of LC composites containing CNTs can be of importance in the development of nanoscopic smart devices such as light-emitting diodes, photovoltaic cells, electrical switches and sensors.[47] The examples are shown in Figure 2.5.

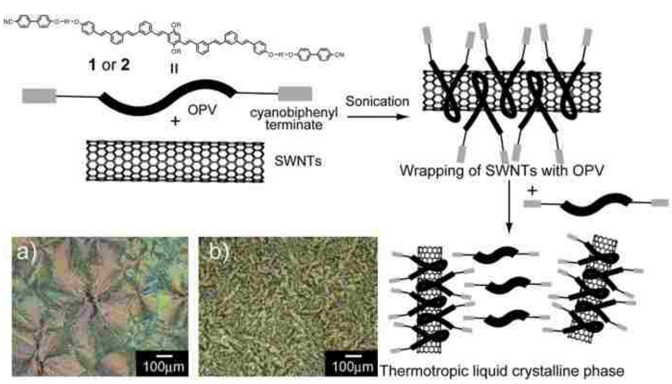

Figure 2.5. Schematic illustration of self-organizing processes for the composite of liquid crystalline oligomers and SWNTs.

2.3. Objective

In this chapter, we report the use of ionic polymers, poly(pyridinium salt)s with various rigid aromatic moieties, to disperse SWNTs in dimethyl sulfoxide (DMSO) and their chemical structures, morphology, solution, and optical properties are characterized by several experimental techniques. We found that SWNTs have better interaction with poly(pyridinium salt)s containing more π cores due to their strong π−π and cationic−π interactions. To our knowledge, this result reported the first example of SWNTs dispersion in DMSO system that affords a high concentration up to 33 wt %. We believe that this series of materials is the cornerstone that would open a new field in materials science.

2.4. Results and Discussion

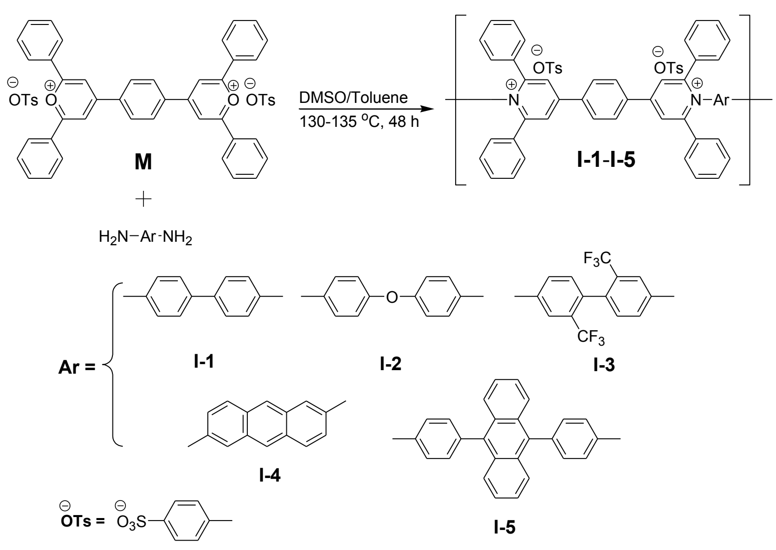

Scheme 2.6. Synthesis of poly(pyridinium salt)s.

Poly(pyridinium salt)s were synthesized by using the ring-transmutation polymerization reaction of bis(pyrylium salt)s with the respective aromatic diamines. The detailed procedures were described in the experimental section. Five different aromatic moieties were introduced along the polymer main chains to study the effect of microstructures of this class of ionic polymers on the dispersion of SWNTs by providing for favorable $\pi-\pi$ or $\pi-$cationic interactions of various aromatic moieties (Scheme 2.6). It is reported in the literature,[48] that amide containing solvents such as *N*,*N*-dimethylformamide (DMF) and *N*,*N*-dimethylacetamide (DMAc) can dissolve the poly(pyridinium salt)s and disperse SWNTs efficiently, undesirable photodecomposition can cause the degradation of polymers in these solvents. To prevent this problem, DMSO was chosen to disperse SWNTs with ionic polymers. Different weight ratio of SWNTs (5, 20, 33 and 50 wt %) to poly(pyridinium salt)s (**I-1**−**I-5**) was solubilized in DMSO using a sonicator at room temperature via a coagulation method. However, note here that the concentration of SWNTs in the composites is subjected to experimental errors because it is hard to determine the exact amount of the SWNTs is present to the polymer matrix in each composition.

In an experiment, the desired amount of SWNTs was added to a solution of polymer in DMSO, and the mixture was sonicated for 2 h. The resulting dark suspension was centrifuged for 1 h to settle down the unbounded SWNTs and the clean dark solution was precipitated in ethyl acetate for the prevention of aggregation that enabled one to obtain a better dispersion of SWNTs in polymer matrix.[49] However, solutions with higher concentrations (>30 wt % SWNTs) became viscous and this property may be related to physical interactions between SWNTs and poly(pyridinium salt)s and similar observation was also reported previously.[50]

The ^1H NMR spectra of polymer/SWNTs composites revealed the non-covalent interactions between these two components. For example, the spectra of polymers (**I-1** and **I-5**) displayed unique aromatic pyridinium proton signals at *ca*. 9.05 ppm and sharp doublet peaks of tosylate aromatic proton signals at 7.46 and 7.09 ppm, respectively (Figures 2.6 and 2.7). After incorporation of SWNTs into the polymer, the intensity of proton signals was significantly broadened and reduced. Similarly, the ^1H NMR spectra of composites of **I-2**, **I-3**, and **I-4** are also provided in Figures S1, S2, and S3 in the Appendix 2. These results supported the strong $\pi{-}\pi$ interactions through main-chain poly(pyridinium salt)s and SWNTs. In general, the proton signals of aromatic moieties that provide $\pi{-}\pi$ interactions with the surface of SWNTs were broader and weaker. On the other hand, the proton signals of alkyl side chain showed less reduced intensity.[51]

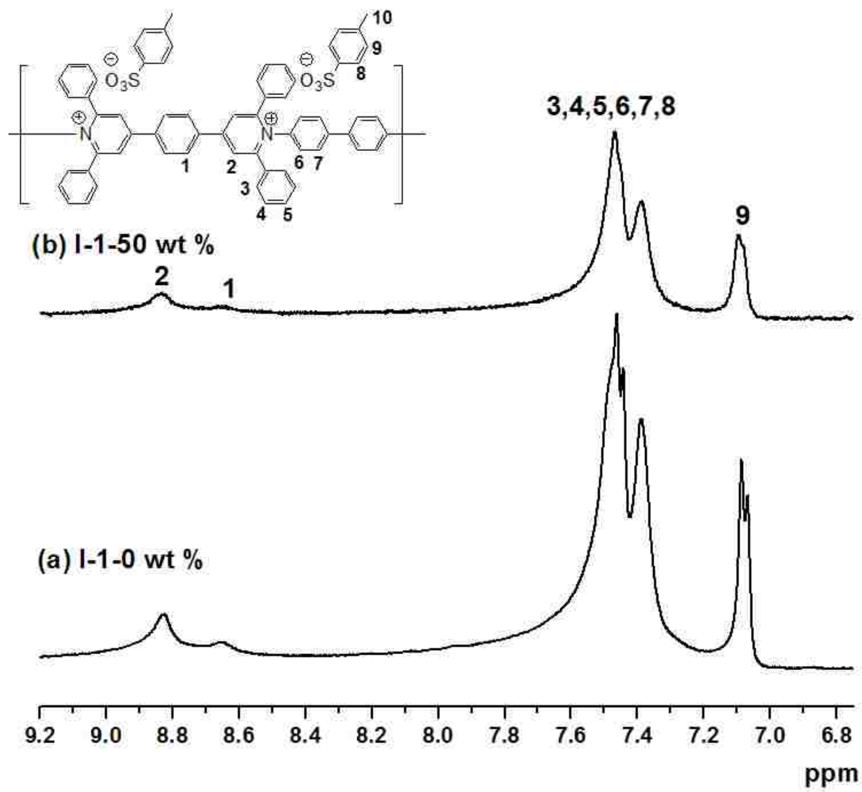

Figure 2.6. Expanded ^{1}H NMR spectra of **I-1**/SWNT composites (delay time = 1 s, number of scans = 16): (a) **I-1** (10 mg/mL in d_6-DMSO); and (b) **I-1**-50 wt % (10 mg/mL in d_6-DMSO).

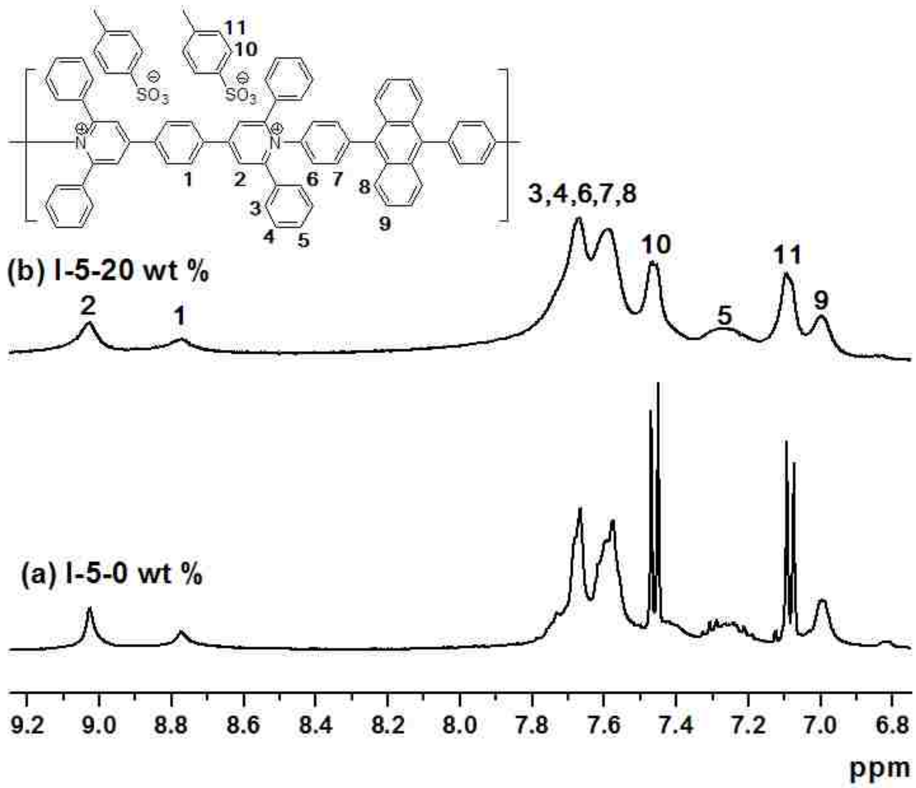

Figure 2.7. Expanded [1]H NMR spectra of **I-5**/SWNTs composites (delay time = 1 s, number of scans = 16): (a) **I-5** (10 mg/mL in d_6-DMSO); and (b) **I-5**-20 wt % (10 mg/mL in d_6-DMSO).

The optical properties of the composites were studied by UV−Vis and photoluminescent spectroscopy. Polymers **I-1**−**I-5** exhibited absorption maxima at 347, 335, 350, 351 and 344 nm in their absorption spectra in DMSO (Figures 2.8, 2.9, S4, S5, and S6). When SWNTs were incorporated to the polymers to produce the composites, their absorption spectra remained essentially identical to those of polymers indicating that there were no significant changes in the electronic structures of their ground states.

In stark contrast, the strong emission of both **I-1** and **I-2** was quenched with the increased ratio of SWNTs. However, more pronounced quenching was observed in **I-2**/SWNTs composite compared to **I-1**/SWNTs. In case of **I-1**/SWNTs composite, the intensity was quenched by 88% while **I-2**/SWNTs composite was 71%. This result implies that different types of interactions between polymers and SWTNs exist that are related to the conformational flexibility or rigidity of the polymers[36a] or better $\pi-\pi$ interaction between polymer **I-1** and SWNTs. To extend the relationship between chemical structures of polymers and SWNTs, the other composites were further studied. Their photoluminescence spectra, recorded in DMSO with excitation wavelengths at 395, 275 and 403 nm, showed λ_{em} peaks at 448, 383 and 530 nm (Figures 2.9, S4, S5, and S6). Like composites **I-1**/SWNTs and **I-2**/SWNTs, the dramatic quenching of light emission from these ionic polymers was observed with the increased weight percentage of SWNTs in polymers. The quenching efficiencies of **I-4**/SWNTs and **I-5**/SWNTs composites were 96 and 90%, respectively, whereas that of **I-3**/SWNTs composite was to an extent of 25% only. The difference in quenching property presumably is related to the fact that polymers **I-4** (anthracene moieties) and **I-5** (phenylated anthracene moieties) provide more $\pi-\pi$ or $\pi-$cationic interactions with SWNTs than **I-3** (fluorinated benzidine moieties) resulting in better dispersion of SWNTs in polymer matrices. Furthermore, the strong quenching of emission most likely stems from the fact that efficient energy or electron transfer between the polymers and SWNTs occurs, instead of disruption of π–conjugation.[51c,d,52]

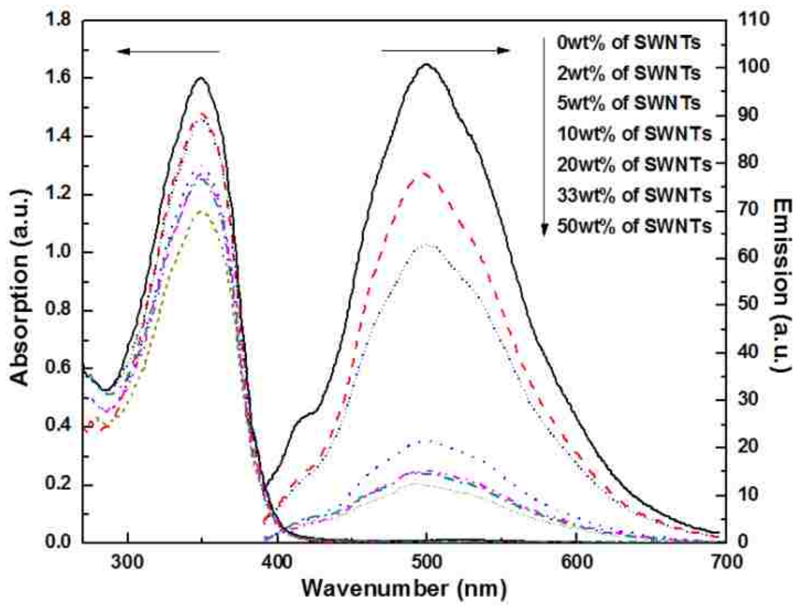

Figure 2.8. UV–Vis absorption spectra of **I-1**/SWNT composites in DMSO (left arrow) and emission spectra of **I-1**/SWNT composites at excitation wavelength of 357 nm in DMSO (right arrow).

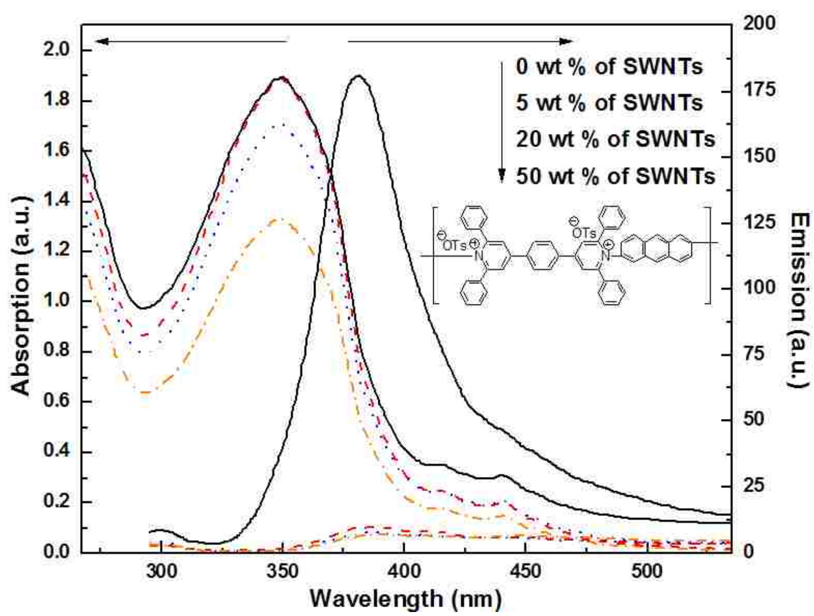

Figure 2.9. UV–Vis absorption spectra of **I-4**/SWNTs composites in DMSO (left arrow) and emission spectra of **I-4**/SWNTs composites at excitation wavelength of 275 nm in DMSO (right arrow).

The dispersion of SWNTs in polymers was studied by using transmission electron microscopy (TEM) technique. Some representative images are shown in Figures 2.10 and 2.11. In general, SWNTs are heavily entangled due to van der waals intercations between adjacent tubes. Upon dispersion of SWNTs with poly(pyridinium salt)s in DMSO, they exfoliated to form much finer bundles. When compared the dispersion of SWNTs, **I-1**/SWNTs, **I-4**/SWNTs, and **I-5**/SWNTs composites revealed more dispersed SWNTs than **I-2**/SWNTs and **I-3**/SWNTs composites due to more π−π interactions supported by ^{1}H and photoluminescent spectroscopy. A high resolution TEM image of polymer/SWNT composite (Figures 2.10d and 2.11c) revealed the presence of a thin layer of an amorphous coating with a thickness around 3 nm on the surface of the SWNT walls in each case. The TEM images of other compoistes are shown in Figure S7 in the Appendix 2.

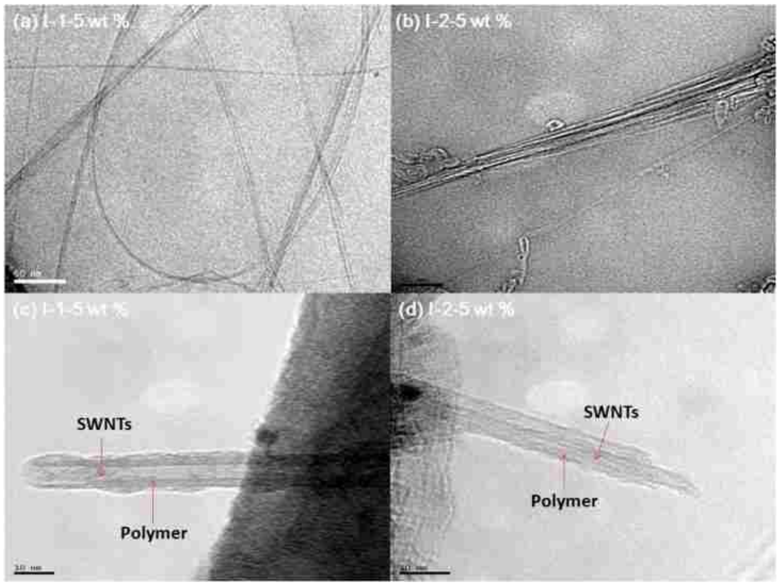

Figure 2.10. TEM images of (a) **I-1**-5 wt % (b) **I-2**-5 wt % and HRTEM images of (c) **I-1**-5 wt %; (d) **I-2**-50 wt % (The scale bars in a, b and c, d represent 50 and 10 nm, respectively).

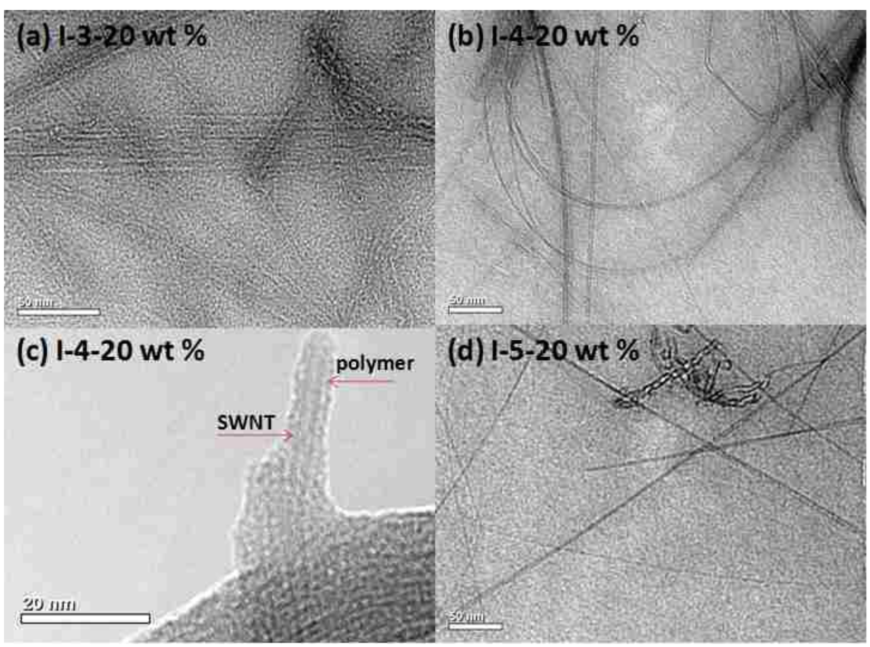

Figure 2.11. TEM images of (a) **I-3-**20 wt %, (b) **I-4-**20 wt %, (c) **I-4-**20 wt % and (d) **I-5-**20 wt % (The scale bars in a, b, c, and d represent 50, 50, 20 and 50 nm).

The poly(pyridinium salt)s used for the dispersion of carbon nanotubes exhibit lyotropic LC properties in DMSO above their critical concentrations at room temperature. These results motivated us to study the lyotropic LC properties of the composites using polarizing optical microscope (POM) technique. For the entire range of concentrations, any entanglement of SWNTs was not observed under POM study. LC structures of polymers **I-1** and **I-2** composed of small and large bâtonnets, polygonal arrays, and rounded droplets were identified as an anisotropic and isotropic phase. These unique textures are indicative of their lamellar phase.[53] However, by increasing the ratio of SWNTs, **I-1**-20 wt % exhibited a biphasic image in which an LC phase coexisted with an isotropic and anisotropic solutions (Figure 2.12). This result is possibly due to an interruption of dispersed SWNTs in the formation of lyotropic phase. However, at the identical concentration of SWNTs (5 wt %), **I-2**/SWNT composites required a little higher concentration for fully-grown lyotropic phase that means the rod-like structure is more favorable to form the LC properties. Furthermore, polymer **I-3** showed a fully-grown LC texture at 20 wt % in DMSO and **I-3**/SWNTs composites with varying SWNT concentrations did not provide any visible entanglement of SWNTs. **I-3-**20 wt % composite displayed a biphasic solution. The birefringence of LC phase of **I-3-**50 wt % was significantly reduced suggesting an interruption of dispersed SWNTs in the formation of lyotropic phase of ionic polymer. Like **I-3**/SWNTs composites, both **I-4-**20 wt % and **I-5-**20 wt % showed significantly reduced birefringence in their LC textures (Figure 2.13). However, at the same concentration of SWNTs (20 wt %), **I-4** and **I-5** composites showed more reduced birefringence LC images than **I-3**/SWNT composites (Figure S9). These results imply that the more conjugated $\pi - \pi$ interactions of rigid aromatic moieties as well as cation–π interactions of pyridinium moieties are favorable for the dispersion of SWNTs, which were also supported by other techniques employed in this study (*vide supra*). On the other hand, these interactions also reduced the birefringence of lyotropic LC phases of poly(pyridinium salt)s in DMSO, especially with the incorporation of higher wt % nanotubes in various composites studied.

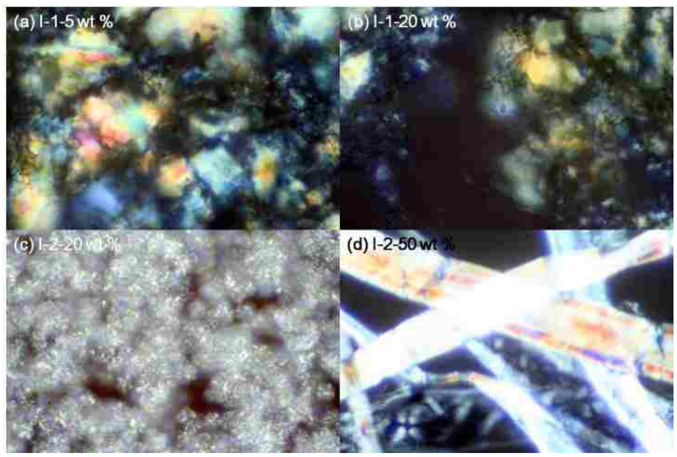

Figure 2.12. Photomicrographs of (a) composite **I-1-**5 wt % SWNTs 30 wt % in DMSO, (b) composite **I-1-**20 wt % SWNTs 30 wt % in DMSO, (c) composite **I-2-**20 wt % SWNTs in 40 wt % DMSO, and (d) composite **I-2-**50 wt % SWNTs 40 wt % in DMSO under crossed polarizers (magnification 400x).

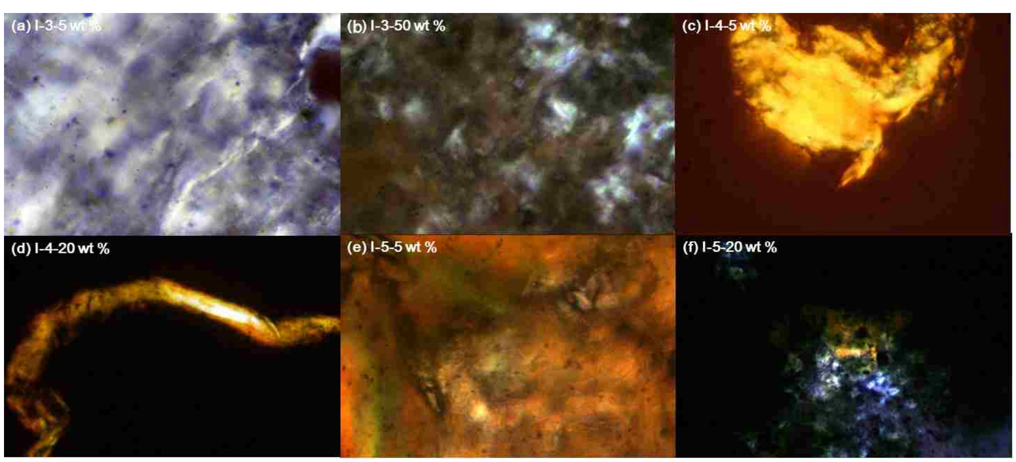

Figure 2.13. Photomicrographs of (a) composite **I-3-**5 wt % SWNTs 20 wt % in DMSO, (b) composite **I-3-**50 wt % SWNTs 20 wt % in DMSO, (c) composite **I-4-**5 wt % SWNTs in 40 wt % DMSO, (d) composite **I-4-**20 wt % SWNTs 40 wt % in DMSO, (e) composite **I-5-**5 wt % SWNTs 20 wt % in DMSO, and (f) composite **I-5-**20 wt % SWNTs 20 wt % in DMSO under crossed polarizers exhibiting lyotropic LC phase, respectively (magnification 400x).

The characterization of polymer/SWNTs composites by Raman spectroscopy revealed no significant change in the signals of SWNTs upon non-covalent functionalization. The spectral shift of tangential mode also known as G band at *ca*. 1590 cm^{-1} remained relatively unchanged when compared with pristine SWNTs (Figure 2.14). The intensity of disorder-induced D band at *ca*. 1320 cm^{-1} was low compared to that of G-band and did not significantly increase suggesting that non-covalent interactions of ionic polymers and nanotubes did not cause any defects on the surfaces of nanotubes. In stark contrast, the intensity of D-band in covalently functionalized nanotubes is comparable to or even larger than that of G-band.[54] More information of other composites is shown in Figures S11 and S12 in the Appendix 2.

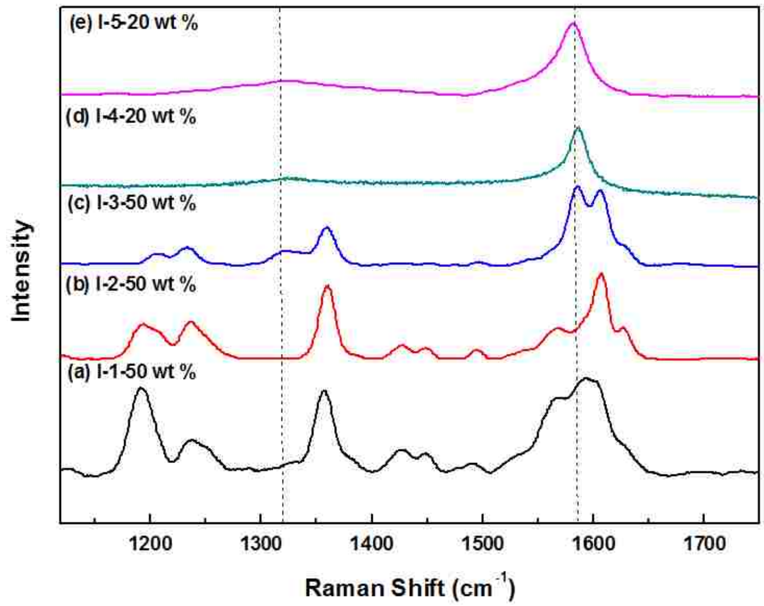

Figure 2.14. Raman spectra of (a) **I-1**-50 wt %, (b) **I-2**-50 wt %, (c) **I-3**-50 wt %, (d) **I-4**-20 wt %, and (d) **I-5**-20 wt %.

To investigate the morphology of the composites, we examined the microstructures with X-ray scattering technique. In Figure 15, the representative X-ray power diffraction (XRD) plots of composites, **I-1**-0 wt % and **I-1**-50 wt % in 30 wt % DMSO, were recorded at room temperature with angle range between 5 and 60°. A broad diffraction peak which means the semi crystalline structure of poly(pyridinium salt)s with relatively low intensities at $2\theta = 20^{o}$ was observed in both composites that corresponded to the *d*-spacing in the range of 4.43−4.96 Å are the results of π−π stacking of the polymer chains.[55]

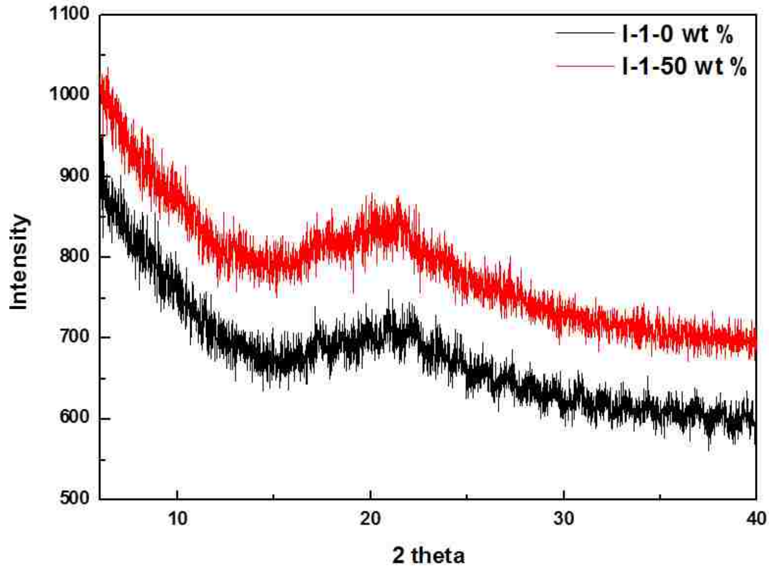

Figure 2.15. XRD plots of **I-1**-0 wt % and (b) **I-1**-50 wt % in 30 wt % DMSO taken at room temperature.

To evaluate thermal stability of the composites, TGA analysis was performed between 30 and 600 ^{o}C under nitrogen atmosphere and thermal decmoposition of SWNTs is provided in Figure S10 in the Appendix 2. The composites without SWNTs displayed two step degradation. The first weight loss was assigned to the decomposition of the tosylate counterion and the second curve was related to the degradation of the polymer main chain (Figure 2.16). Even though the poly(pyridinium salt)s showed the good thermal stability in nitrogen, the addition of SWNTs into the polymer increased the degradation temperature of the composites approximately 30−70 ^{o}C. The observed results concluded that a well-dispersed SWNTs induces better interfacial adhesion beween SWNTs and polymer resulting in higher thermal stability. Furthermore, the SWNTs may restrict the thermal motion of the poly(pyridinium salt)s hindering the diffusion of the degradation products from solid to gas phase.[44a,c]

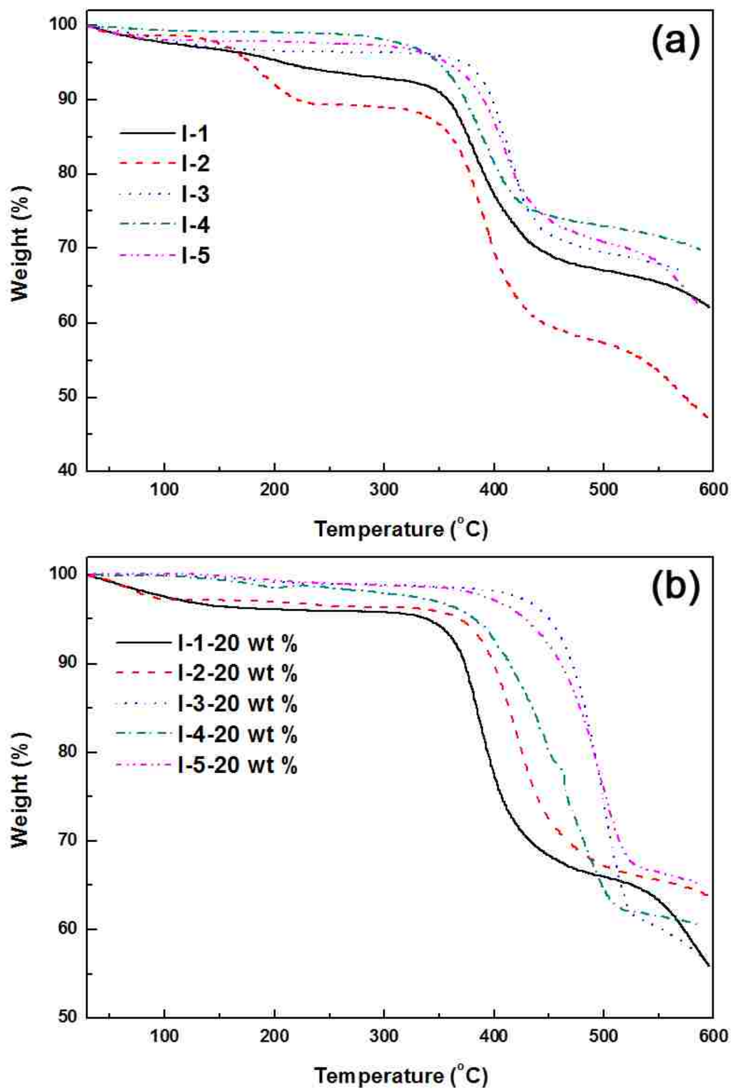

Figure 2.16. TGA thermograms of (a) polymers **I-1**−**I-5** and (b) composites **I-1-**20 wt %−**I-5-**20 wt % obtained at a heating rate of 10 °C/min in nitrogen.

2.5. Experimental

2.5.1. General Comments

Benzidine, 4,4´-oxydianiline, DMSO, lithium triflimide and common organic solvents were purchased from commercial vendors (Sigma-Aldrich, Alfa-Aesar, Acros Organics, and TCI America) and used without any further purification. 2,2′-

Bis(trifluoromethyl)benzidine was received as a gift from Polaroid Corporation and it was then purified by recrystallization from ethanol/water mixture before use. The 4,4′-(1,4-phenylene)bis(2,6-diphenylpyrylium *p*-toluene sulfonates), **M**, 2,6-diaminoanthracene and 9,10-bis(4-aminophenyl)anthracene was synthesized according to the reported procedure.[56] Single-walled carbon nanotubes (*ave*. diameter = 1.1 nm, length = 5–30 μm and data for SWNTs: C, 98.52; Co, 0.79; Fe, 0.06; Mo, 0.22; Cl, 0.23; S, 0.18) were purchased from Cheap Tubes Inc. and used without further purification.

The ^{1}H NMR spectra were recorded with a Varian NMR spectrometer operating at 400 MHz at room temperature. The proton chemical shifts were referenced to tetramethylsilane (TMS). The NMR samples were prepared in d_6-DMSO with a concentration of 10 mg/mL. Dilute solution for UV–Vis and photoluminescence spectroscopy study was prepared by dissolving 0.5 mg of the dry polymer/SWNTs composite in 15 mL of the DMSO at room temperature. A few drops of the resulting solutions were transferred to a quartz cell and diluted further with DMSO to adjust the optical density to obtain a light colored solution. UV–Vis absorption spectra were recorded with a Varian Cary 3 Bio UV–Vis spectrophotometer at room temperature. Photoluminescence spectra in solutions were recorded with a Perkin–Elmer LS 55 luminescence spectrometer with a xenon lamp light source. Lyotropic LC properties of the composites were studied using a polarized optical microscope (POM, Nikon, Model Labophot 2) equipped with crossed polarizer. Samples of these composites for lyotropic properties were made by dissolving known amounts of composites into known amounts of DMSO. Thermogravimetric analyses (TGA) of the composites were performed using a TGA Q50 instrument in nitrogen. The TGA data was collected at temperatures between

30 and 600 ºC at a heating rate of 10 ºC/min. A Tecnai-G2-F30 supertwin transmission electron microscope (TEM) system with a 300 keV Schottky field emission gun was used to characterize the morphology of the samples. Bulk morphology was analyzed using the conventional bright field (BF) mode, and all TEM images were recorded using a slow-scan CCD camera attached to a Gatan GIF 2000 energy filter. To prepare samples by the solution-drop method, 3 wt % of composite in DMSO was placed onto a 3 mm diameter carbon-coated copper grid using a small tipped transfer-pipette. The solvent was evaporated from the sample under reduced pressure inside TEM chamber, leaving the fine particulate objects deposited on the carbon film, which was then used in the TEM study. The major components of the Raman microscope are a Lexel RamanIon krypton ion laser (647.1 nm), a Nikon MM-40 measuring microscope, a Jobin-Yvon TRIAX 550 monochromator, and a Princeton Instruments Spec-10 liquid nitrogen cooled CCD. The Raman system is calibrated using emission lines from a neon lamp.

2.5.2. General Procedure for Synthesis of Polymers **I-1**−**I-5**

The bis(pyrylium salt), **M**, (1.00 g, 1.13 mmol) and diamine (1.13 mmol) was dissolved in DMSO (25 mL) under nitrogen atmosphere. The solution was stirred at 130−135 °C for 48 h. The water generated during the reaction was removed by a toluene/water azeotrope. After the reaction completed, the solution was concentrated under reduced pressure and it was precipitated in distilled water. It was further purified by re-dissolving in methanol and by subsequent re-precipitation with the addition of distilled water. The solid was collected and dried *in vacuo* at 110 °C for 72 h. Data for polymer **I-1**: Anal. Cacld for $C_{66}H_{50}N_2O_6S_2$ (1031.24): C, 76.87; H, 4.89; N, 2.72; S, 6.22. Found: C, 73.56; H, 5.10; N, 2.52; S, 7.50; for polymer **I-2**: Anal. Cacld for $C_{66}H_{50}N_2O_7S_2$ (1047.24): C, 75.70; H, 4.81; N, 2.67; S, 6.12. Found: C, 72.96; H, 4.78; N, 2.58; S, 6.00; for polymer **I-3**: Anal. Cacld for $C_{68}H_{48}N_2O_6F_6S_2$ (1167.26): C, 69.97; H, 4.14; N, 2.40; S, 5.49. Found: C, 66.92; H, 4.44; N, 2.39; S, 5.53; for polymer **I-4**: Anal. Cacld for $C_{68}H_{50}N_2O_6S_2$ (1055.26): C, 77.40; H, 4.78; N, 2.65; S, 6.08. Found: C, 76.81; H, 5.34; N, 2.73; S, 5.18; for polymer **I-5**: Anal. Cacld for $C_{80}H_{58}N_2O_6S_2$ (1207.49): C, 79.58; H, 4.84; N, 2.32; S, 5.31. Found: C, 77.05; H, 5.58; N, 2.27; S, 5.07.

2.5.3. General Procedure for Preparation of Polymer/SWNTs composites

An amount of 50 mg of polymer was dissolved in 4 mL of DMSO and 25 mg of SWNTs (33 wt % of SWNTs content based on the total weight) was transferred into the polymer solution. The dark solution was mixed by sonication for 2 h with a water-bath temperature maintained at room temperature. The resulting solution was centrifuged (30 min under ≈ 20,000 g) to settle down insoluble solids. The homogeneous dark solution was precipitated in ethyl acetate and the precipitated black solid was filtered and dried *in vacuo* at 80 ^{o}C for 48 h.

2.6. Conclusion

In summary, we have demonstrated the dispersion of SWNTs using poly(pyridinium salt)s of rigid aromatic moieties via non-covalent interactions in DMSO. The chemical structures of the composites were investigated by ^{1}H NMR spectroscopy. The UV−Vis absorption spectra were indicative of closely spaced π−π* transitions suggesting that their absorption maxima were less sensitive to the incorporation of SWNTs. In stark contrast, in their PL spectra recorded for various composites prepared varying the weight percentage of SWNTs in poly(pyridinium salt) matrices in DMSO, a strong quenching effect of light emission of each of the ionic polymers was observed due to the efficient energy or electron transfer between the polymer and SWNTs. The morphology of the composites was further studied by TEM analysis suggestive of exfoliation of nanotubes that occurred in the ionic polymer matrices and the TGA analysis revealed the increased thermal stability of the composites. This method allows the convenient preparation of a new family of SWNTs dispersions in main-chain ionic polymers.

CHAPTER 3

SOLUTION, OPTICAL AND THERMAL PROPERTIES OF BIS(PYRIDINIUM SALT)S INCLUDING IONIC LIQUIDs

3.1. Abstract

Bis (pyridinium salt)s containing different alkyl chain lengths and various organic counterions were prepared by the ring-transmutation reaction of bis(pyrylium tosylate) with aliphatic amines in dimethyl sulfoxide at 130−135 °C for 18 h and their tosylate counterions were exchanged to other anions such as triflimide, methyl orange, and dioctyl sulfosuccinate by the metathesis reaction in a common organic solvent. Their chemical structures were investigated by ^{1}H, ^{19}F, and ^{13}C NMR spectroscopic techniques. The thermal properties of bis(pyridinium salt)s were studied by DSC and TGA measurements. Some of the dicationic salts provided low melting points below 100 ^{o}C and some of them displayed amorphous properties. Polarized optical microscopy studies revealed the crystal structures prior to melting temperatures in some cases. Their optical properties were examined by using UV−Vis and photoluminescent spectroscopy; and they emitted blue light both in the solution and solid states regardless of their microstructures, counterions, and the polarity of organic solvents. However, most of these salts exhibited hypsochromic shift in their emission peaks in the solid state when compared with those of their solution spectra. Due to unique properties of methyl orange anion as a pH indicator, two of the salts showed different color change in varying concentrations of triflic acid in

common organic solvents, demonstrating their potential use as an acid sensor in methanol, acetonitrile and acetone.

3.2. Introduction

Ionic liquids (ILs) are molten salts at room temperature and composed of cations and anions in their chemical structures. These new liquids have received great interest because of their unusual properties as liquids. The most important properties of electrolyte solutions are nonvolatility and high ion conductivity. These are essential characteristics of advanced electrolyte solutions that are critical to energy devices put in outdoor use. Moreover, environmental problems are becoming very important issues for upcoming future and the nonvolatile electrolyte solution can be a good candidate to approach the field of green chemistry. ILs will have unlimited structural vibrations due to the easy preparation of many components. So there are unlimited possibilities open to the new field of ionic liquids. The properties of organic ionic liquids are summarized in Table 3.1.

Table 3.1. Basic characteristics of organic ionic liquids

Low melting point	· Treated as liquid at ambient temperature · Wide usable temperature range
Non-volatility	· Thermal stability · Nonflammability
Composed by ions	· High ion density · High ion conductivity
Organic ions	· Various kinds of salts · Designable · Unlimited combination

Because ILs are composed of only ions, they show very high ionic conductivity, nonvolatility, and nonflammability. The nonflammable liquids with high ion conductivity are practical materials for use in electrochemistry. Furthermore, the nonflammability and nonvolatility inherent in ion conductive liquids open new possibilities in other fields as well. Most of the interest in ILs is concentrated on the design of new solvents. While the development of "new solvents" has led the direction of possible applications for ionic liquids, there is more potential for the development of electrochemical applications.

ILs have been known for a long time, but their extensive use as solvents in chemical processes for synthesis and catalysis has recently become significant. Some of ILs reported in early 1900s.[1,2] In 1940s, aluminum chloride-based molten salts were utilized for electroplating at ambient temperatures. In the early 1970s, Wilkes and co-workers tried to develop better batteries for nuclear warheads and space probes which required molten salts to operate.[3] Wilkes and his colleagues continued to improve their ILs for use as battery electrolytes and then a small community of researchers began to make ILs and test their properties.[4] In the late 1990s, ILs became one of the most promising chemicals as solvents.

Initial ILs such as organo-aluminate ILs have some limitations due to their instability to air and water.[5] After the air stable ILS such as 1-n-butyl-3-methlyimidazolium tetrafluoroborate ([bmim][BF_4]) and 1-n-butyl-3-methlyimidazolium hexafluorophosphate ([bmim][PF_6]) reported, the number of air and water stable ILs has been studied extensively. Recently, many research groups have found that ILs are more than just green solvents and they have found several applications such as replacing them with volatile organic solvents, making new materials, conducting heat effectively, supporting enzyme-catalyzed reactions, hosting a variety of catalysts, purification of gases, homogenous and heterogeneous catalysis, biological reactions media and removal of metal ions. The chemical structures of ILs are shown in Figure 3.1 and Table 3.2.

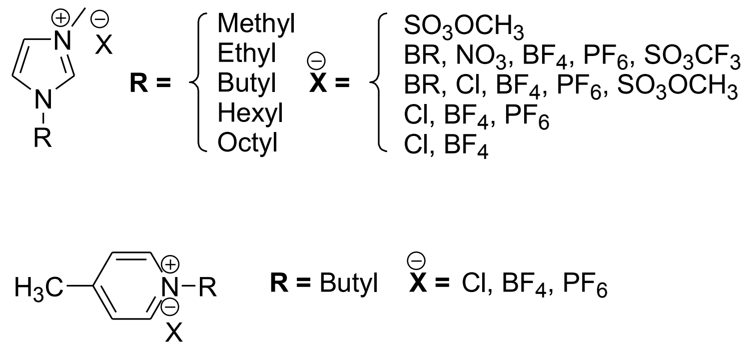

Figure 3.1. Common ionic liquids based on imidazolium and pyridinium.

Table 3.2. Most widely used ILs and their structures

Ionic liquid	**Structure**	**Common name**
1-Butyl-3-methylimidazolium tetrafluoroborate	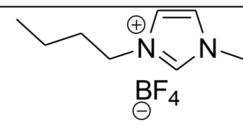	[bmim][BF_4]
1-Butyl-3-methylimidazolium triflate	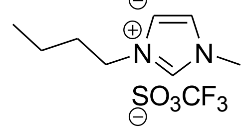	[bmim][TfO]
1-Butyl-3-methylimidazolium methide	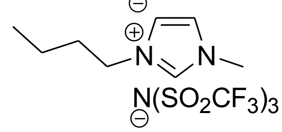	[bmim][methide]
1-Butyl-3-methylimidazolium dicyanamide	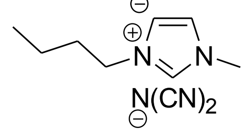	[bmim][DCA]
1-Butyl-3-methylimidazolium hexafluorophosphate	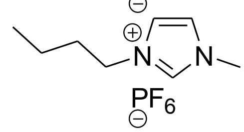	[bmim][PF_6]
1-Butyl-3-methylimidazolium nitrate	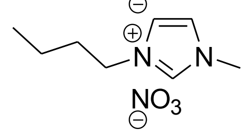	[bmim][NO_3]
1-Butyl-3-methylimidazolium bis(trifluoromethylsulfonyl) imide	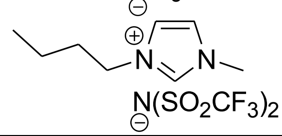	[bmim][Tf_2N]

There are a great number of different cation and anion combinations to synthesize ILs. The wide variety of cation and anion combinations can tune the physical and chemical properties of ILs. The well-known cations for ILs are based on imidazolium, pyridinium, phosphonium and ammonium structures. The properties of ILs can be determined by mutual fit of cation and anion, size, geometry, and charge distribution. Among the similar class of salts, small chemical modification in types of ions can influence the physico-chemical properties and the overall properties of ILs result from the composite properties of the cations and anions and include those that are superacidic, basic, hydrophilic, water miscible, water immiscible and hydrophobic. It has been reported that the anion controls the water miscibility, but the cation also has an influence on the hydrophobicity or hydrogen bonding ability (Figure 3.2).[6]

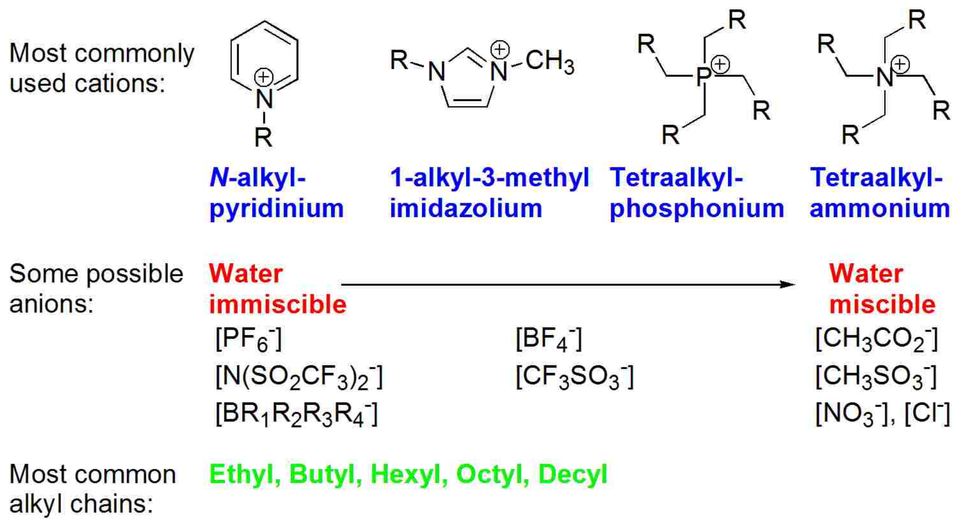

Figure 3.2. Most commonly used cation structures and possible anion types.

In general, the properties of ILs can be determined by the types of anions. The incorporation of different anions results in an increasing number of alternative ILs with various properties. The incorporation of different anions results in an increasing number of alternative ILs with various properties. The types of anions can be divided by two different anions: anions with fluorine group such as $^{-}PF_6$, $^{-}BF_4$, $CF_3SO_3^{-}$, $(CF_3SO_2)_2N^{-}$ and without fluorine groups such as $^{-}AlCl_4$. The most popular anions consist of chloride, nitrate, acetate, hexafluorophosphate and tetrafluoroborate.[7] The most widely investigated ILs are with $^{-}PF_6$ and $^{-}BF_4$. Especially $^{-}PF_6$ is the most prominent anion in ILs research. Since the anion chemistry has a large effect on the properties of ILs, although the cations are the same, significant differences can be observed with different anions in ILs. For example ILs with 1-*n*-butyl-3-methylimidazolium cation and PF_6^{-} anion is immiscible with water, whereas ILs with same cation and BF_4^{-} anion is water soluble. The results indicate that different ion pairs can determine physical and chemical properties of the liquid. Even though PF_6^{-} and BF_4^{-} anions are commonly used in ILs research, they have some limitation to be used in real applications such as decomposition of anions in the presence of water and liberate HF.[8]

The cation of ILs is generally a bulk organic structure with low symmetry. Most ILs are based on ammonium, sulfonium, phosphonium, imidazolium, pyridinium, picolinium, pyrrolidinium, thiazolium, oxazolium and pyrazolium cations. Many research groups mainly focus on room temperature ILs composed of asymmetric *N*,*N*-dialkylimidazolium cations associated with a variety of anions. The melting point of ILs is generally below 100 ^{o}C and Chiappe and Pieraccini have reported as the size and asymmetry of the cation increases, the melting point decreases. Further, an increase in the branching on the alkyl chain increases the melting point. The melting point of ILs is essential because it represents the lower limit of the liquidity and with thermal stability it defines the interval of temperatures within which it is possible to use ILs as solvents.[9]

To synthesize ILs, there are three basic methods: metathesis reactions, acid–base neutralization, and direct combination. Alkylammonium halide can be obtained by the reaction between the appropriate halogenoalkane and amine. Pyridinium and imidazolium halides are also synthesized by metathesis reaction. On the other hand, monoalkyllammonium nitrate salts are best prepared by the neutralization of aqueous solutions of the amine with nitric acid. Tetraalkylammonium sulfonates are also prepared by mixing sulfonic acid and tetraalkylammonium hydroxide. In order to obtain pure ILs, products are dissolved in an organic solvent such as acetonitrile and treated with activated carbon, and the organic solvent is removed under vacuum. The final method for the synthesis of ILs is the direct combination of halide salt with a metal halide. Halogenoaluminate and chlorocuprate ILs are prepared by this method.[10]

ILs can have reasonable ionic conductivities compared with those of organic solvents/electrolyte systems at elevated temperatures. However, at room temperature the conductivity is generally lower than those of concentrated aqueous electrolytes. Due to the ion pair formation and/or ion aggregation, their conductivity can be reduced.[11] Generally, ILs are more viscous than common molecular solvents and their viscosities are range from 10 mPas to about 500 mPas at room temperature. There are several factors which can control the viscosity of ILs such as van der Waals interactions, electrostatic forces, and alkyl chain lengths in the cation. This is because stronger van der Waals forces between cations can lead to increase in the energy requirement for molecular motion. Furthermore, hydrogen bonding in the anions has a pronounced effect on viscosity. For example, the anions such as $^{-}BF_4$ and $^{-}PF_6$ can from viscous ILs due to their formation of hydrogen bonding.[12]

In general, ILs have higher density than water with values range from 1.0 to 1.6 g/cm^3 and the density can be decreased with increase in the length of alkyl chain in the cation. The chemical structure of anion can affect the density of ILs. For example, the order of increasing density for ILs with different anions is $CH_3SO_3^-$, $^-BF_4$, $CF_3CO_2^-$, $CF_3SO_3^-$, $C_3F_7CO_2^-$ and $^-N(Tf)_2$.[13] As a class, ILs have been defined to have melting points below 100 °C and most of them are liquid at room temperature. Like the density of ILs, there are several factors affecting the melting points of ILs. The increase size of anions can lead to a decrease in melting points.[14] Furthermore, cation size and symmetric structures play an important role on the melting points of ILs. For example, large cations and increased asymmetric substitution result in a decreased melting point.[15] Moreoever, ILs are thermally stable up to 450 ^{o}C and the thermal stability is limited by the strengths of their heteroatom-carbon and heteroatom-hydrogen bond, respectively.[14]

To date, most chemical reactions have been carried out in molecular solvents and most of our understanding of chemistry has been based upon the behavior of molecules in the solution phase in molecular solvents. Recently, however, ILs has emerged as a new class of solvents for green chemistry. They have many fascinating properties which make them of fundamental interest to all chemists, since both the thermodynamics and kinetics of reactions carried out in ionic liquids are different to those in conventional molecular solvents. These results stem from the fact that ionic liquids have no measurable vapor pressure, and hence can emit no volatile organic compounds (VOCs) in the enviroment.

As a favorable separation technique in industry, extraction is an energy-efficient technology using two immiscible phases (conventionally an organic phase and an aqueous phase). Many organic solvents, however, are toxic and flammable VOCs. To improve the safety and environmental friendliness of this conventional separation technique, ILs can be used as ideal substitutes because of their stability, nonvolatility and adjustable miscibility and polarity. ILs can be hydrophilic and hydrophobic depending on the structures of cations and anions.[16] Some ILs with hydrophobic character allows them to extract hydrophobic compounds in biphasic separations. Metal cations (Li^+, K^+, Na^+, Cs^+, Mg^{2+}, Pb^{2+}, Ni^{2+}, Cd^{2+}, Zn^{2+}, Hg^{2+}, Fe^{2+}, among others) tend to remain in the aqueous solution being hydrated. Therefore, in order to remove metal ions from the aqueous phase into hydrophobic ILs, extractants are normally needed to form complexes to increase the metal's hydrophobicity.[17] The solvation of crown-ether complexes in ILs is more thermodynamically favored than conventional organic solvents.[18] This is why ILs can be used to solvate metal ions from aqueous solution.

It has been reported that ILs could dissolve transition metal complexes and support organic chemistry. For example, nickel complexes dissolved in acidic chloroaluminate ionic liquids catalyze the dimerization of alkenes[19] while Ziegler-Natta catalysts in a similar solvent can polymerize ethylene.[20] However Zaworotko's water-stable ionic liquids containing tetrafluoroborate, hexafluorophosphate, nitrate, sulfate and acetate anions expanded the ILs applications. With these ILs Chauvin and Dupont demonstrated their potential in hydrogenation catalysis[21] and showed that reaction rates and selectivities could be enhanced. It has been proven that activation of a pre-catalyst can be thermodynamically hindered in IL, affording no catalysis at all if reaction conditions are not adapted properly.[22] In addition to catalyst activation, sufficient retention of the catalyst in the IL is important in order to provide good recycling. The most versatile approach used to anchor homogeneous catalysts in IL phases is to attach charged groups to the ligands bound to the metal catalyst center. The imidazolium tagged liganda/catalysts are shown in Figure 3.3.

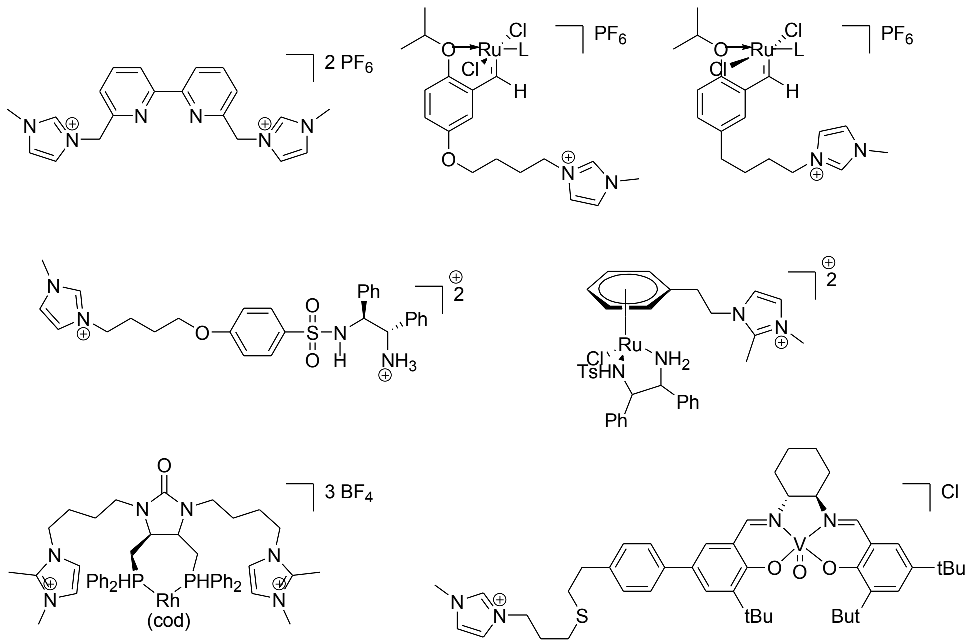

Figure 3.3. Imidazolium tagged ligands/catalysts that enhance immobilization in ionic liquids and improve catalyst recycling/use.

Applications of ILs in sensor are recently being explored by many researchers. One of the early achievements is the use of ILs as the sensing materials for organic vapors.[23,24] Furthermore, ILs containing methyl orange (MO) or methyl red (MR) displayed the potential use in aqueous and non-aqueour acid sensors. Imidazolium and pyridinium based ILs with methyl orange and methyl red exhibited different color change and absorption based on acid concentrations (Figure 3.4).[25] The melting points of MO and MR are 300 and 180 ^{o}C, respectively. However, the incorporation of cations significantly decreases the melting points due to their disruption of the crystal packing by bulky and asymmetric cations.

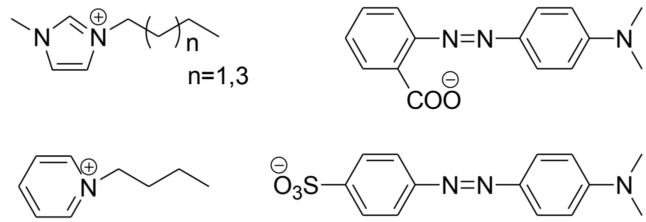

Figure 3.4. Chemical structures of IL-modified dyes.

ILs are being considered as alternatives to conventional electrolyte materials. It has been reported that some ILs exhibit ionic conductivity of over 10^{-2} S/cm at room temperature which is close to the level for fuel cell applications.[26] Doyle et al. synthesized proton conducting membranes based on perfluorinated ionomer and ILs. In this system, proton conductivitiy of synthesized materials provided 0.1 S/cm at 180 ^{o}C.[27] Generally, traditional membranes lose their proton conductivity above 130 ^{o}C. However, it was thought that ILs could be used thermally stable solvents in transporting protons due to their nonvolatility. Moreover, ILs have been studied for proton transfer toward fuel cell electrolytes under water-free condition and these ILs are called Brønsted acid-base ILs.[28]

In general, multi-charged ILs have been shown to have a greater range of physical properties than traditional monocationic types such as higher density, glass transition, melting point, surface tension, and shear viscosity.[29] Since the number of possible combinations of cationic and anionic moieties in multi-charged ILs are greater than those of monocationic such liquids, multi-charged ILs can be considered as an extension to the structural variations of ILs, when properly designed. For example, ammonium-based dicationic phosphate salt liquids,[30,31] imidazolium-based dicationic ILs,[32] pyridinium based dicationic ILs,[33] and pyrrolidinium cation based ILs[34] were synthesized to explore their physical properties. Note here that they displayed better physical properties than those of monocationic ILs. Even though materials chemist face a challenge to synthesize multi-charged ILs because of strong, long-range intermolecular interactions, however, the incorporation of the bulky organic anions such as bis(trifluoromethylsulfonyl)imide ($^{-}N(Tf)2$) not only decreases the melting point but also increases the thermal stability of ILs. Some representative structures of dicationic ILs are shown in Figure 3.5.

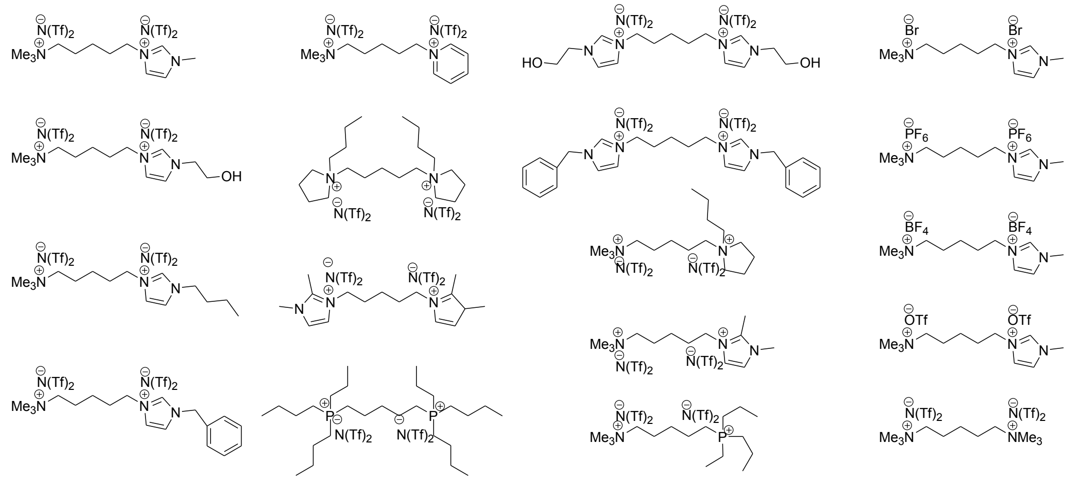

Figure 3.5. Chemical structures of dicationic ionic liquids.

Armstrong and co-workers reported the effect of chemical structural modifications on the physicochemical properties of symmetrical tricationic ILs containing $^{-}N(Tf)_2$, hexafluorophosphate ($^{-}PF_6$), tetrafluoroborate ($^{-}BF_4$), and trifluoromethanesulfonate (TfO^{-}). The densities of ILs with similar cationic moieties are affected by the counterions in the order $^{-}N(Tf)_2 > {}^{-}PF_6 > TfO^{-} > {}^{-}BF_4$; and the thermal decomposition temperatures of multi-charged ILs are higher than those of monocationic ionic liquids. The melting points of tricationic ILs are affected by the flexibility of the central core systems while keeping their solubility in water and heptanes which is similar to that of monocationic and dicationic ILs.[35] Furthermore, the mesitylene core with bis and trisimidazolium salts can have thermotropic liquids-crystalline (LC) properties with various organic anions ($^{-}$I, $^{-}BF_4$, and $^{-}N(Tf)_2$).[36] Their versatile applications, but not limited to, range from stationary phases for gas chromatography to high-temperature lubricants to dye-sensitized solar cells to even photocontrollability of liquid crystal alignment.[37] Furthermore, dicatioinic ILs such as dicationic arginine-diglycerides,[38] viologen-based dicationic organic salts,[39,40] imidazolium-based dicationic organic salts,[41] and bisamidinium-based dicationic tectons[42] showed LC properties.

It has been reported that aromatic bis(pyridinium salt)s with various counterions such as tosylate, triflimide, tetraphenylborate and tetrakis[3,5]bis(trifluoromethyl)phenyl]borate (Figure 3.6). They displayed good thermal stabilities in the range of 257−461 °C which are dependent on the nature of both the anions and dications. Furthermore, good solubilities in a wide range of common organic solvents are observed which is suitable for thin films and fiber processing and they displayed blue and green light in both solution and solid state.[43]

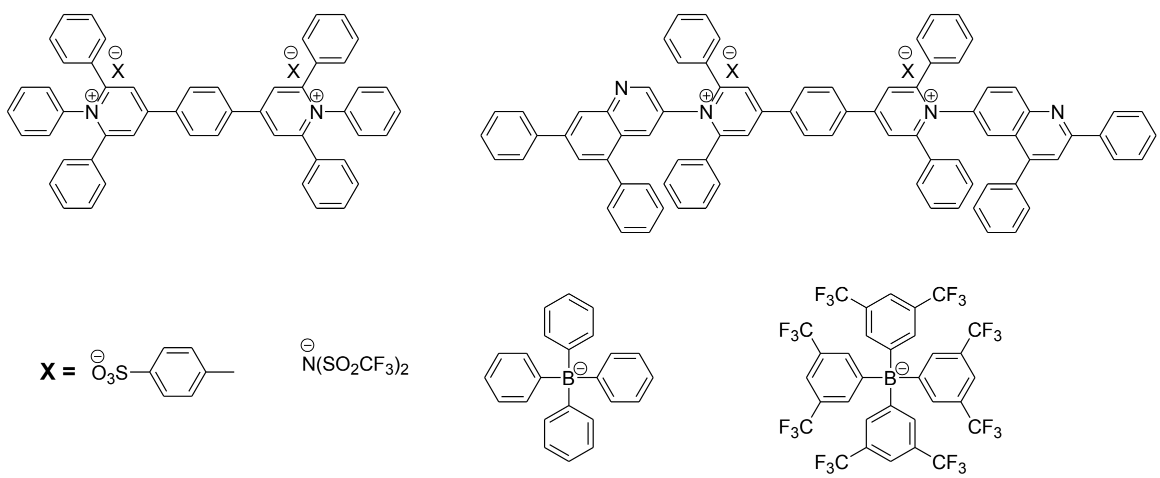

Figure 3.6. Chemical structures of bis(pyridinium salt)s.

3.3. Results and Discussion

The two organic salts **1a** and **2a** were synthesized by using a ring-transmutation reaction of bispyrylium salt, **M**, with the respective aliphatic amines in DMSO. To increase the reactivity of reaction, small amount of toluene was added into the solution to remove the water generated in the reaction by a Dean-Stark trap set-up. The crude products were purified by column chromatography and tosylate counterions were further exchanged to other counterions such as triflimide, dioctyl sulfosuccinate (AOT), and methyl orange through the metathesis reactions in a common organic solvent. The overall reaction is shown in Scheme 3.1.

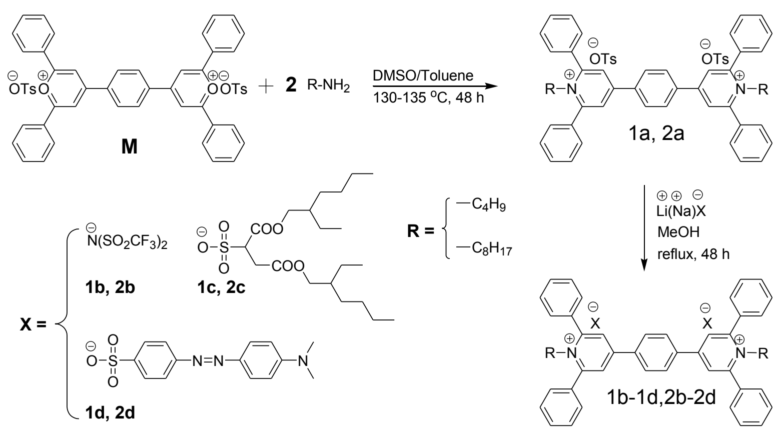

Scheme 3.1. Chemical structures of bis(pyridinium salt)s **1a−1d** and **2a−2d**.

The chemical structures of these salts were characterized by the analyses of ^{1}H, ^{19}F, and ^{13}C NMR spectra. Their ^{1}H NMR spectra are provided in Figure S1 to S8 in the Appendix 3. The salt **1a** showed aliphatic protons at 0.354 ($-CH_2CH_3$), 0.710 ($-CH_2CH_3$), and 1.28 ($-CH_2CH_2CH_3$) ppm, respectively. Unique $-^{+}NCH_2CH_2-$ appeared at 4.39 ppm due to the quaternary nitrogen. Tosylate peaks were observed at 7.65 (H_{arom}), 7.00 (H_{arom}), and 2.23 ($C_6H_4CH_3$) ppm, respectively. After exchanging tosylate to triflimide, the tosylate peaks disappeared and the two protons of $-^{+}NCH_2CH_2-$ and aromatic peaks (**1** in

Figure 7) from the pyridinium moiety slightly were shifted to upfield in the spectrum. In the case of **1c** these proton signals were shifted to down field, but in the case of **1d** they were shifted to upfield with respect to those of **1a**. These results suggested that chemical structures of anions have an effect on the chemical shifts of methylene and aromatic protons of quaternary nitrogen of dicationic moiety. These findings are in excellent agreement with those observed in imidazolium salts either in ionic liquids or in polymerized ionic liquids with various organic and inorganic counterions[44-46] as well as in other tricationic salts of mesitylene and stilbazolium moieties.[47] Moreover, a fluorine peak of triflimide at −78.7 ppm in the ^{19}F NMR spectrum and elemental analysis further supported the completion of exchange reaction. To have bulky counterion in the salt, AOT counterion was introduced in the bis(pyridinium salt) moieties via the identical metathesis reactions. The appearance of additional unique peaks of dioctyl sulfosuccinate counterion was confirmed by the analyses of ^{1}H and ^{13}C NMR spectra, which were suggestive of the complete exchange reaction of counterions. Additionally, the methyl orange counterions were also incorporated into bis(pyridinium salt)s. The introduction of methyl orange was revealed by the appearance of unique dimethyl protons ($-N(CH_3)_2$) signal at 2.98 ppm in the ^{1}H NMR spectrum and their integral ratio was consistent with the aromatic moieties suggesting of the completion of exchange reaction. The carbon signal of $-N(CH_3)_2$ at 40.3 ppm in ^{13}C NMR spectrum further supported the presence of counterions.

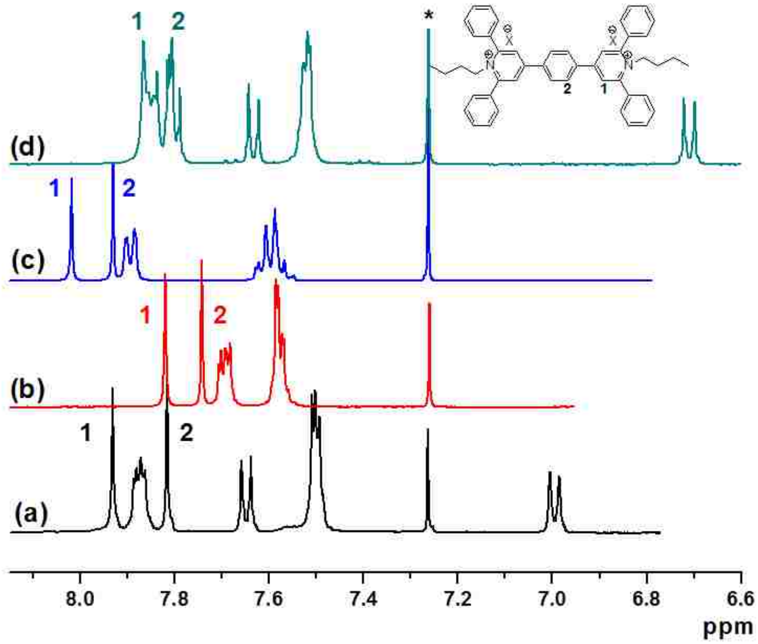

Figure 3.7. Expanded aromatic region of ^{1}H NMR spectra of (a) **1a**, (b) **1b**, (c) **1c**, and (d) **1d** (An asterisk indicates $CDCl_3$). X^- in the generalized chemical structures in this figure represents the corresponding anions.

Like the salt **1a**, **2a** showed similar ^{1}H NMR spectrum. Two doublet and methyl peaks from tosylate counterions were detected at 7.63, 7.01 and 2.25 ppm, respectively. The unique triplet peak from $-^+NCH_2CH_2-$ was found to be located at chemical shift of 4.38 ppm. The extra aliphatic protons appeared in the range of 0.68 to 1.50 ppm. After exchanging the tosylate to triflimide, all protons of tosylate completely disappeared and a new set of fluorine signal of triflimide appeared at −78.8 ppm which is a similar characteristic of salt **1a**. Similarly, the salts **2c** and **2d** showed characteristics to those of **1c** and **1d**. In case of **2d**, dimethyl protons ($-N(CH_3)_2$) signal of methyl orange appeared at 3.06 ppm and that of carbon of $-N(CH_3)_2$ at 40.3 ppm in its ^{1}H and ^{13}C NMR spectra, respectively. The whole ^{1}H NMR spectra of pyridinium salts **1a−2d** are shown in Figures S1−S8 in the Appendix 3.

Table 3.3. Unique chemical shifts of **1a−2d** from their ^{1}H NMR spectra recorded in $CDCl_3$ at room temperature

Entry	aromatic meta to N^+ (ppm) (**1**)	aromatic (ppm) (**2**)	$-^{+}NCH_2CH_2-$ (ppm)
1a	7.93	7.82	4.39
1b	7.82	7.74	4.31
1c	8.02	7.93	4.46
1d	–[a]	–[a]	4.39
2a	7.93	7.82	4.38
2b	7.82	7.74	4.29
2c	8.02	7.93	4.43
2d	–[a]	–[a]	4.37

[a] Could not be determined due to the overlapped peaks from methyl orange counterion.

High thermal stability is generally required for high-operating temperature devices. Therefore, thermal stabilities of organic salts were studied by thermogravimetric analysis (TGA) measurements between 30 and 600 ^{o}C in nitrogen and their plots are displayed in Fig 4. Although highly π−conjugated aromatic materials can exhibit high thermal stability of materials, their poor solubility in organic solvents often is encountered due to their rigid chemical structures.[48,49] In this study, bis(pyridinium salt)s with varying short and long alkyl chain lengths (butyl and octyl) and various organic counterions were found to have T_ds in the range of 202−305 ^{o}C. Generally, organic salts **1a−1d** showed higher thermal stability than those of **2a−2d**. These results stemmed from the fact that the longer aliphatic chains reduced the thermal stability of bis(pyridinium salt)s. Moreover, **1b** and **2b** containing triflimide as a counterion provided better stability among other counterions. This characteristic trend may be attributed to the decomposition temperature and nucleophilic character of lithium triflimide. Generally, the anions of strong acids being the weak nucleophiles impart excellent thermal stability of cationic moieties.[50]

Table 3.4. Thermal stabilities of bis(pyridinium salt)s

Compounds	**1a**	**1b**	**1c**	**1d**	**2a**	**2b**	**2c**	**2d**
T_d^a (°C)	233	305	238	202	220	286	234	225

[a] Thermal decomposition was recorded at 5 wt % weight loss in nitrogen.

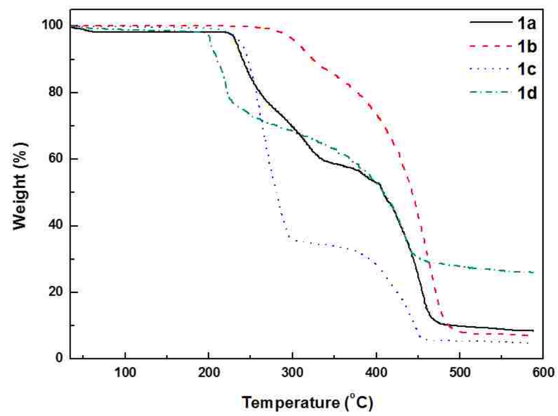

Figure 3.8. TGA thermograms of the compounds **1a−1d** obtained at a heating rate of 10 °C/min in nitrogen.

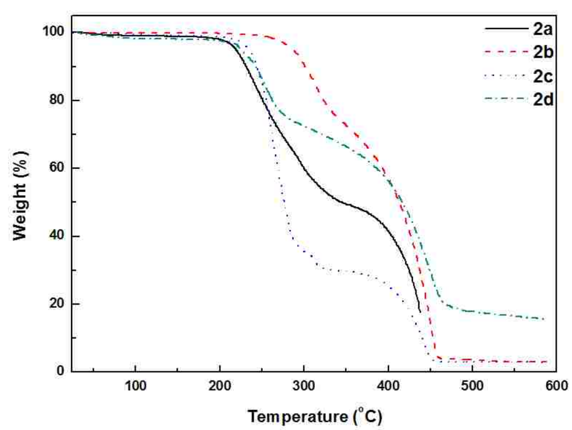

Figure 3.9. TGA thermograms of the compounds **2a−2d** obtained at a heating rate of 10 °C/min in nitrogen.

Amorphous ionic materials[43] have drawn much attention over the past decades due to their easy processing into thin films or fibers thereby avoiding cumbersome and expensive techniques such as vapor deposition technique.[51] Therefore, the thermal transitions of organic salts were evaluated by DSC measurements to explore these properties. The salt **1a** showed several endotherms prior to its melting endotherm (T_m) at 220 ^{o}C in the first heating cycle, which was then followed by its thermal decomposition at higher temperature (Figure 3.10). The low-temperature endotherms (124 and 180 ^{o}C) were related to crystal-to-crystal transitions, which were verified by polarizing optical microscopy (POM) studies (Figure 3.13) and **1a** showed a stable glass transition T_g at ca. 75 ^{o}C upon slow cooling at a rate of 10 ^{o}C/min after melting. From the second heating cycle, **1a** only showed a distinct T_g at ca. 72 ^{o}C without any other thermal transitions. These results suggested **1a** could not revert to its crystallinity after melting and it became an amorphous material.

Unlike the organic salt **1a**, **1b** containing triflimide counterion also exhibited several endotherms prior to its T_m at 260 ^{o}C and then followed decomposition at higher temperature. All of the low-temperature endotherms are related to polymorphism which was also verified on observation of highly birefringent crystal phases by using POM studies (Figure 3.13). There were sharp textural defects and absence of homogeneity in the domains suggesting their crystalline phases. The polymorphism phenomenon is quite common in many ionic liquids and liquid-crystalline ionic compounds.[47,52-55] Furthermore, their crystallization processes of **1b** from liquid phase were observed in the cooling cycle (10 ^{o}C/min) and T_m from the second heating was found to be at 200 ^{o}C. These thermal transitions were at variance to those of **1a** suggesting that **1b** possessed crystalline properties as opposed to amorphous properties. In contrast to **1a** and **1b**, **1c** provided T_g at 77 ^{o}C from the first heating cycle, but no T_m in the DSC thermogram; while **1d** did not provide any detectible melting transition in the DSC thermogram. This result stemmed from the fact that the bulky counterions (AOT) promoted the amorphous state of salt **1c**. In the case of **2a**, T_g appeared at 47 ^{o}C and the melting point was found to be *ca*. 90 ^{o}C by using Fisher Jones melting point apparatus. In contrast to **1a**, the glass transition of **2a** was recorded from the first heating cycle and the thermal transition trend may be attributed to that fact that the longer aliphatic groups can provide the increase of the segmental mobility of bis(pyridinium salt)s resulting in the appearance of T_g from the first heating cycle.

Like salt **1b**, **2b** showed crystal to crystal transitions at 80 and 86 ^{o}C, respectively, and T_m was observed at 143 ^{o}C. The lowered T_m was attributed to the decrease in molecular packing of the longer octyl groups. Note here that no liquid-to-crystal phase transition (T_c) appeared from the slow cooling cycle, however, and its T_m appeared in the second heating cycle. These results suggested that during the cooling cycle it did not crystallize because octyl aliphatic moiety may hinder the crystallization process, but did crystallize in the heating cycle exhibiting melting peak (Figure S9). The salts **2c** and **2d** did not provide any meaningful transitions in the respective DSC thermograms.

The ILs, whose melting points are generally below 100 ^{o}C, are usually considered as ionic liquids in the field of ionic liquids, and Chiappe and Pieraccini have reported as the size and asymmetry of the cation increases, the melting point decreases. Further, an increase in the branching on the alkyl chain increases the melting point. The melting point of ILs is crucial because it represents the lower limit of the liquidity and with thermal stability it defines the interval of temperatures within which it is possible to use ILs as solvents.[56] As recorded from the DSC thermograms, **1a** and **1b** had T_m at 220 and 260 °C, respectively. Even though no T_m of **1c** was detected in DSC thermogram, the melting point of **1c** was found to be at ca. 180 °C as determined in the Fisher Jones melting point apparatus and the decomposition of **1d** was prior to its melting point. These results supported that size and asymmetry of the anions had an effect on the T_m of organic salts. In the series of **2a−d**, the melting points of **2a** and **2c** were observed at *ca*. 90 and 60 °C which can be considered as ionic liquids while **2b** melted at 143 °C. The DSC thermograms of **2a−2d** are shown in Figures S9 in the Appendix 3.From the results of thermal properties, the increase size and chemical structures of anions and long alkyl chains can lead to decrease in melting transitions. Therefore, dicationic bis(pyridinium salt)s, when properly designed, could be the basis of new generation of ionic liquids that expands further the repertoire of this novel type of solvents.

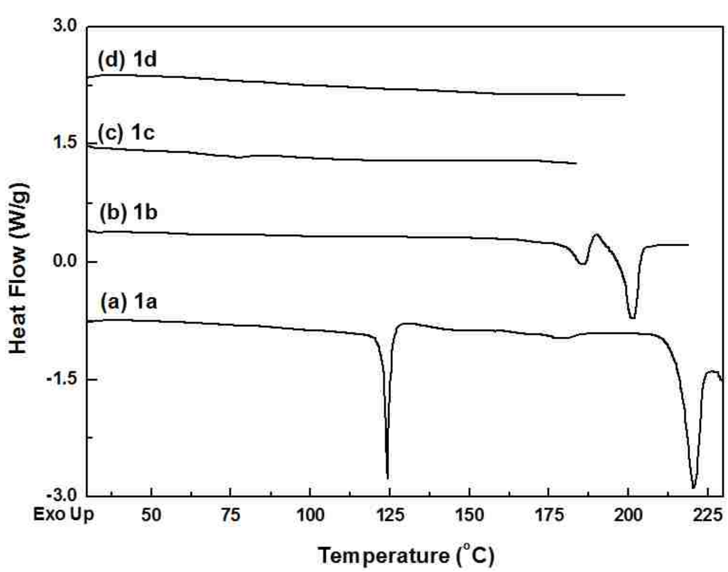

Figure 3.10. DSC thermograms of **1a−1d** obtained from the first heating cycle at a rate of 10 °C/min in nitrogen.

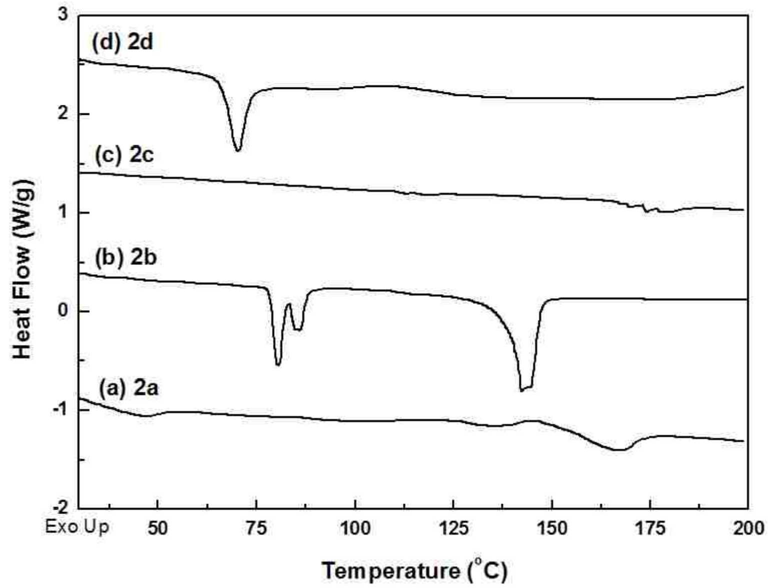

Figure 3.11. DSC thermograms of **2a−2d** obtained from the first heating cycle at a rate of 10 °C/min in nitrogen.

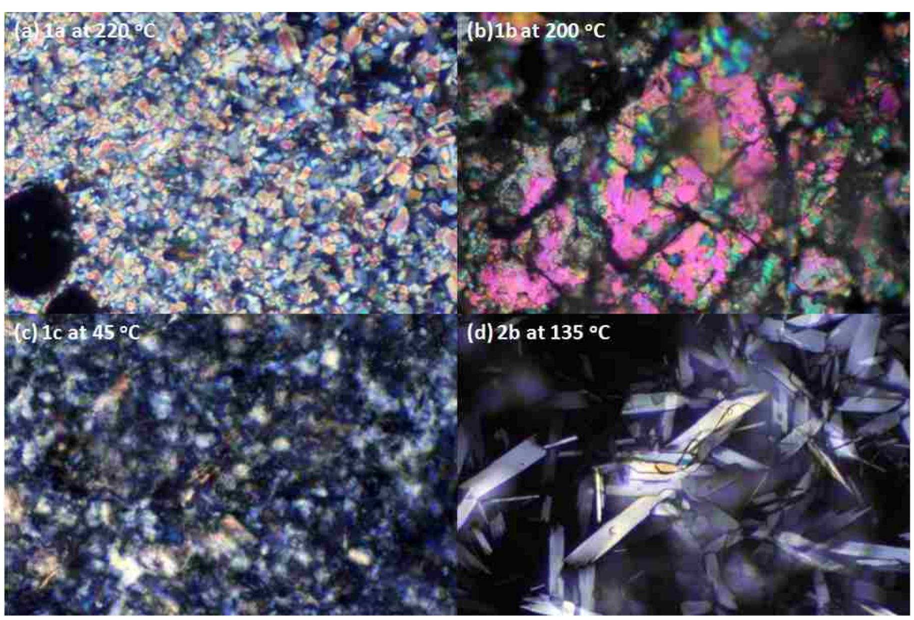

Figure 3.12. Photomicrographs of (a) **1a** taken at 220 ^{o}C, (b) **1b** taken at 200 ^{o}C, (c) **1c** taken at 45 ^{o}C, and (d) **2b** taken at 135 ^{o}C under crossed polarizers exhibiting crystal phase (magnification 400x).

One of the interesting characteristics of conjugated compounds is about their optical property in solution and solid states. The bis(pyridinium salt)s synthesized in this study exhibited good solubility in common organic solvents due to their long aliphatic groups and organic counterions. Therefore, the optical properties of synthesized organic salts were characterized by UV−Vis and photoluminescent spectroscopy (PL). All of the salts showed essentially almost identical λ_{max} in the range of 327−337 nm in various organic solvents such as CH_3CN, CH_3OH, acetone, tetrahydrofuran (THF) or $CHCl_3$ as detected in their absorption spectra with the exception of **1d** and **2d**. These absorption spectra could be an indication of closely spaced π–π^* transitions of aromatic moieties of bis(pyridinium salt)s. In the cases of **1d** and **2d,** there was an additional absorption peak of methyl orange at 421 and 424 nm, respectively, that stems from the conjugated π–π^* transitions of this organic counterion. These results suggest that the interactions between various organic solvents and the chemical structures of ionic compounds did not cause any significant changes in the energies of their ground states. The optical band gaps (E_g) of all of the organic salts as determined from the onset of wavelength (low energy region) in each of the UV−Vis absorption spectra are summarized in Table 3.5. These values were in the range of 3.18−3.24 eV that are comparable to those of other bis(pyridinium salt)s with organic counterions reported previously.[43]

Table 3.5. Optical properties of bis(pyridinium salt)s

Compounds	**1a**	**1b**	**1c**	**1d**	**2a**	**2b**	**2c**	**2d**
UV abs (nm)[a]	328	329	329	327, 421	328	337	332	327, 424
Band gap (eV)[b]	3.21	3.21	3.21	3.24	3.20	3.20	3.18	3.23
PL λ_{em} CH_3CN (nm)	442	440	442	442	441	443	442	442
PL λ_{em} CH_3OH(nm)	442	441	442	443	442	443	442	442
PL λ_{em} Acetone (nm)	442	442	441	442	442	443	442	443
PL λ_{em} THF (nm)	378,[d] 439	442	439	381	439	443	439	444
PL λ_{em} $CHCl_3$ (nm)	439	441	441	–[e]	441	441	441	–[e]
PL λ_{em} film (nm)[c]	441	424	424	–[e]	433	423	420	–[e]

[a] Obtained in MeOH.
[b] Determined from onest of wavelengths in MeOH.
[c] Cast from $CHCl_3$.
[d] Shoulder peak.
[e] Not detected.

The light emission properties of organic salts were studied in several organic solvents (both low and high polarity) in which their UV−Vis spectra are recorded; and their solid-state light- emission properties were also examined. Salts **1a−d** emitted visible light having the λ_{em} peaks in the narrow range of 439−442 nm in various organic solvents with the exception of **1d,** which showed a λ_{em} peak at 381 nm (> 400 nm) in THF (Figure 3.13). The salt **1d** emitted UV light in THF when excited at 300 nm wavelength of light. These results suggested that λ_{em} peaks were independent of the types of organic anions used. As discussed (*vide supra*), long alkyl chains in bis(pyridinium salt)s had an effect on their thermal properties. However, there was no significant difference in the light emission properties for **1a−d** and **2a−d** (Figures 3.13 and 3.14**)**. These results supported that the light emission properties in various organic solvents were independent of the chemical structures of bis(pyridinium salt)s used. Note here that the recoded excitation spectra of these salts (not shown) faithfully reproduced their UV-vis absorption spectra that provided the compelling evidence for their photoluminescent properties. The light emission properties for the majority of salts in solutions did not exhibit positive solvatochromic effect.[57,58] Moreover, In contrast to other bis(pyridinium salt)s with conjugated aromatic and heterocyclic moieties,[43] the synthesized ionic compounds emitted blue light because of lack of conjugated moieties, since they are connected to butyl or octyl groups.

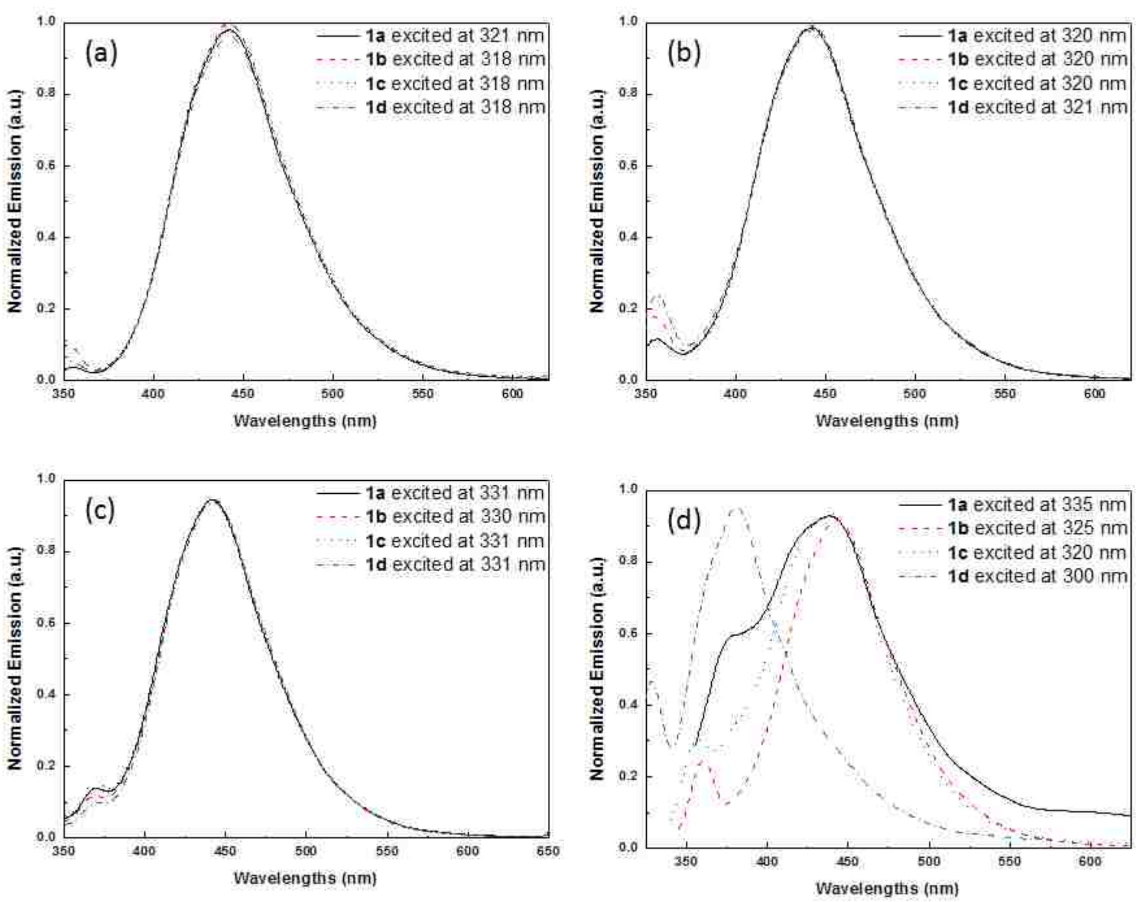

Figure 3.13. Emission spectra of **1a−1d** in (a) CH_3CN, (b) CH_3OH, (c) Acetone, and (d) THF at various excitation wavelengths.

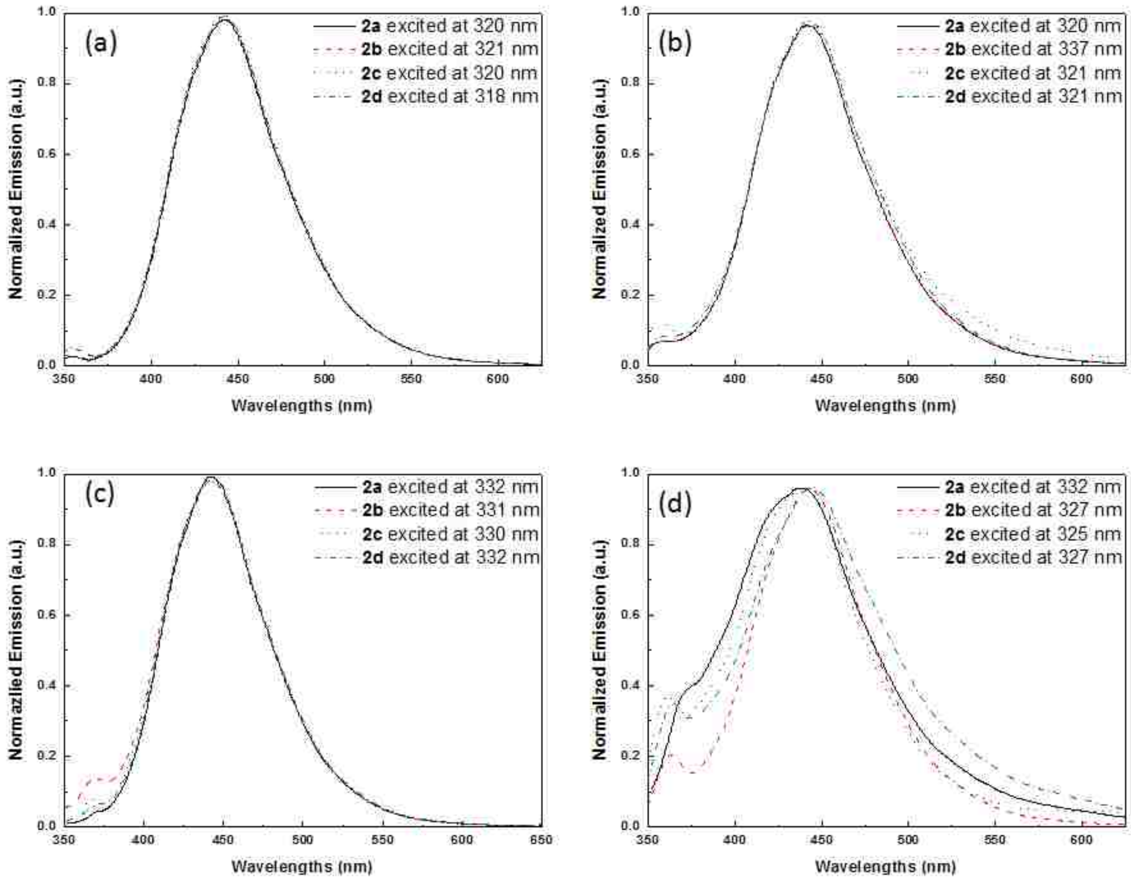

Figure 3.14. Emission spectra of **2a**−**2d** in (a) CH_3CN, (b) CH_3OH, (c) Acetone, and (d) THF at various excitation wavelengths.

We also explored the photoluminescence properties of these organic salts in the thin films cast from $CHCl_3$ to assess their potential for optoelectronic applications. The salts **1a**−**c** exhibited λ_{em} values in the blue region similar to those in solutions (Figures 3.15 and 3.16 and Table 3.5) in the solid state. However, **1a** showed a slight bathochromic shift by 2 nm, but **1b** and **1c** showed a hypsochromic shift of 17 nm. These results indicated that **1b** and **1c** were less ordered in the solid state due to the bulky size of counterions reducing the π−π stacking and causing a blue shift. Similarly, **2a**−**c** showed similar light emission properties in the solid state like **1a**−**c** as shown in Figure 3.16**.**

However, the λ_{em} value of **2a** (433 nm with excitation wavelength at 310 nm) showed a hypsochromic effect compared to that of **1a** (441 nm with excitation wavelength at 330 nm). It also showed a hypsochromic shift in the solid state when compared with that solution spectrum. Salts **2b** and **2c** showed relatively large hypsochromic shifts in their spectra when compared with those of solution spectra.[43,57,58] This blue shift might be caused by the variation of alkyl chain lengths of bis(pyridinium salt)s which means that the longer aliphatic groups could reduce the π−π stacking of chromophores resulting in a hypsochromic shift in thin films. Their full-width at half-maximum (fwhm) values of **2a−c** were wider than those of compounds **1a−c** suggesting their light-emission stemmed from a number of chromophoric species.

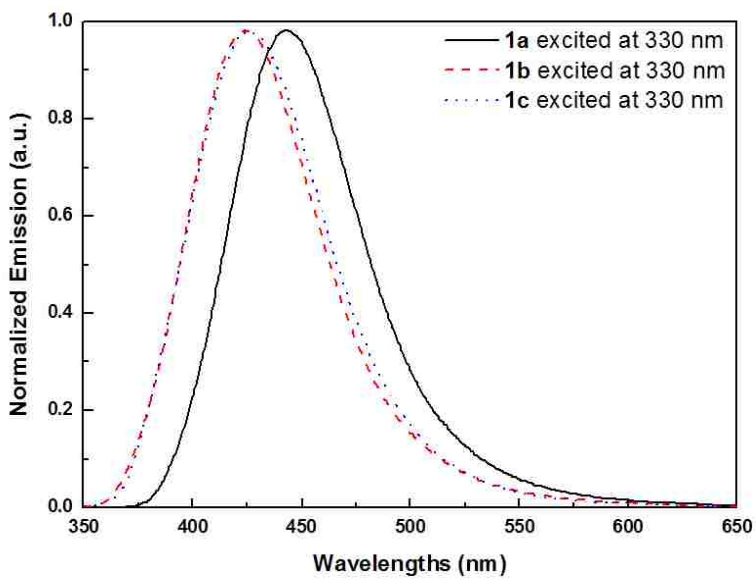

Figure 3.15. Emission spectra of **1a−1c** cast from $CHCl_3$ with excitation wavelength at 330 nm.

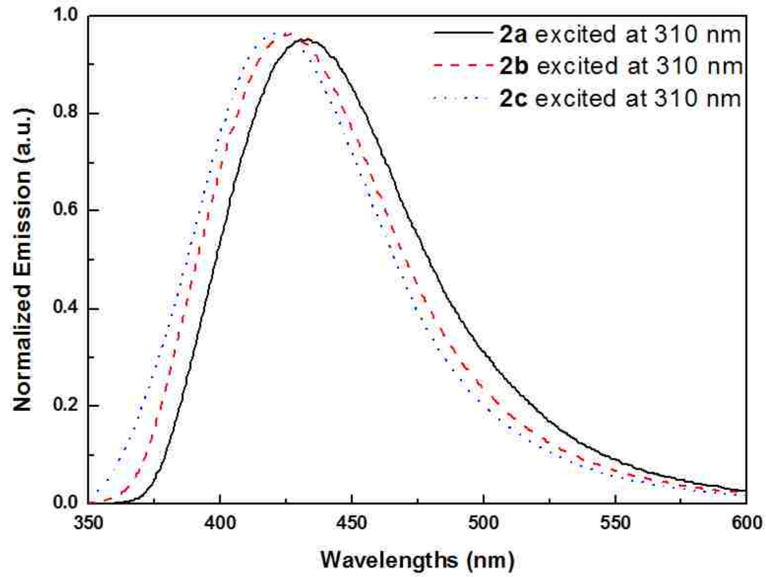

Figure 3.16. Emission spectra of **2a−2c** cast from $CHCl_3$ with excitation wavelength at 310 nm.

The traditional dye such as methyl orange (MO) is widely used in the chemistry laboratory and industrial processes. However, due to insolubility of MO in common organic solvents, the use and availability of MO is somewhat limited. One of the most well-known properties of MO is about its pH sensing application in aqueous media. It has been already studied that monocationic ionic liquids with MO and MR displayed their pH sensing performance in aqueous and non-aqueous solutions.[25]

For organic salts **1d** and **2d** containing MO as counterions were soluble in many organic solvents such as DMSO, CH_3CN, methanol, ethanol, acetone, chloroform, and ethyl acetate. The good solubility of **1d** and **2d** can make them to be used as an organic acid sensor in these organic solvents. The absorption spectra of **1d** and **2d** in three organic solvents (CH_3CN, CH_3OH, and acetone) were studied with the variation of HOTf (CF_3SO_3H) concentrations (10^{-1} to 10^{-4} M). Generally, the differences in sensing performance might be caused by different degrees of dissociation of the strong acid HOTf in various organic solvents.[25] These results stemmed from the fact that the dissociation of HOTf mainly depends on the deprotonation ability of the solvent (Scheme 3.2). However, no significant color changes were observed based on the polarity of solvents. In contrast, the indicator performance between **1d** and **2d** was clearly different. While the color of **1d** and **2d** was deep red with the 0.1 M HOTf concentration in methanol, the color of **2d** changed to light orange by decreasing the concentration of HOTf to 0.01 M; while the red color of salt **1d** did not visibly change on decreasing the identical concentration of HOTf (Figures 3.17 and 3.18). Similar results were also found in acetone and acetonitrile media (Figures S10−S13). Since the color change of the solutions are mainly caused by the transformation between the azo from and the zwitterionic form, the differences in indicator performance of **1d** and **2d** might be affected by different alkyl chain lengths in bis(pyridinium salt)s. By changing the HOTf to weak acid such as lactic acid in the identical solvents, there was no visibly color change suggestive of no dissociation of lactic acid occurred in the organic solvents examined.[25]

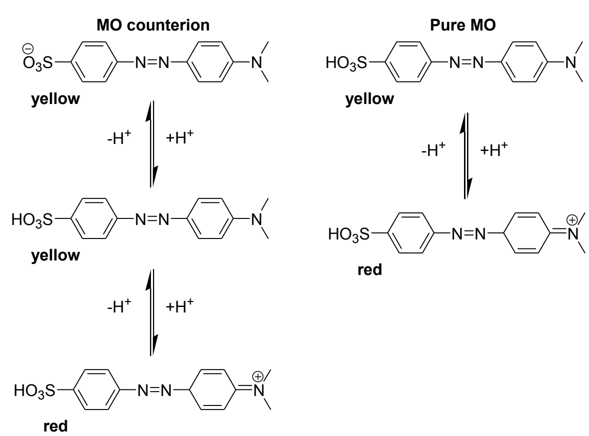

Scheme 3.2. Possible mechanism of MO counterion and pure MO in organic solvents.

From the UV−Vis spectra, there are two distinctive absorption peaks at 326 and 425 nm in methanol which are related to pyridinium salts and MO counterions, respectively. By adding the different HOTf concentrations, the absorption of MO (λ_{abs} = 425 nm) shifted to higher wavelengths (λ_{abs} = 516) nm while the bis(pyridinium salt) absorption still remained unchanged (Figures 3.17 and 3.18). The observed absorption behavior suggested that only MO counterion formed zwitterionic form from the dissociated proton of HOTf. Other solvents (acetonitrile and acetone) provided the identical absorption spectra. Moreover, the emission spectra of **1d** and **2d** in methanol with different concentrations of HOTf were studied to see the effect of organic acid in their emission properties. However, no significant change in the light emission was observed suggesting the concentrations of HOTf have negligible effect on their emission properties.

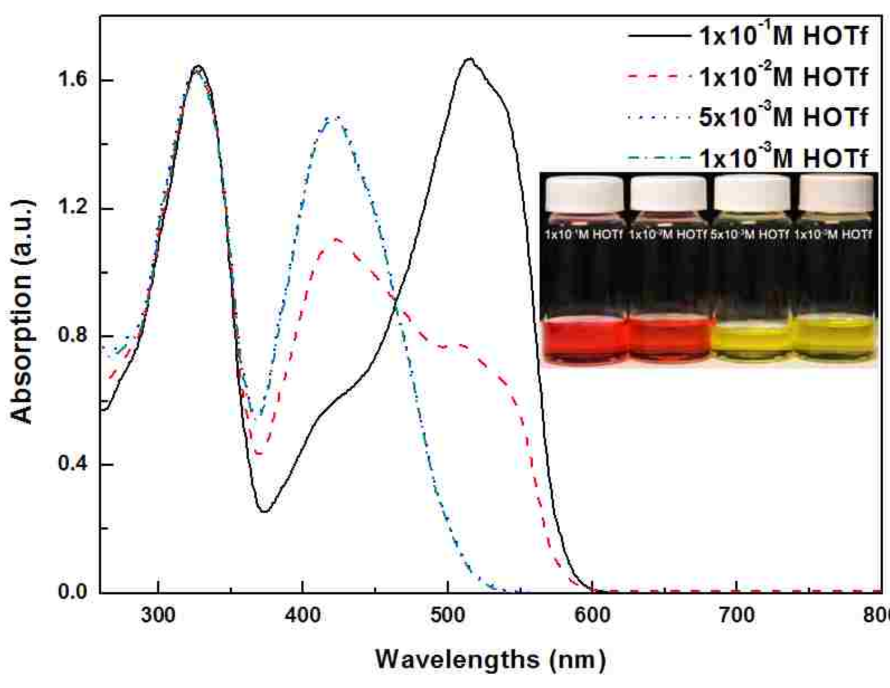

Figure 3.17. UV−Vis spectra of **1d** (2 x 10^{-5} M) in methanol with varied HOTf concentrations.

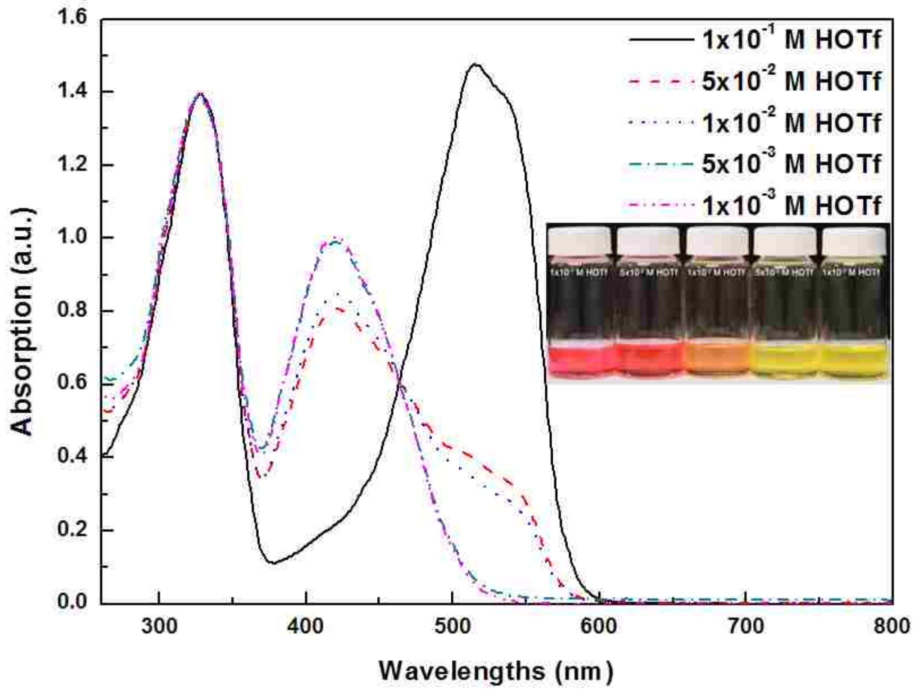

Figure 3.18. UV−Vis spectra of **2d** (2×10^{-5} M) in methanol with varied HOTf concentrations.

3.4. Experimental

3.4.1. General Comments

Butylamine, hexylamine, lithium triflimide, methyl orange, dodecylbenzene sulfonic acid (sodium salt), dioctyl sulfosuccinate (sodium salt) and common organic solvents were purchased from commercial vendors (Sigma-Aldrich, Alfa-Aesar, Acros Organics, and TCI America) and used without any further purification.

^{1}H, ^{19}F, and ^{13}C NMR spectra were obtained using a Varian NMR spectrometer (400 MHz for ^{1}H 376 MHz for ^{19}F, and 100 MHz for ^{13}C) with three RF channels at room temperature, and chemical shifts were referenced to tetramethylsilane (TMS). The NMR samples were prepared in $CDCl_3$ with a concentration of 10 mg/mL and 30 mg/mL, respectively. Differential scanning calorimetry (DSC) of ionic compounds was conducted on TA module DSC Q200 series under a nitrogen atmosphere at heating and cooling rates of 10 ^{o}C/min. Thermo gravimetric anlaysis (TGA) of the compounds were performed using a TGA Q50 instrument in nitrogen. The TGA data was collected at temperatures between 30 and 600 ºC at a heating rate of 10 ºC/min. The temperature axis of the DSC thermograms was calibrated before using the reference standard of high purity indium and tin. UV–Vis absorption spectra were recorded with a Varian Cary 3 Bio UV−Vis spectrophotometer at room temperature. Photoluminescence spectra in the solution and solid states were recorded with a Perkin−Elmer LS 55 luminescence spectrometer with a xenon lamp light source.

3.4.2. General Procedure for Synthesis of Compounds **1a** and **2a**

The bis(pyrylium salt), **M**, (4.00 g, 4.53 mmol) and aliphatic amine (10.4 mmol, 2.30 equiv based on **M**) was dissolved in DMSO (100 mL) and toluene (10 mL) under nitrogen atmosphere. The solution was stirred at 130−135 ^{o}C for 18 h. The water generated during the reaction was removed by a toluene/water azeotrope. After the reaction completed, the solution was removed under reduced pressure and the viscous residue was washed with water. The crude product was dried *in vacuo* at 80 ^{o}C for 24 h and it was further purified by column chromatography ($CHCl_3$:MeOH = 4.5v:0.5v).

Data for compound **1a**: Anal. Cacld. for $C_{62}H_{60}N_2O_6S_2$ (993.28): C, 74.97; H, 6.09; N, 2.82; S, 6.46. Found: C, 73.65; H, 6.05; N, 2.83; S, 6.09; ^{1}H NMR (400 MHz, $CDCl_3$, ppm) δ = 0.35 (t, 6H, $-CH_2CH_3$), 0.72 (q, 4H, $-CH_2CH_2CH_3$), 1.26 (q, 4H, $-NCH_2CH_2-$), 2.23 (s, 6H, $C_{arom}CH_3$), 4.38 (t, 4H, $-NCH_2CH_2-$), 7.00 (d, 4H, H_{arom}), 7.47−7.51 (m, 12H, H_{arom}), 7.64 (d, 4H, H_{arom}), 7.80 (s, 4H, H_{arom}), 7.86−7.89 (m, 8H, H_{arom}), 7.92 (s, 4H, H_{arom}); ^{13}C NMR (100 MHz, $CDCl_3$, ppm) δ = 12.5, 19.2, 21.2, 31.4, 54.6, 126.0, 127.8, 128.8, 129.1, 129.5, 129.6, 130.8, 132.8, 136.7, 138.5, 144.6, 153.6, 156.4.

Data for compound **2a**: Anal. Cacld. for $C_{70}H_{76}N_2O_6S_2$ (1105.49): C, 76.05; H, 6.93; N, 2.53; S, 5.80. Found: C, 73.69; H, 7.01; N, 2.62; S, 5.69; ^{1}H NMR (400 MHz, $CDCl_3$, ppm) δ = 0.69 (br, 8H, $-CH_{aliphatic}$), 0.81 (t, 6H, $-CH_2CH_3$), 0.86−1.15 (m, 12H, $-CH_{aliphatic}$), 1.33 (t, 4H, $-NCH_2CH_2-$), 2.25 (s, 6H, $C_{arom}CH_3$), 4.38 (t, 4H, $-NCH_2CH_2-$), 7.01 (d, 4H, H_{arom}), 7.50−7.53 (m, 12H, H_{arom}), 7.64 (d, 4H, H_{arom}), 7.85−7.88 (m, 12H, H_{arom}), 7.99 (s, 4H, H_{arom}); ^{13}C NMR (100 MHz, $CDCl_3$, ppm) δ = 14.0, 21.2, 22.4, 25.9, 27.8, 28.4, 29.4, 31.4, 54.8, 125.9, 126.9, 128.4, 129.1, 129.4, 129.6, 130.8, 132.8, 136.8, 138.7, 144.2, 153.6, 156.4.

3.4.3. General Procedure for Synthesis of Compounds **1b-1d−2b-2d**

The compounds **1a** or **2a** were reacted with target counterions through a metathesis reaction in MeOH under reflux. For example, the compound **1a** (430 mg, 0.389 mmol) was dissolved MeOH (20 mL) and excess of lithium triflimide (246 mg, 0.856 mmol) were added. The solution was stirred under reflux for 48 h and the solvent was removed by a rotary evaporator. The remained solid was completely washed water to remove any residual salt. The reaction step was repeated one or two more times until all the tosylate counterions were completely exchanged to triflimide counterions, which was confirmed by ^{1}H NMR spectrum. The washed solid was dried *in vacuo* at 80 ^{o}C for 48 h.

Data for compound **1b**: Anal. Cacld. for $C_{52}H_{46}N_4O_8F_{12}S_4$ (1211.18): C, 51.57; H, 3.83; N, 4.63; S, 10.59. Found: C, 51.71; H, 3.80; N, 4.59; S, 10.64; ^{1}H NMR (400 MHz, $CDCl_3$, ppm) δ = 0.41 (t, 6H, $-CH_2C\mathit{H}_3$), 0.77 (q, 4H, $-CH_2C\mathit{H}_2CH_3$), 1.41 (q, 4H, $-NCH_2C\mathit{H}_2-$), 4.39 (t, 4H, $-NC\mathit{H}_2CH_2-$), 7.54−7.61 (m, 12H, $\mathit{H}_{\mathrm{arom}}$), 7.68−7.71 (m, 8H, $\mathit{H}_{\mathrm{arom}}$), 7.74 (s, 4H, $\mathit{H}_{\mathrm{arom}}$), 7.82 (s, 4H, $\mathit{H}_{\mathrm{arom}}$); ^{19}F NMR (376 MHz, $CDCl_3$, ppm) δ = −78.8; ^{13}C NMR (100 MHz, $CDCl_3$, ppm) δ =12.4, 19.3, 31.5, 54.7, 118.2, 121.4, 124.6, 127.1, 128.9, 129.3, 129.4, 131.2, 132.4, 137.0, 154.1, 156.5.

Data for compound **1c**: Anal. Cacld. for $C_{88}H_{120}N_2O_{14}S_2$ (1494.03): C, 70.74; H, 8.10; N, 1.88; S, 4.29. Found: C, 66.90; H, 8.31; N, 1.67; S, 4.63; ^{1}H NMR (400 MHz, $CDCl_3$, ppm) δ = 0.42 (t, 6H, $-CH_2C\mathit{H}_3$), 0.76−0.89 (m, 32H, $-C\mathit{H}_{\mathrm{aliphatic}}$), 1.22−1.61 (m, 34H, $-C\mathit{H}_{\mathrm{aliphatic}}$), 2.98−3.03 (m, 2H, $-C\mathit{H}_{\mathrm{aliphatic}}$), 3.15−3.22 (m, 2H, $-C\mathit{H}_{\mathrm{aliphatic}}$), 3.87−4.06 (m, 12H, $-C\mathit{H}_{\mathrm{aliphatic}}$), 4.46 (t, 4H, $-NC\mathit{H}_2CH_2-$), 7.54−7.63 (m, 12H, $\mathit{H}_{\mathrm{arom}}$), 7.88−7.91 (m, 8H, $\mathit{H}_{\mathrm{arom}}$), 7.93 (s, 4H, $\mathit{H}_{\mathrm{arom}}$), 8.02 (s, 4H, $\mathit{H}_{\mathrm{arom}}$); ^{13}C NMR (100 MHz, $CDCl_3$, ppm) δ = 10.8−10.9,12.6, 14.0, 14.1, 19.3, 23.0, 23.4, 23.7, 28.8−28.9, 30.0 (d), 30.3 (d), 31.6, 34.1, 38.4, 38.5, 28.6, 38.7, 46.6, 54.7, 61.1, 67.0, 67.8, 126.8, 129.2, 129.5, 129.7, 130.9, 132.8, 136.8, 153.7, 156.6, 169.3, 171.8.

Data for compound **1d**: Anal. Cacld. for $C_{76}H_{74}N_8O_6S_2$ (1259.58): C, 72.47; H, 5.92; N, 8.90; S, 5.09. Found: C, 70.75; H, 6.04; N, 8.36; S, 4.73; ^{1}H NMR (400 MHz, $CDCl_3$, ppm) δ = 0.36 (t, 6H, $-CH_2C\mathit{H}_3$), 0.72 (m, 4H, $-CH_2C\mathit{H}_2CH_3$), 1.29 (br, 4H, $-NCH_2C\mathit{H}_2-$), 3.07 (s, 12H, $-N(C\mathit{H}_3)_2$), 4.39 (t, 4H, $-NC\mathit{H}_2CH_2-$), 6.71 (d, 2H, $\mathit{H}_{\mathrm{arom}}$), 7.51−7.63 (m, 12H, $\mathit{H}_{\mathrm{arom}}$), 7.63 (d, 2H, $\mathit{H}_{\mathrm{arom}}$), 7.78−7.87 (m, 24H, $\mathit{H}_{\mathrm{arom}}$); ^{13}C NMR (100 MHz, $CDCl_3$, ppm) δ =12.5, 19.2, 31.5, 40.3, 54.6, 121.6, 125.0, 126.6, 126.9, 129.2, 120.4, 129.5, 130.1, 132.7, 136.5, 143.5, 147.9, 152.5, 153.0, 153.4, 156.4.

Data for compound **2b**: Anal. Cacld. for $C_{60}H_{62}N_4O_8F_{12}S_4$ (1323.40): C, 54.45; H, 4.72; N, 4.23; S, 9.69. Found: C, 54.39; H, 4.74; N, 4.04; S, 9.45; ^{1}H NMR (400 MHz, $CDCl_3$, ppm) δ = 0.73 (br, 8H, $-CH_{aliphatic}$), 0.81 (t, 6H, $-CH_2CH_3$), 0.86−1.17 (m, 12H, $-CH_{aliphatic}$), 1.42 (t, 4H, $-NCH_2CH_2-$), 4.29 (t, 4H, $-NCH_2CH_2-$), 7.52−7.60 (m, 12H, H_{arom}), 7.67−7.71 (m, 8H, H_{arom}), 7.74 (s, 4H, H_{arom}), 7.81 (s, 4H, H_{arom}); ^{19}F NMR (376 MHz, $CDCl_3$, ppm) δ = −78.8; ^{13}C NMR (100 MHz, $CDCl_3$, ppm) δ =14.0, 22.4, 26.0, 27.8, 28.4, 29.5, 31.4, 54.9, 115.0, 118.2, 121.4, 127.1, 128.9, 129.3, 129.4, 131.2, 132.4, 137.0, 154.1, 156.5.

Data for compound **2c**: Anal. Cacld. for $C_{96}H_{136}N_2O_{14}S_4$ (1606.24): C, 71.78; H, 8.53; N, 1.74; S, 3.99. Found: C, 68.74; H, 8.61; N, 1.68; S, 4.31; ^{1}H NMR (400 MHz, $CDCl_3$, ppm) δ = 0.73 (br, 8H, $-CH_{aliphatic}$), 0.79−1.60 (m, 80H, $-CH_{aliphatic}$), 2.98−3.03 (m, 2H, $-CH_{aliphatic}$), 3.15−3.22 (m, 2H, $-CH_{aliphatic}$), 3.87−4.06 (m, 12H, $-CH_{aliphatic}$), 4.43 (t, 4H, $-NCH_2CH_2-$), 7.52−7.62 (m, 12H, H_{arom}), 7.87 (d, 8H, H_{arom}), 7.93 (s, 4H, H_{arom}), 8.02 (s, 4H, H_{arom}); ^{13}C NMR (100 MHz, $CDCl_3$, ppm) δ =10.8 (d), 10.9 (d), 14.0, 14.1 (d), 22.4, 23.0, 23.4, 23.6, 26.0, 27.9, 28.5, 28.8 (d), 28.9, 29.6, 30.0, 30.1, 30.3 (d), 34.2, 38.4, 38.5, 38.7 (d), 55.0, 61.8, 67.0, 67.7 (d), 126.9, 129.2, 129.4, 129.7, 130.9, 132.8, 136.9, 153.8, 156.6, 169.2, 171.7.

Data for compound **2d**: Anal. Cacld. for $C_{84}H_{90}N_8O_6S_2$ (1371.79): C, 73.55; H, 6.61; N, 8.17; S, 4.67. Found: C, 73.04; H, 6.70; N, 8.05; S, 4.59; ^{1}H NMR (400 MHz, $CDCl_3$, ppm) δ = 0.68 (br, 8H, $-CH_{aliphatic}$), 0.80 (t, 6H, $-CH_2CH_3$), 0.86−1.00 (m, 8H, $-CH_{aliphatic}$), 1.14, (q, 4H, $-NCH_2CH_2CH_2-$), 1.32 (br, 4H, $-NCH_2CH_2-$), 3.06 (s, 12H, $-N(CH_3)_2$), 4.37 (t, 4H, $-NCH_2CH_2-$), 6.69 (d, 4H, H_{arom}), 7.52 (m, 12H, H_{arom}), 7.63 (d, 4H, H_{arom}), 7.78−7.86 (m, 20H, H_{arom}), 7.90 (s, 4H, H_{arom}); ^{13}C NMR (100 MHz, $CDCl_3$, ppm) δ = 14.0, 22.4, 25.9, 27.8, 28.5, 29.4, 31.4, 40.3, 54.8, 111.5, 121.6, 125.0, 126.0, 126.6, 126.8, 128.3, 129.2, 129.4, 129.5, 130.9, 132.7, 136.6, 143.5, 147.9, 152.5, 153.0, 153.4, 156.4.

3.5. Conclusions

A series of bis(pyridinium salt)s with different alkyl chain lengths and organic counterions were prepared via the ring-transmutation and metathesis reactions. The chemical structures of synthesized organic salts were fully characterized by ^{1}H, ^{19}F, and ^{13}C NMR spectroscopy techniques and elemental analysis. All of the organic salts had excellent thermal stabilities (> 200 ^{o}C), dicationic salts with long octyl group exhibited lower thermal stabilities than those with butyl group. Some of bis(pyridinium salt)s displayed amorphous properties based on the DSC analyses while some showed ionic liquid properties. Because of the presence of chromophores, the photoactive properties of these salts were examined by UV−Vis and photoluminescence spectroscopy. No significant differences in their UV−Vis spectra were found suggesting an indication of closely spaced π–π^* transitions and they emitted blue light in the various organic solvents and in the solid states. In the solutions, they usually emitted blue light; and majority of them exhibited no positive solvatochromic effect. Their λ_{em} peaks were shifted hypsochromically in the solid states when compared with those of their solution spectra. Due to the pH indicating property of MO counterions, bis(pyridinium salt)s with MO showed different visual color change properties in several organic solvents with the variation of concentrations of HOTf.

APPENDIX 1

SUPPLEMENTARY INFORMATION FOR CHATPER 1

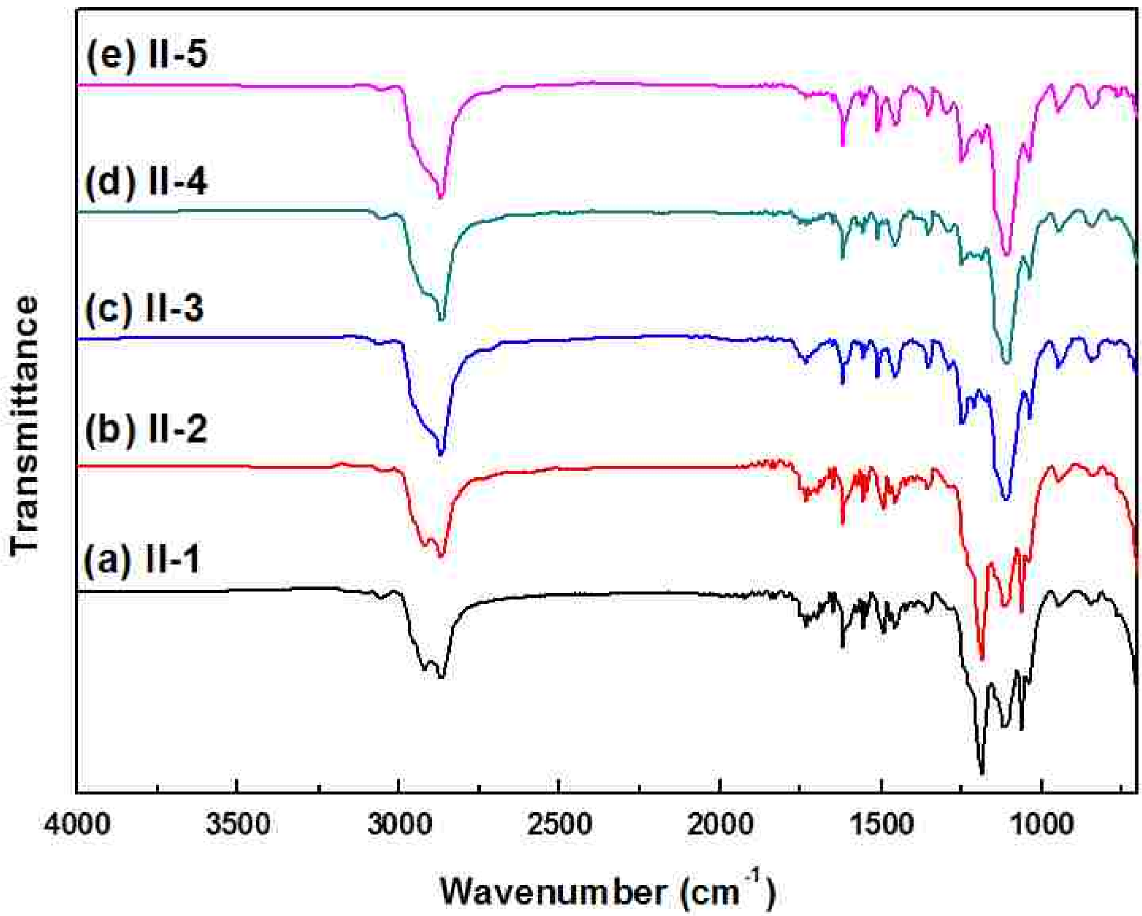

Figure S1. FTIR spectra of polymers **II-1−II-5** taken at room temperature.

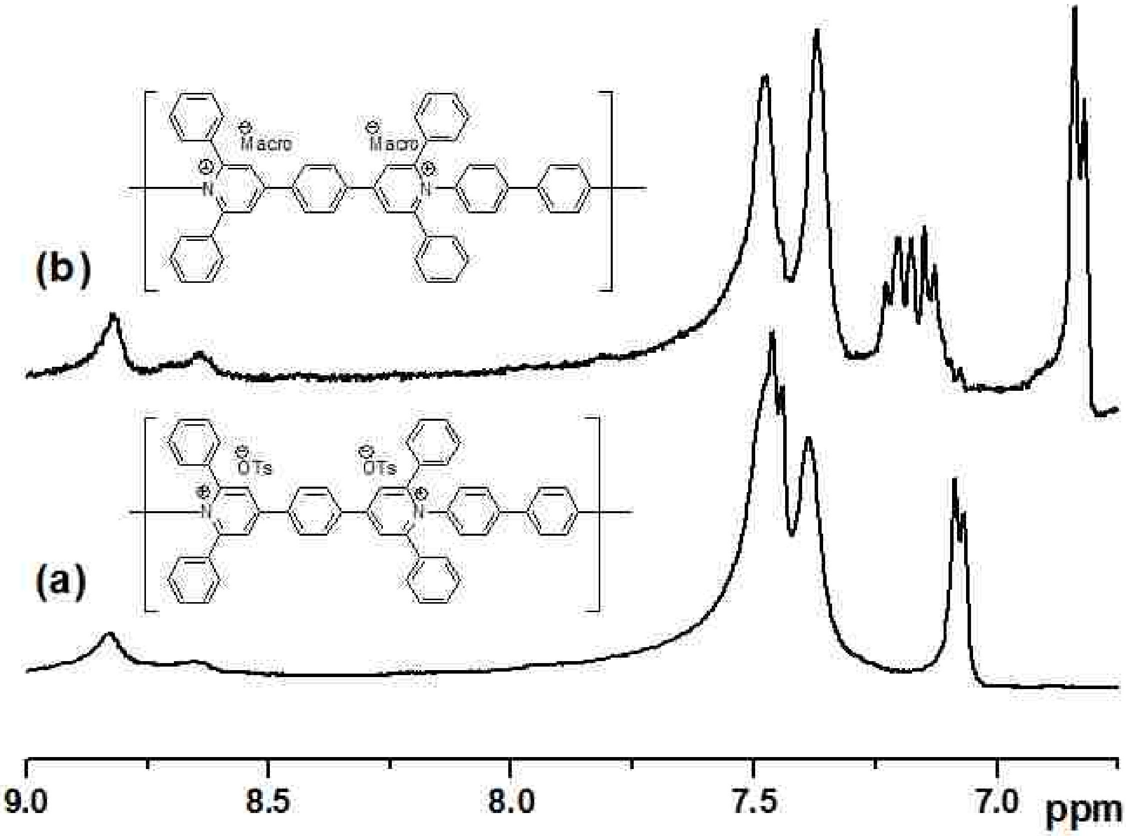

Figure S2. Expanded ^{1}H NMR spectra [delay time = 1 s, number of scans = 16] of polymers (a) **I-1** and (b) **II-1** [10 mg/mL in d_6-DMSO at 25 ^{o}C].

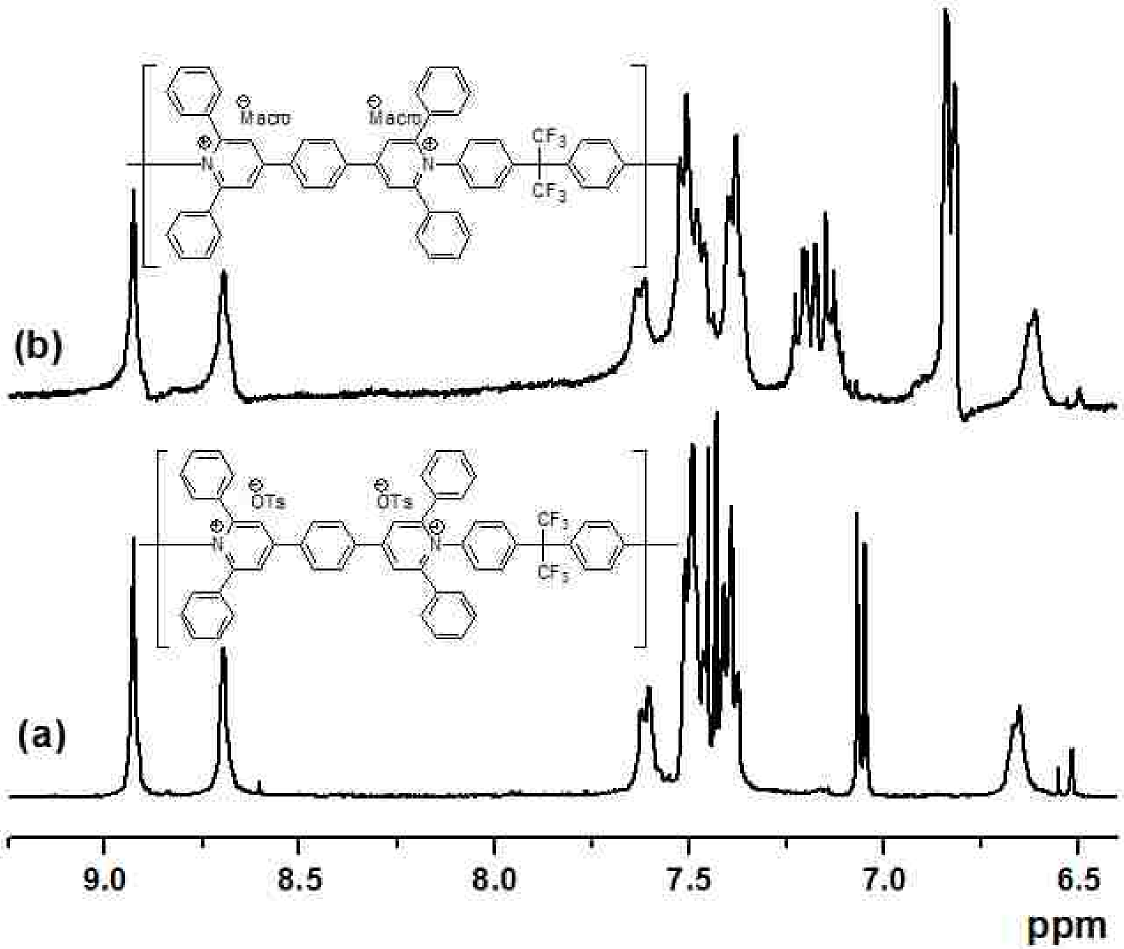

Figure S3. Expanded [1]H NMR spectra [delay time = 1 s, number of scans = 16] of polymers (a) **I-3** and (b) **II-3** [10 mg/mL in d_6-DMSO at 25 ^{o}C].

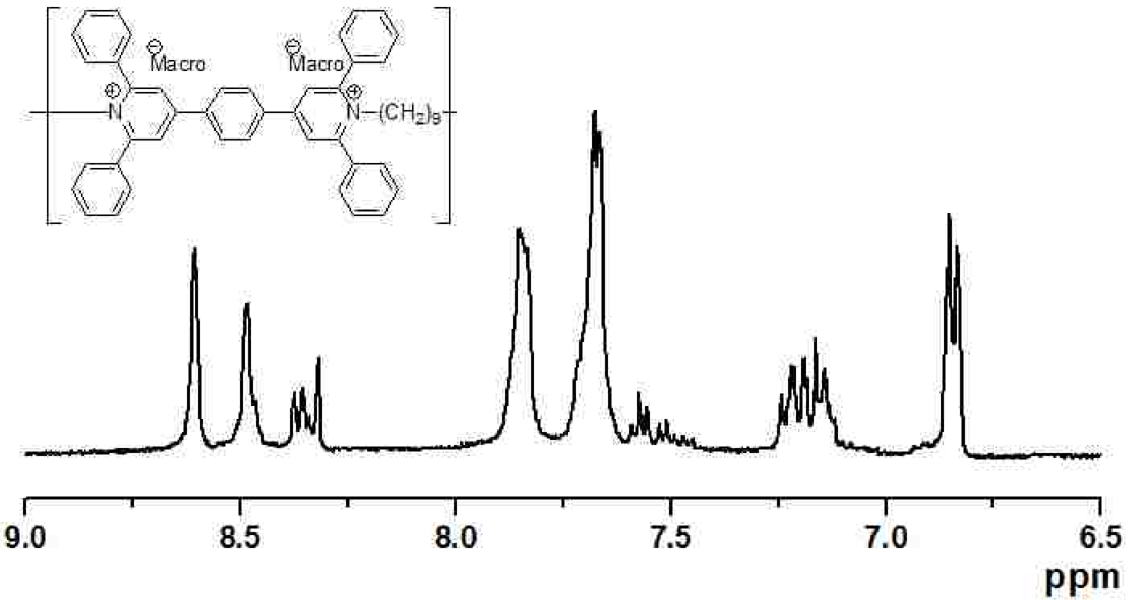

Figure S4. Expanded [1]H NMR spectrum [delay time = 1 s, number of scans = 16] of polymer **II-4** [10 mg/mL in d_6-DMSO at 25 °C].

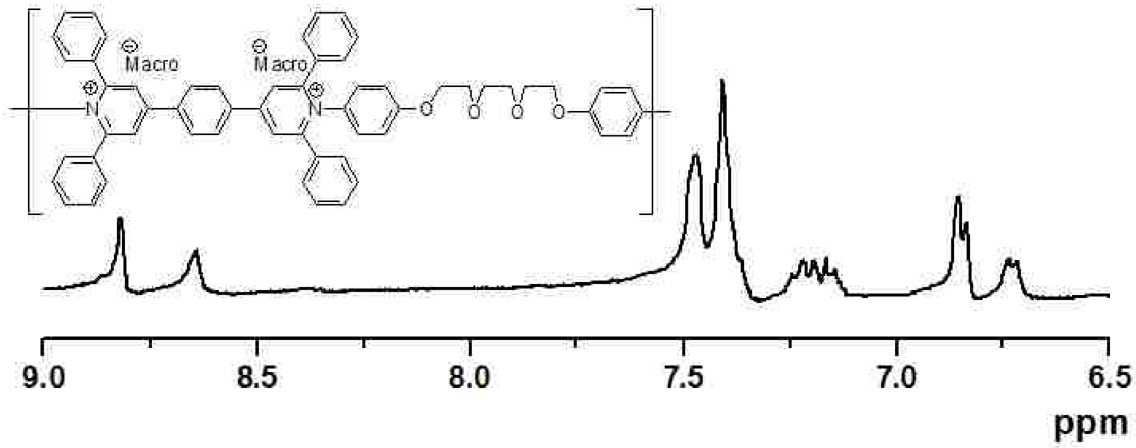

Figure S5. Expanded ^{1}H NMR spectrum [delay time = 1 s, number of scans = 16] of polymer **II-5** [10 mg/mL in d_6-DMSO at 25 ^{o}C].

APPENDIX 2

SUPPLIMENTARY INFORMATION FOR CHATPER 2

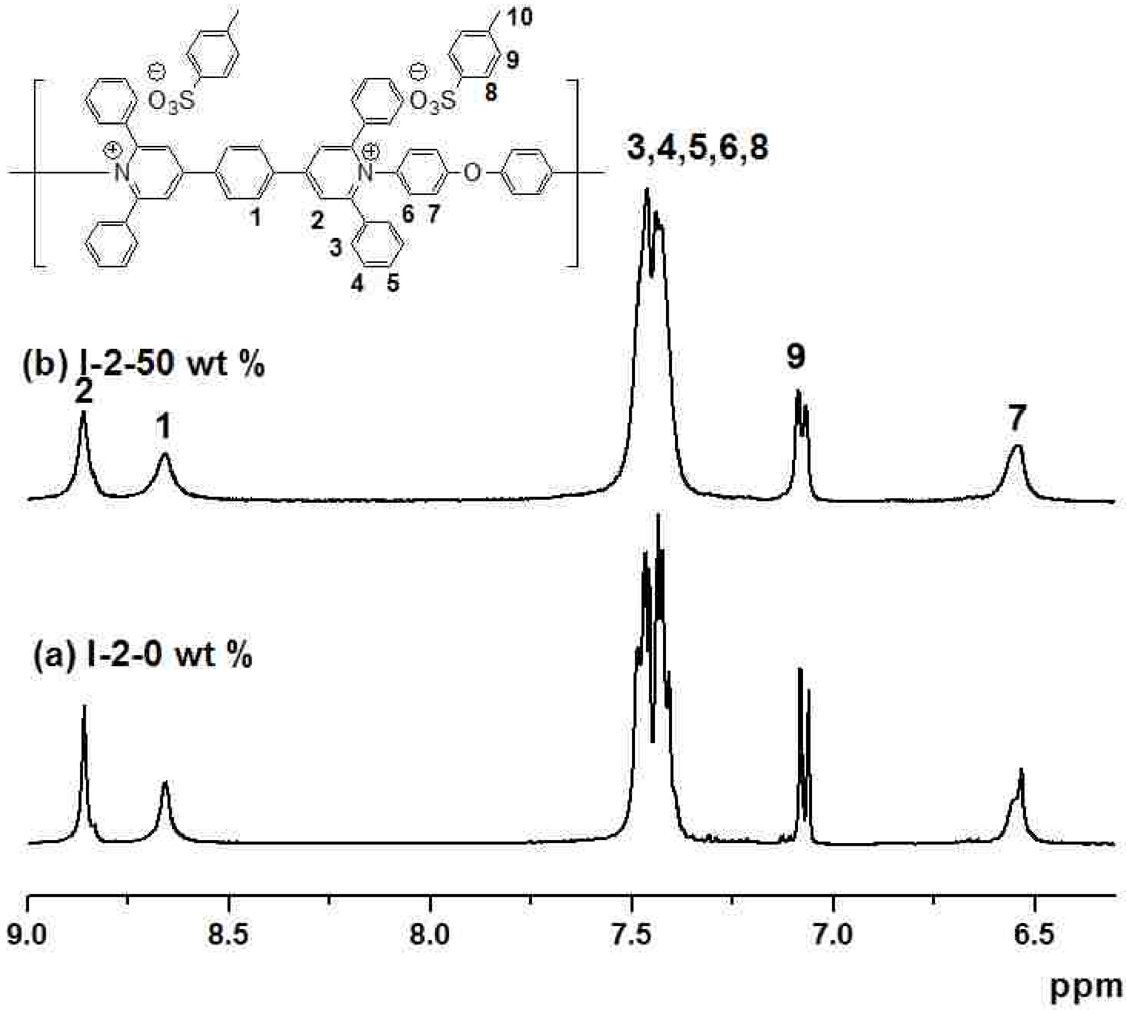

Figure S1. ^{1}H NMR spectra of **I-2**/SWNT composites (delay time = 1 s, number of scans = 16): (a) **I-2** (10 mg/mL in d_6-DMSO); and (b) **I-2**-50 wt % (10 mg/mL in d_6-DMSO).

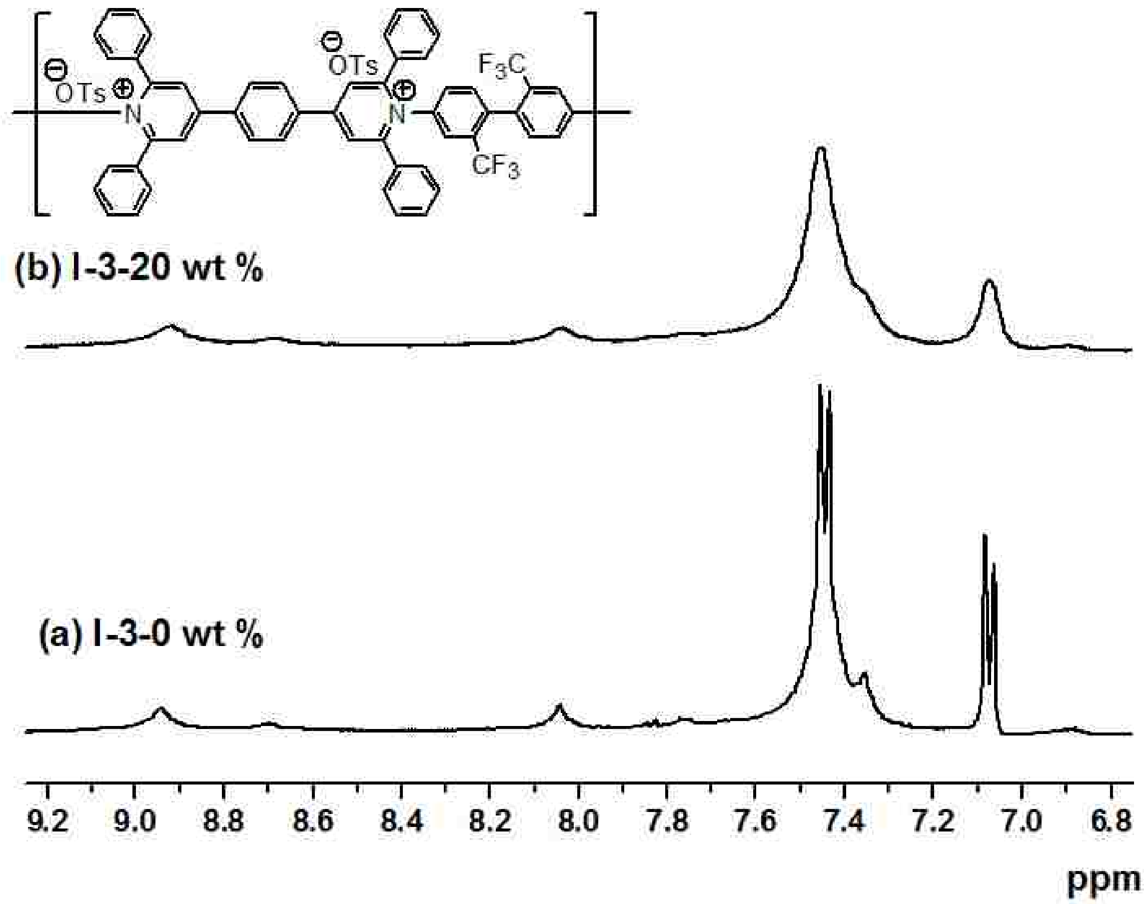

Figure S2. ^{1}H NMR spectra of **I-3**/SWNTs composites (delay time = 1 s, number of scans = 16): (a) **I-3** (10 mg/mL in d_6-DMSO); and (b) **I-3**-20 wt % (10 mg/mL in d_6-DMSO).

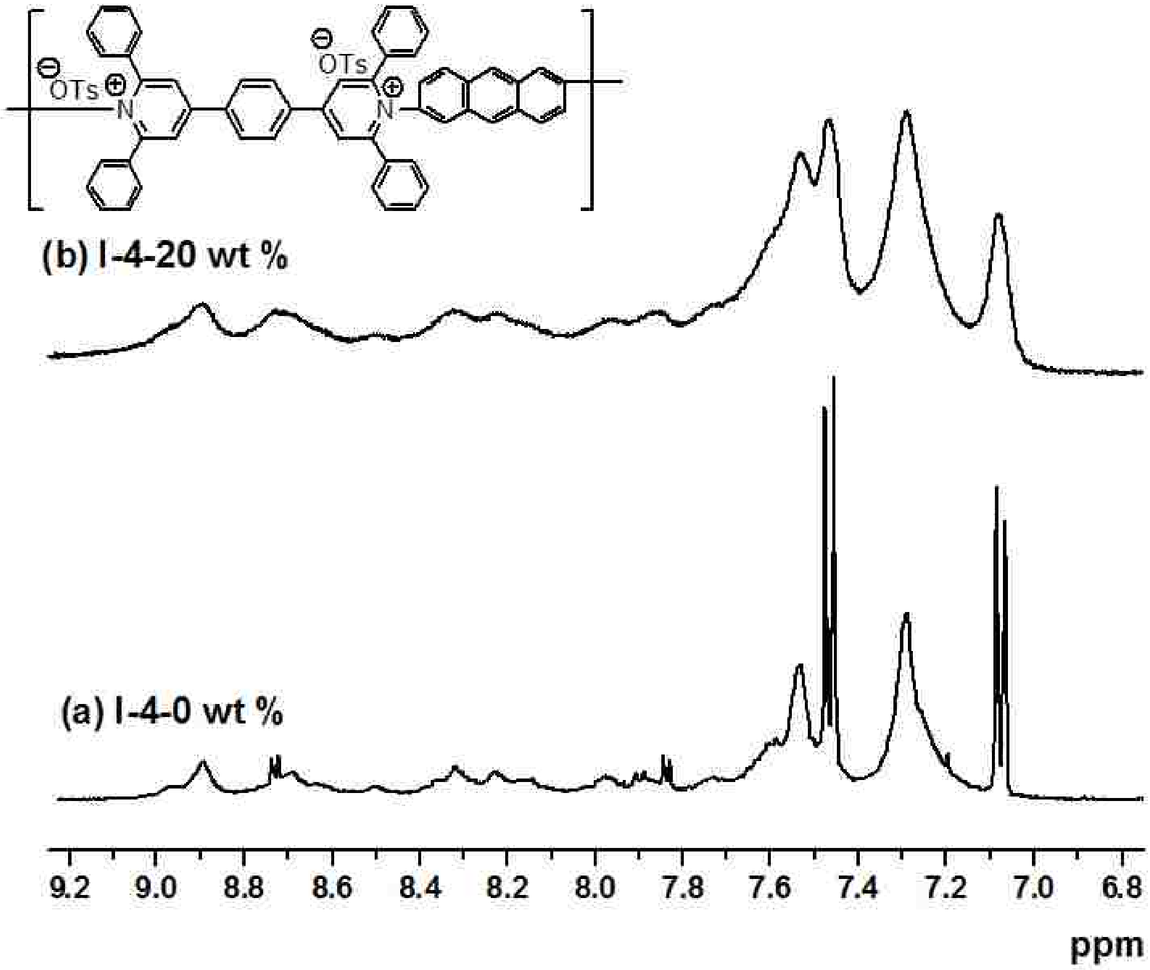

Figure S3. ^{1}H NMR spectra of **I-4**/SWNTs composites (delay time = 1 s, number of scans = 16): (a) **I-4** (10 mg/mL in d_6-DMSO); and (b) **I-4**-20 wt % (10 mg/mL in d_6-DMSO).

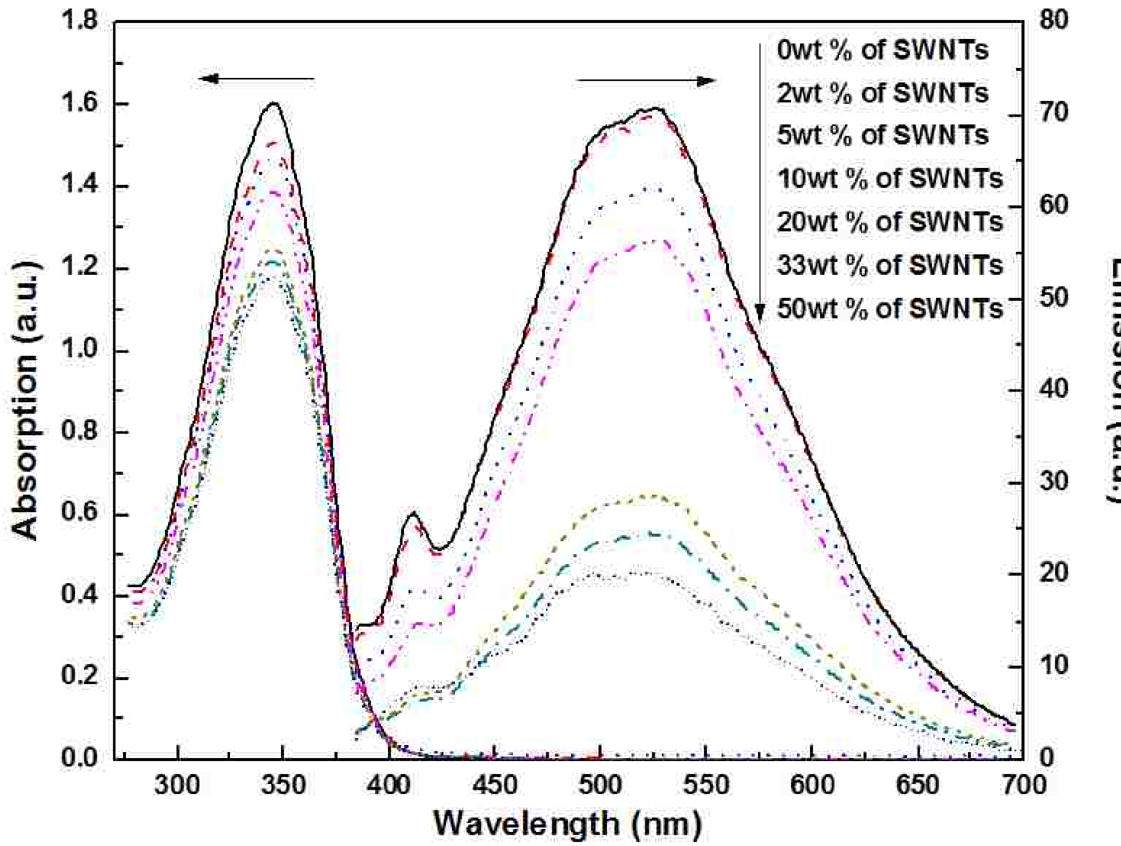

Figure S4. UV–Vis absorption spectra of **I-2**/SWNT composites in DMSO (left arrow) and emission spectra of **I-2**/SWNT composites at excitation wavelength of 364 nm in DMSO (right arrow).

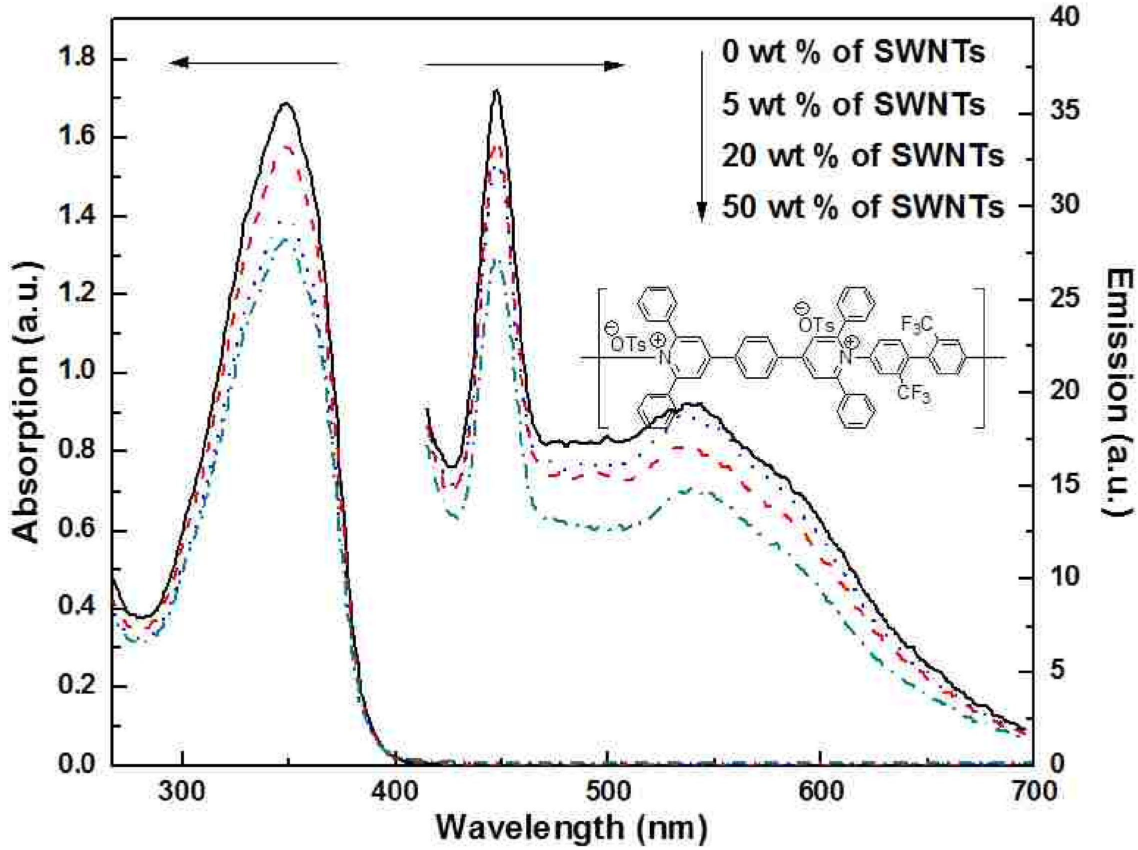

Figure S5. UV–Vis absorption spectra of **I-3**/SWNTs composites in DMSO (left arrow) and emission spectra of **I-3**/SWNTs composites at excitation wavelength of 395 nm in DMSO (right arrow).

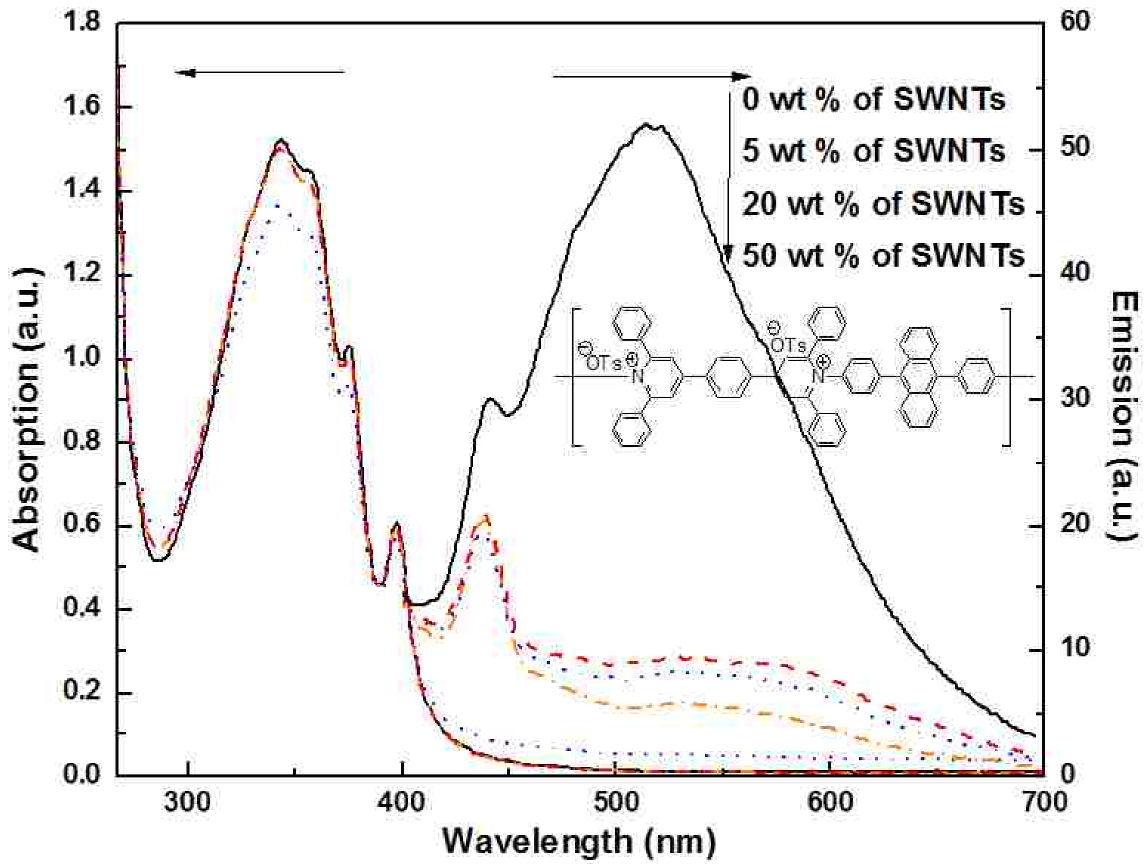

Figure S6. UV–Vis absorption spectra of **I-5**/SWNTs composites in DMSO (left arrow) and emission spectra of **I-5**/SWNTs composites at excitation wavelength of 403 nm in DMSO (right arrow).

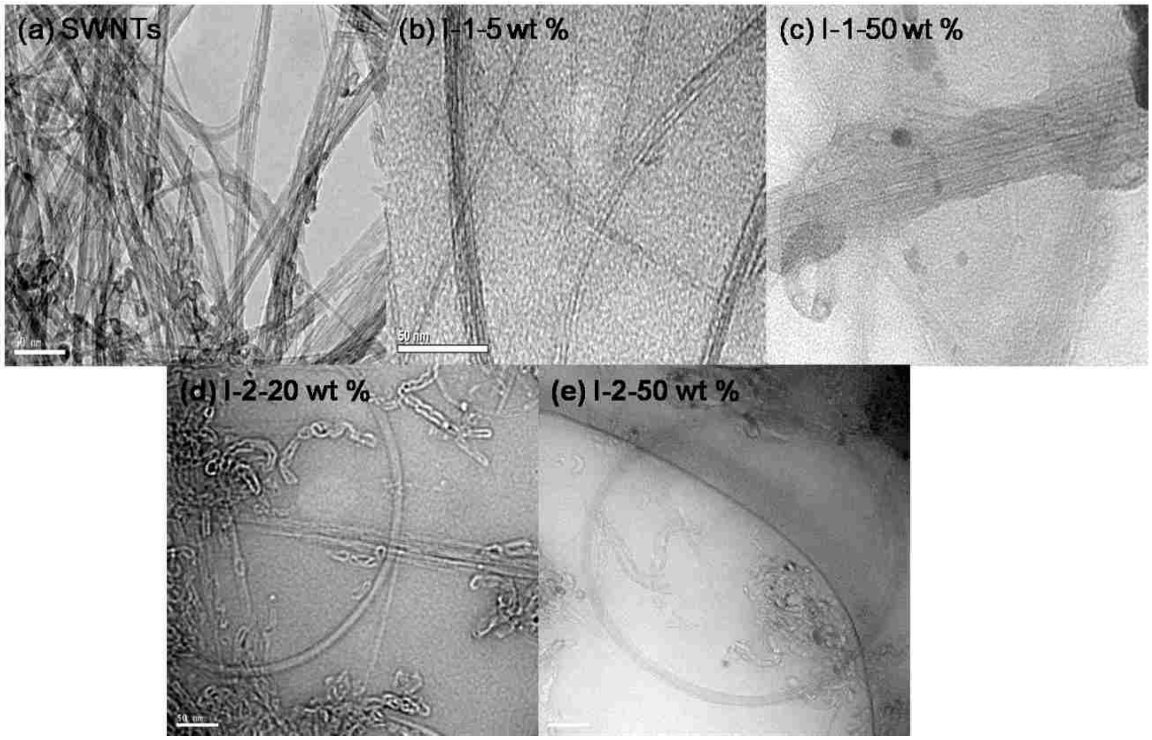

Figure S7. TEM images of (a) SWNTs, (b) **I-1**-20 wt %, (c) **I-1**-50 wt %, (d) **I-2**-20 wt % and (e) **I-2**-50 wt %.

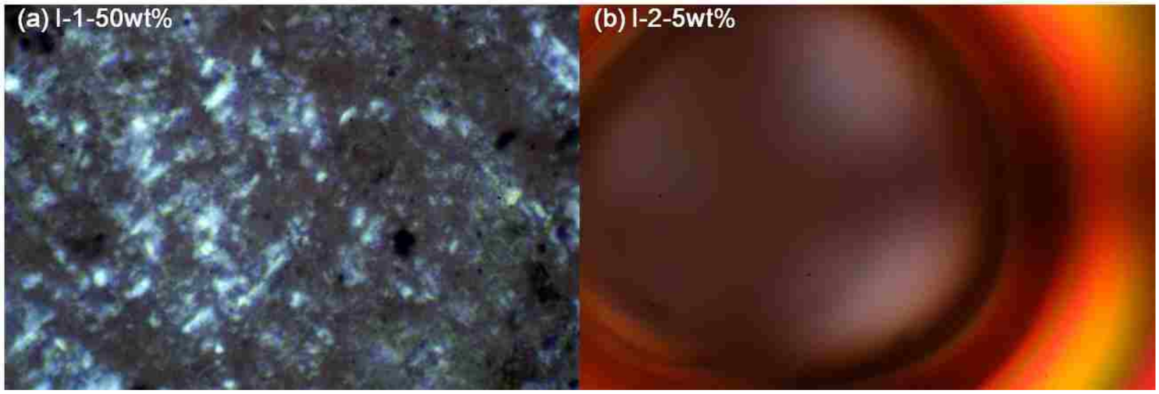

Figure S8. Photomicrographs of (a) **I-1**-50 wt %, and (b) **I-2**-5 wt % taken under crossed polarizers at room temperature exhibiting lyotropic solutions (magnification 400×).

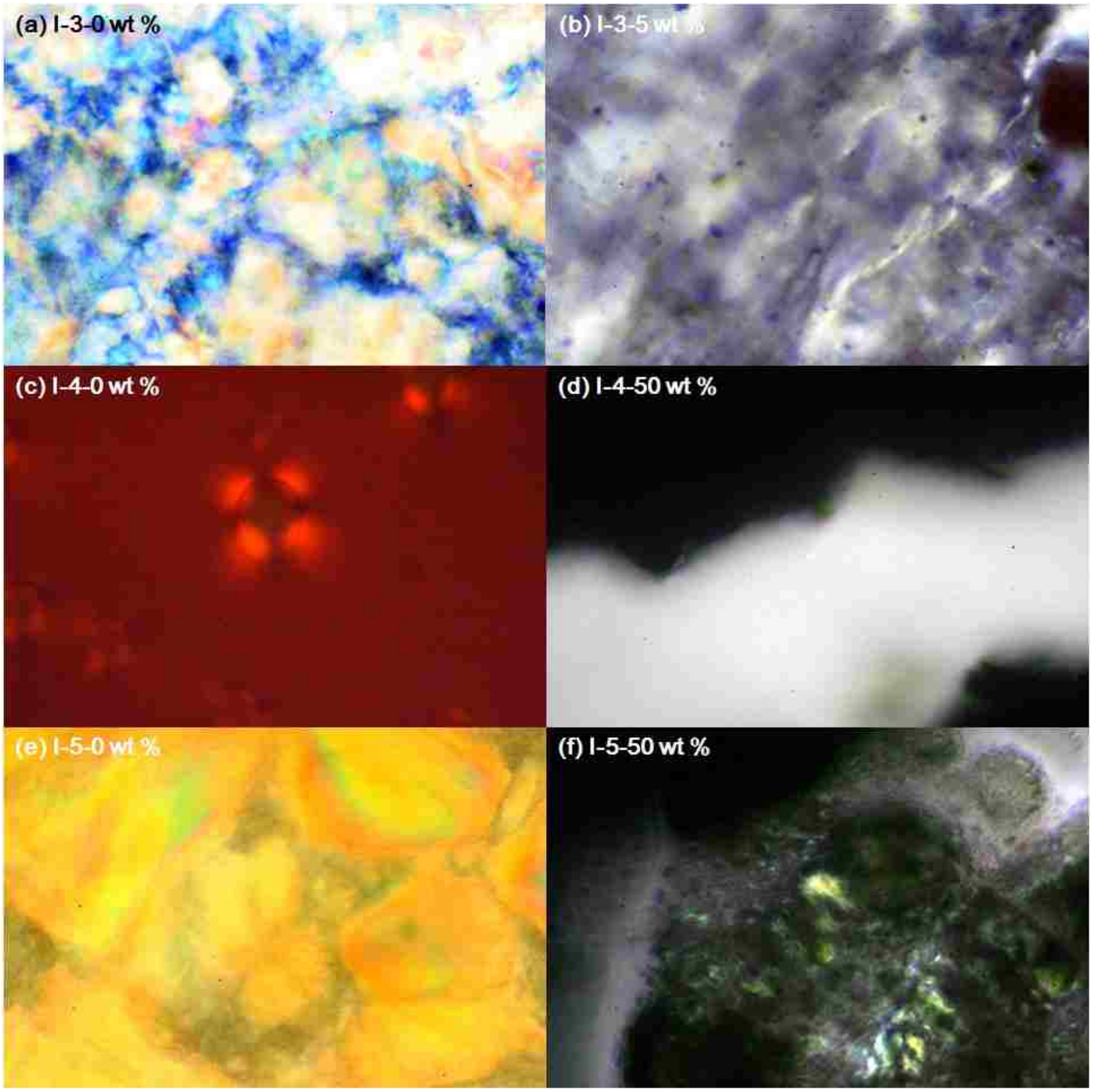

Figure S9. Photomicrographs of (a) composite **I-3**-0 wt % SWNTs 20 wt % in DMSO, (b) composite **I-3**-5 wt % SWNTs 20 wt % in DMSO, (c) composite **I-4**-0 wt % SWNTs in 40 wt % DMSO, (d) composite **I-4**-50 wt % SWNTs 40 wt % in DMSO, (e) composite **I-5**-0 wt % SWNTs 20 wt % in DMSO, and (f) composite **I-5**-50 wt % SWNTs 20 wt % in DMSO under crossed polarizers exhibiting lyotropic LC phase, respectively (magnification 400x).

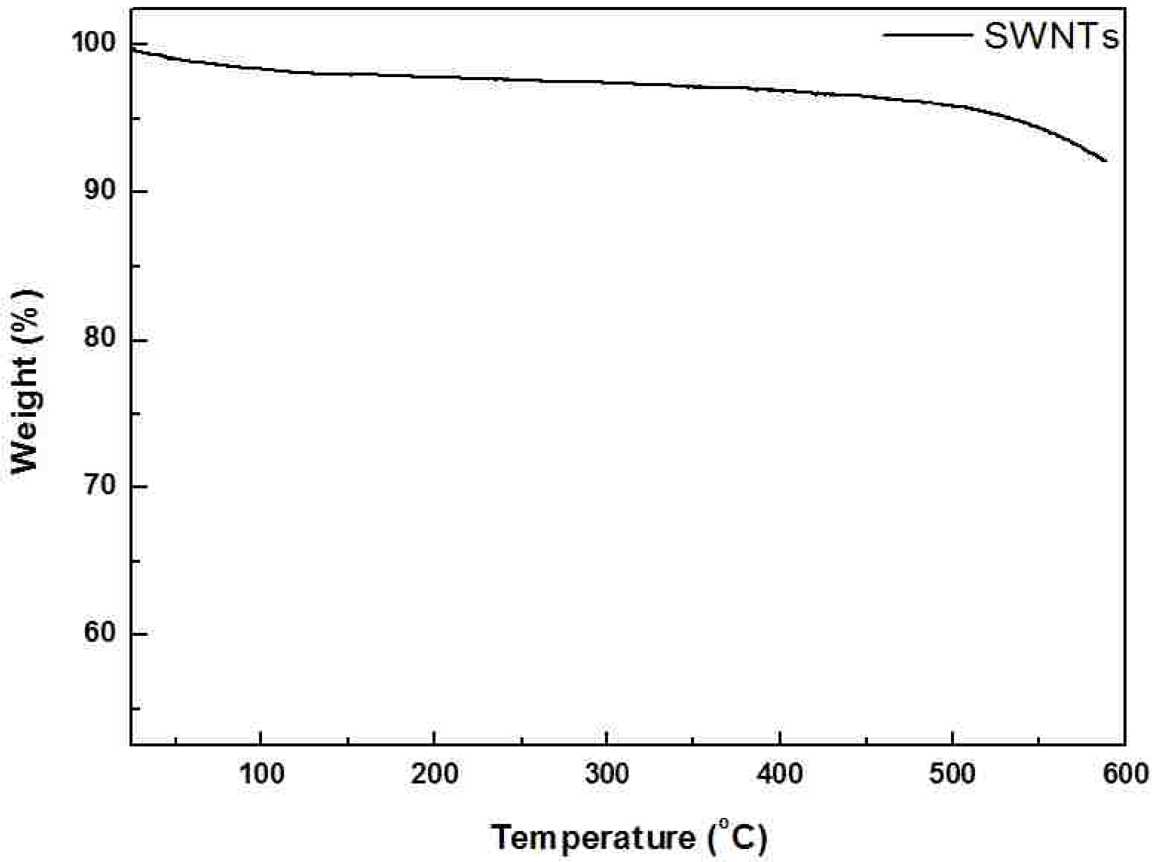

Figure S10. TGA thermogram of the SWNTs obtained at a heating rate of 10 ^{o}C/min in nitrogen.

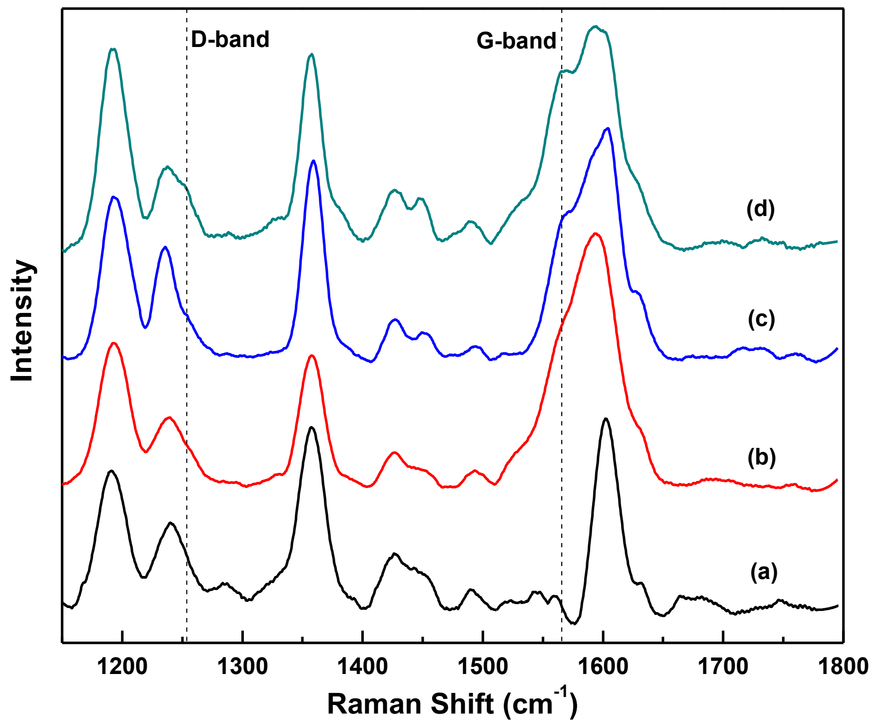

Figure S11. Raman spectra of (a) **I-1**, (b) **I-1**-20 wt %, (c) **I-1**-33 wt %, and (d) **I-1**-50 wt %.

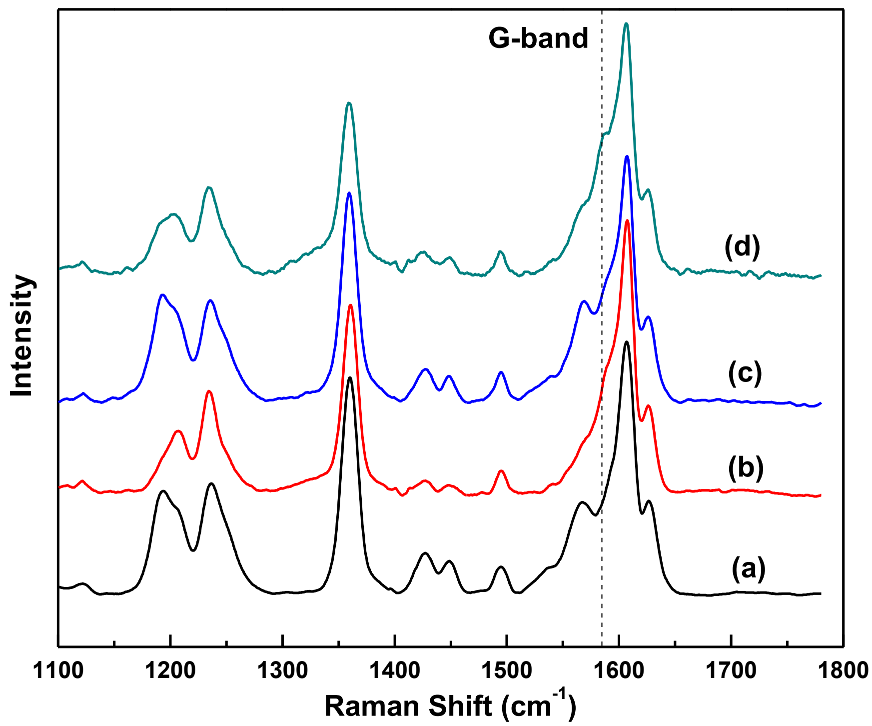

Figure S12. Raman spectra of (a) **I-2**, (b) **I-2**-20 wt %, (c) **I-2**-33 wt %, and (d) **I-2**-50 wt %.

APPENDIX 3

SUPPLIMENTARY INFORMATION FOR CHATPER 3

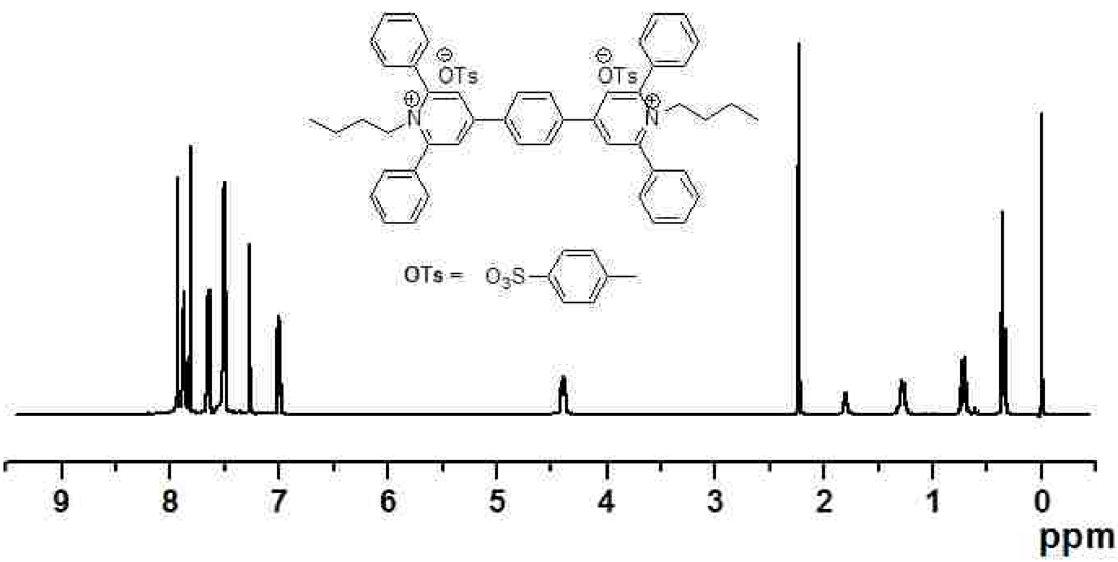

Figure S1. ^{1}H NMR spectrum of **1a** [delay time = 1 s, number of scans = 16; 10 mg/mL in $CDCl_3$ at 25 ^{o}C].

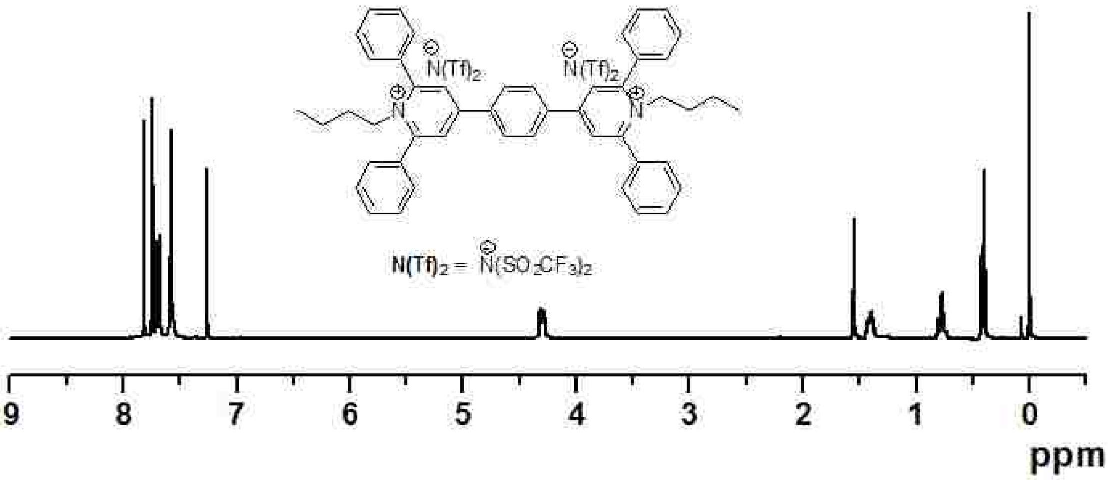

Figure S2. ^{1}H NMR spectrum of **1b** [delay time = 1 s, number of scans = 16; 10 mg/mL in $CDCl_3$ at 25 ^{o}C].

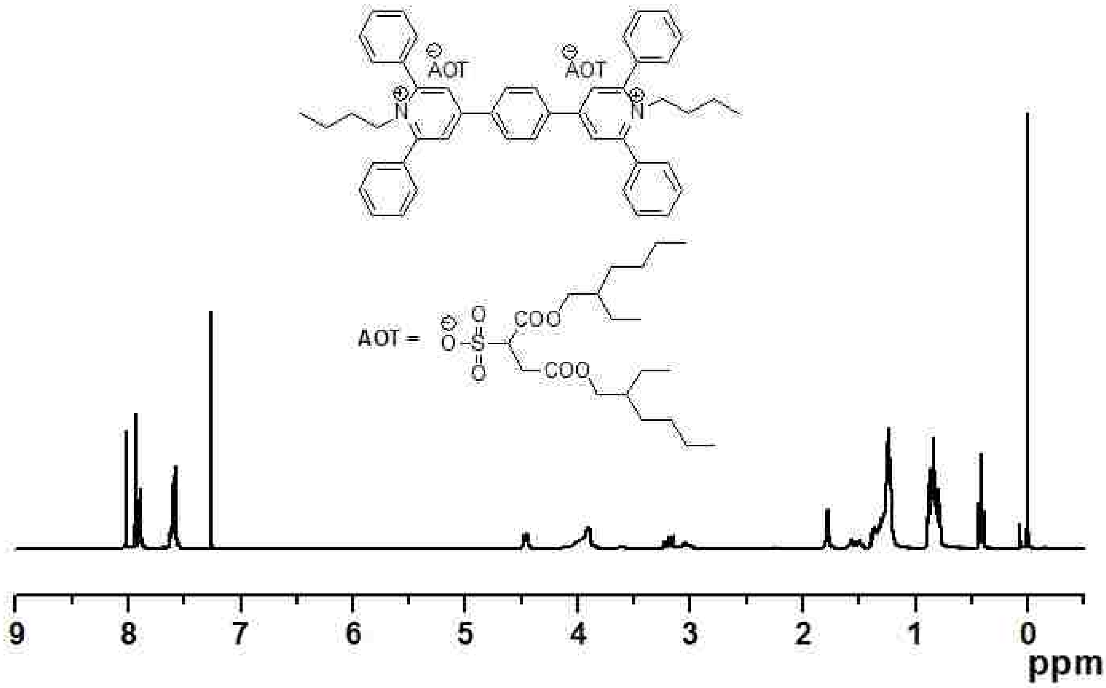

Figure S3. ^{1}H NMR spectrum of **1c** [delay time = 1 s, number of scans = 16; 10 mg/mL in $CDCl_3$ at 25 ^{o}C].

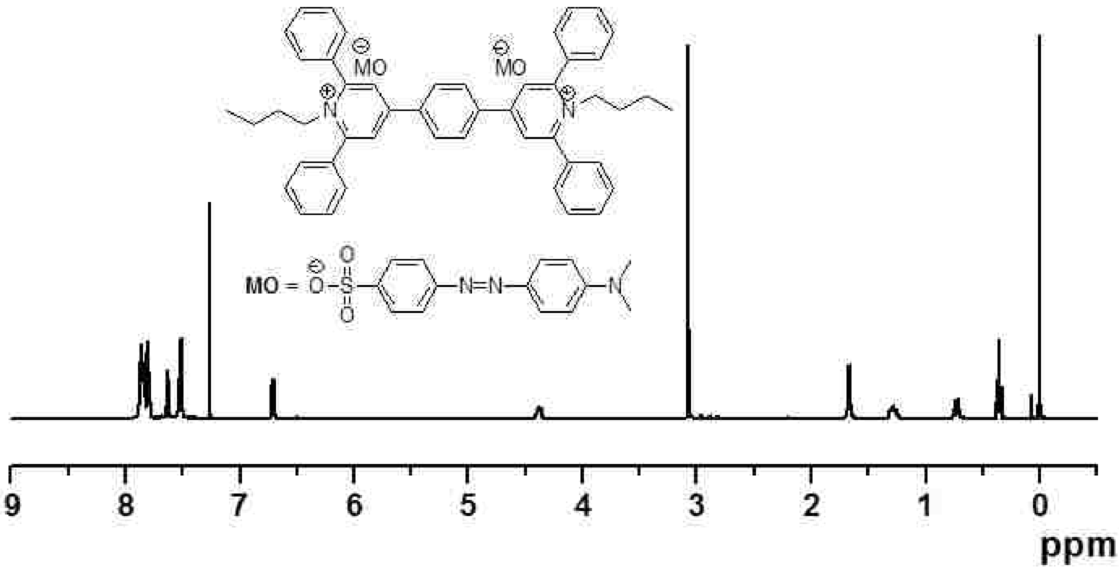

Figure S4. ^{1}H NMR spectrum of **1d** [delay time = 1 s, number of scans = 16; 10 mg/mL in $CDCl_3$ at 25 ^{o}C].

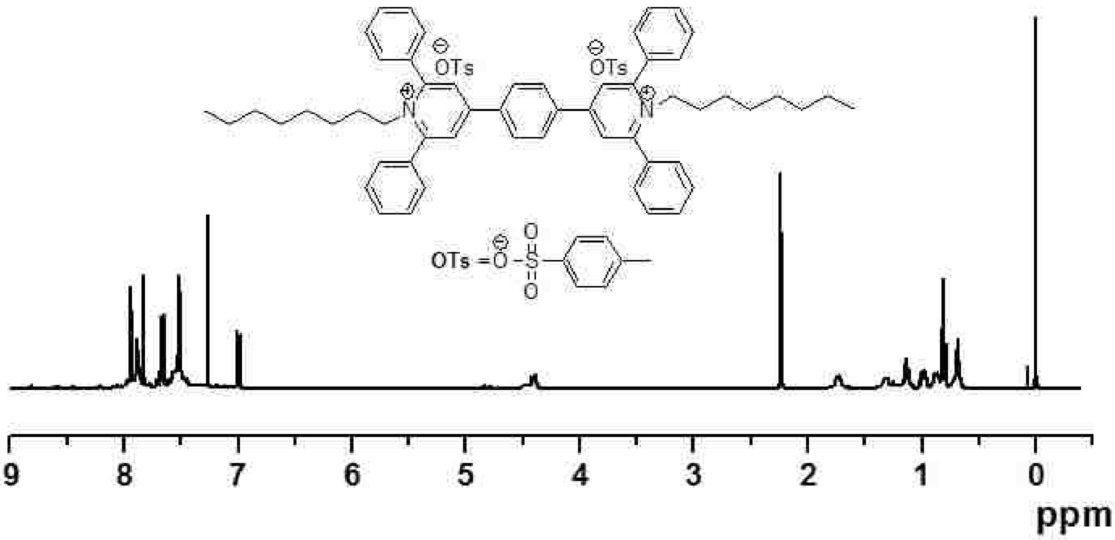

Figure S5. ^{1}H NMR spectrum of **2a** [delay time = 1 s, number of scans = 16; 10 mg/mL in $CDCl_3$ at 25 ^{o}C].

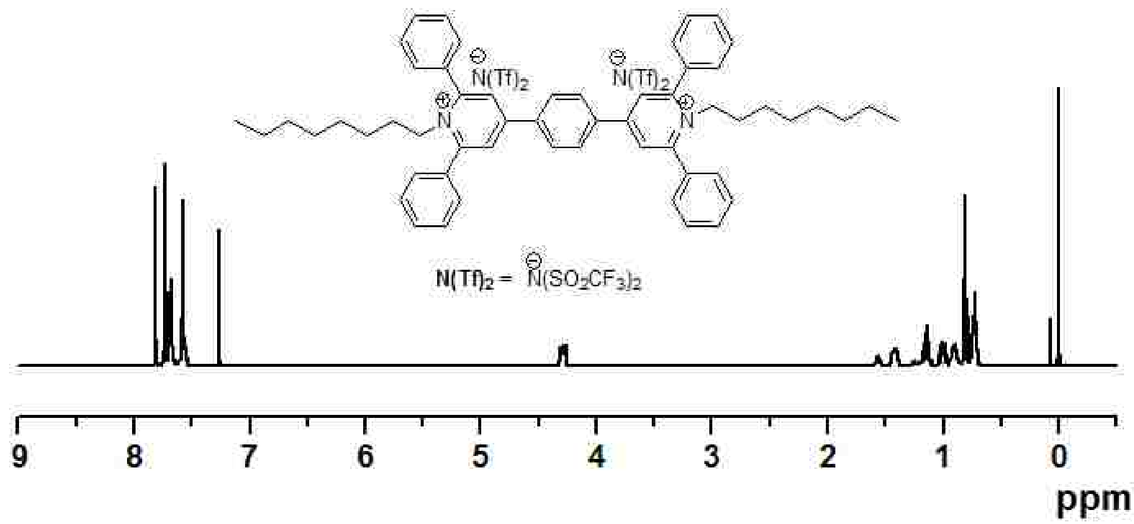

Figure S6. ^{1}H NMR spectrum of **2b** [delay time = 1 s, number of scans = 16; 10 mg/mL in $CDCl_3$ at 25 ^oC].

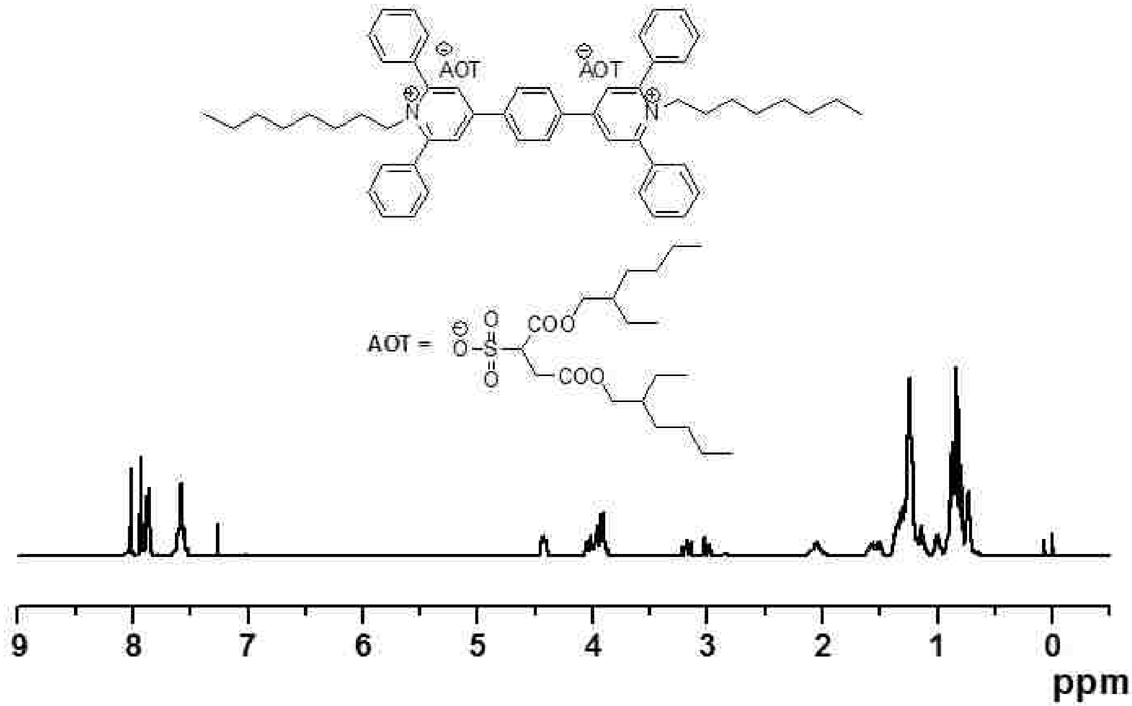

Figure S7. ^{1}H NMR spectrum of **2c** [delay time = 1 s, number of scans = 16; 10 mg/mL in $CDCl_3$ at 25 ^{o}C].

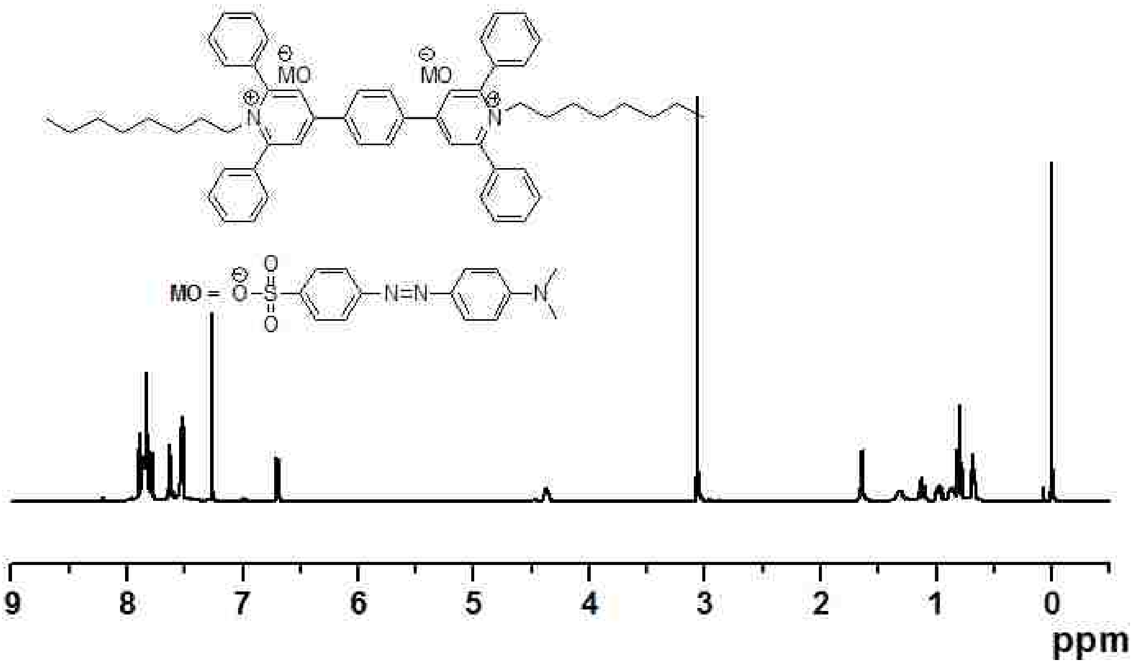

Figure S8. ^{1}H NMR spectrum of **2d** [delay time = 1 s, number of scans = 16; 10 mg/mL in $CDCl_3$ at 25 ^{o}C].

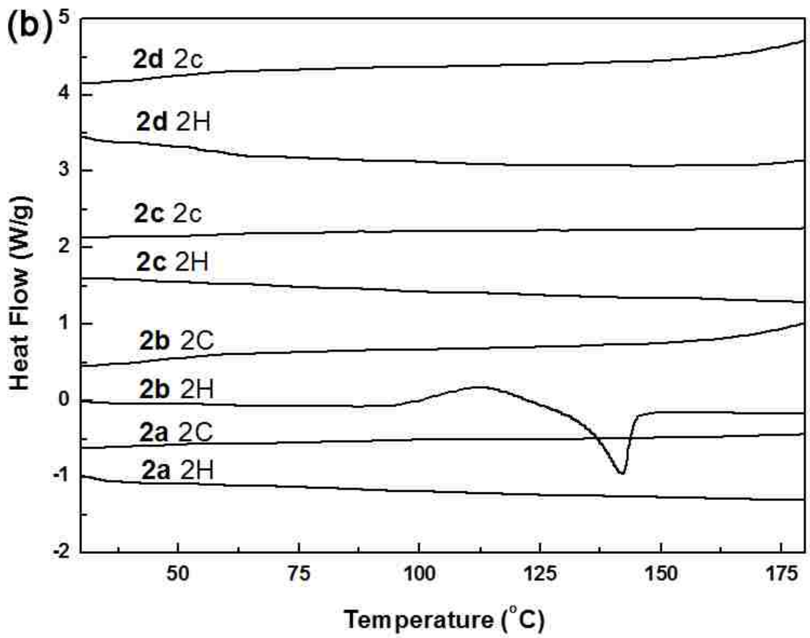

Figure S9. DSC thermograms of **2a−d** obtained from (a) 1st and (b) 2nd heating and cooling cycles at a rate of 10 ^{o}C/min in nitrogen.

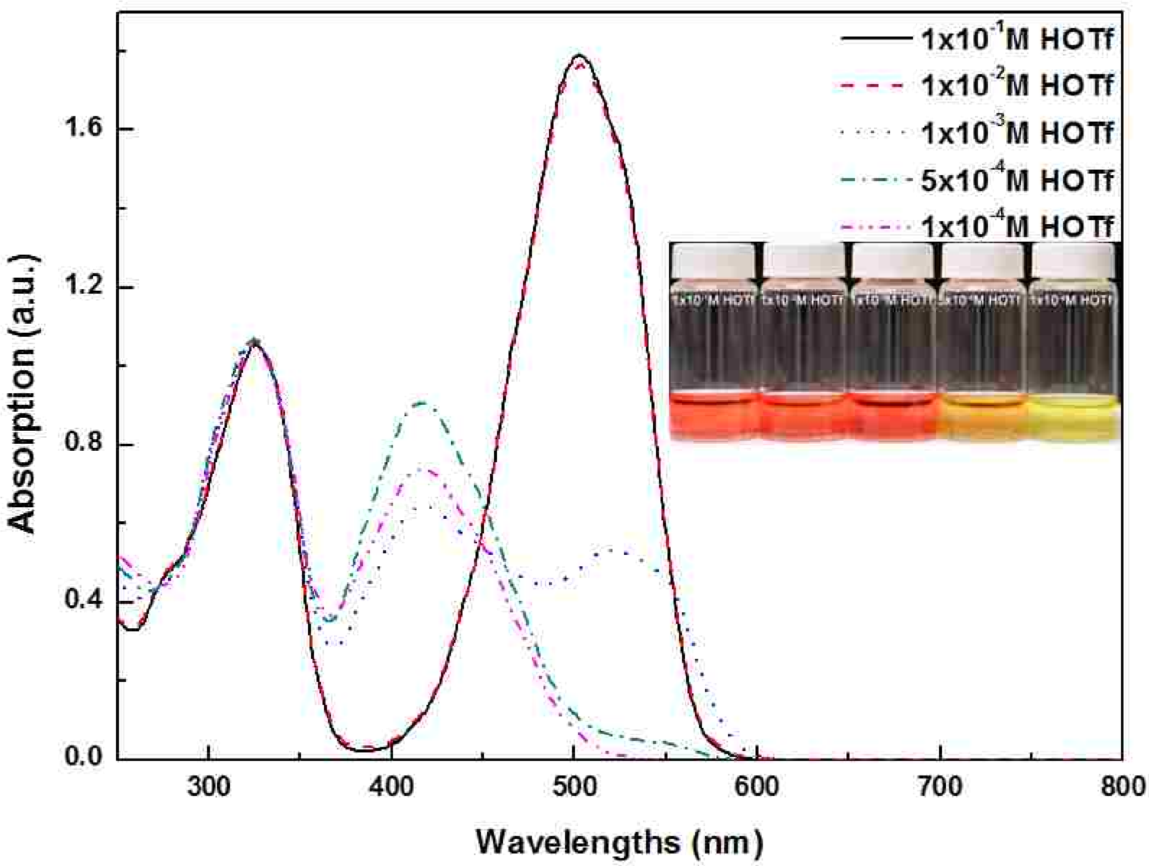

Figure S10. UV−Vis spectra of **1d** (2×10^{-5} M) in CH_3CN with varied HOTf concentrations.

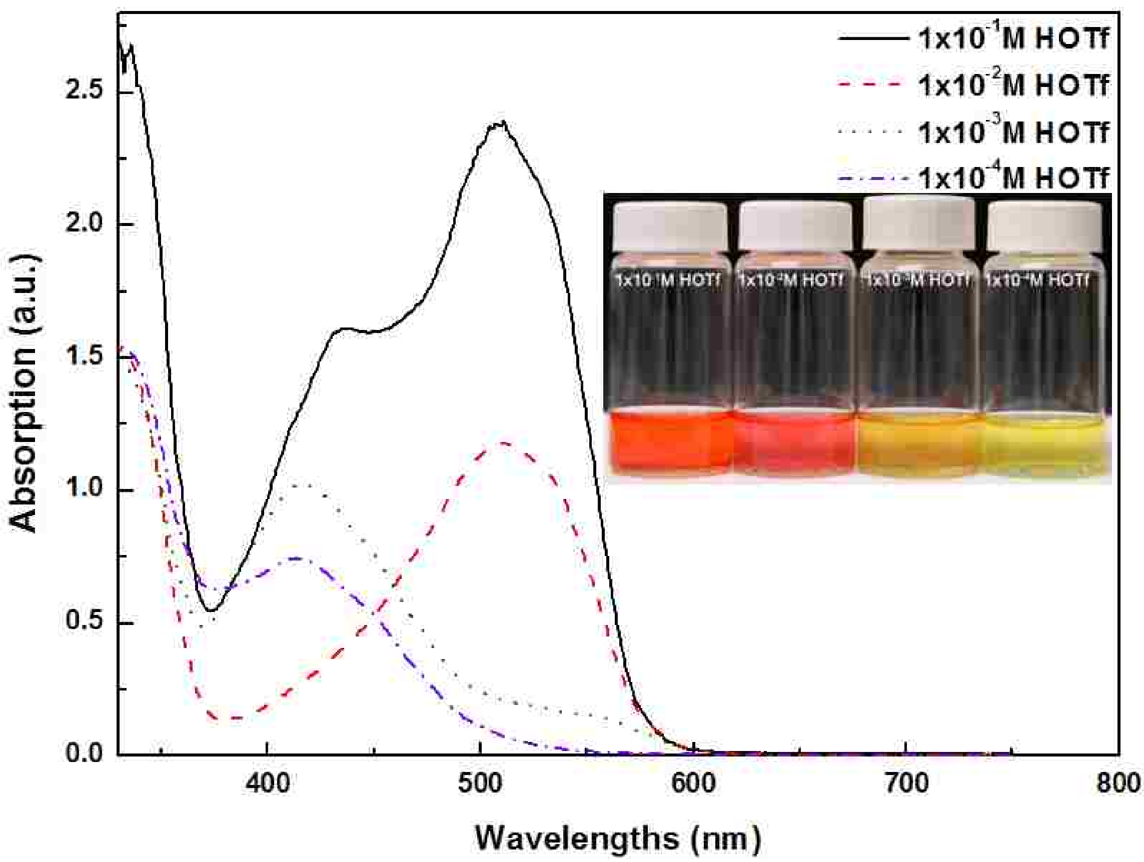

Figure S11. UV−Vis spectra of **1d** (2×10^{-5} M) in acetone with varied HOTf concentrations.

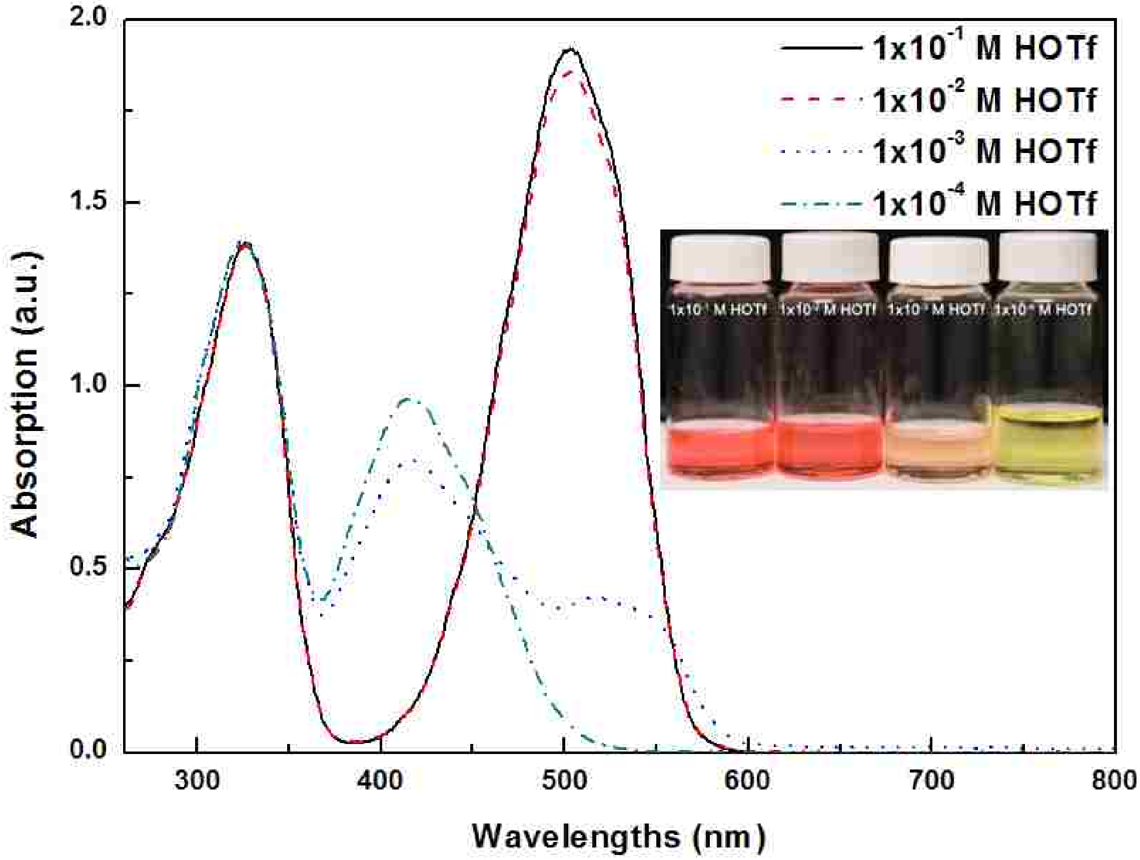

Figure S12. UV−Vis spectra of **1d** (2 x 10^{-5} M) in CH_3CN with varied HOTf concentrations.

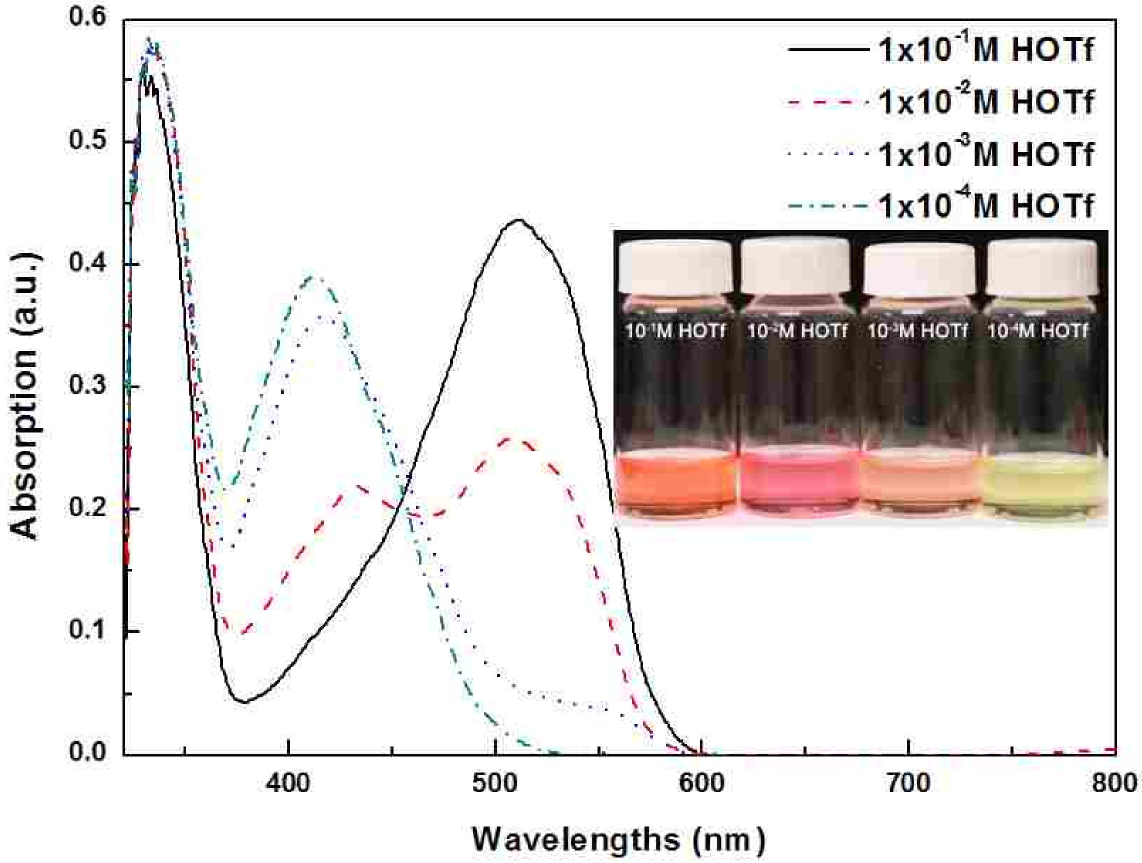

Figure S13. UV−Vis spectra of **1d** (2 x 10^{-5} M) in acetone with varied HOTf concentrations.

RERFENCES

Chapter 1 (1−50)

1. (a) Shirakawa, H.; Louis, E. J.; MacDiarmid, A. G.; Chiang, C. K.; Heeger, A. J. *J. Chem. Soc. Chem. Commun.* **1977**, 578. (b) Burroughes, J. H.; Bradley, D. D. C.; Brown, A. R.; Marks, R. N.; Mackay, K.; Friend, R. H.; Burns, P. L.; Holmes, A. B. *Nature* **1990**, *347*, 539–541.
2. McQuade, D. T.; Pullen, A. E.; Swager, T. M. *Chem. Rev.* **2000**, *100*, 2537.
3. Hove, V.; Garcia, A.; Bazan, G. C.; Nguyen, T.-Q. *Adv. Mater.* **2008**, *20*, 3793.
4. Huyal, I. O.; Koldemir, U.; Ozel, T.; Demir, H. V.; Tuncel, D. *J. Mater. Chem.* **2008**, *18*, 3568.
5. Tuncel, D.; Artar, M.; Hanay, S. B. *J. Polym. Sci Part A: Polym. Chem.* **2010**, *48*, 4894.
6. (a) Shirakawa, H. *Angew. Chem. Int. Ed.* **2001**, *40*, 2575. (b) MacDiarmid, A. G. *Angew. Chem. Int. Ed.* **2001**, *40*, 2581. (c) Heeger, A. J. *Angew. Chem. Int. Ed.* **2001**, *40*, 2591.
7. Pei, Q.; Yu, G.; Zhang, C.; Yang, Y.; Heeger, A. J. *Science* **1995**, *269*, 1086.
8. Yu, G.; Gao, J.; Hummelen, J.; Heeger, A. J. *Science* **1995**, *270*, 1789.
9. Yu, G.; Wang, J.; McElvain, J.; Heeger, A. J. *Adv. Mater.* **1998**, *10*, 1431.
10. Li, H.; Yang, R.; Bazan, G. C. *Macromolecules* **2008**, *41*, 1531−1536.
11. Liang, W. Y. *Phys. Educ.* **1970**, *5*, 226.
12. Filhol, J.-S. *J. Chem. Edu.* **2009**, *86*, 72.
13. (a) Osaka, I.; McCullough, R. D. *Acc. Chem. Res.* **2008**, *41*, 1202. (b) Blouin, N.; Leclerc, M. *Acc. Chem. Res.* **2008**, *41*, 1110.

14. (a) Roncali, J. *Chem. Rev.* **1997**, 97, 173. (b) Roncali, J. *Macromol. Rapid Commun.* **2007**, *28*, 1761.

15. (a) Kroon, R.; Lenes, M.; Hummelen, J. C.; Blom, P. W. M.; de Boer, B. *Polym. Rev.* **2008**, *48*, 531. (b) Bundgaard, E.; Krebs, F. C. *Sol. Energy Mater. Sol. Cells* **2007**, *91*, 954.

16. (a) Yamamoto, T. *Macromol. Rapid Commun.* **2002**, *23*, 583. (b) Babudri, F.; Farinla, G. M.; Naso, F. *J. Mater. Chem.* **2004**, *14*, 11. (c) Barbarella, G.; Melucci, M.; Sotgiu, G. *Adv. Mater.* **2005**, *17*, 1581.

17. (a) Kraft, A.; Grimsdale, A. C.; Holmes, A. B. *Angew. Chem. Int. Ed.* **1998**, *37*, 402. (b) Becker, H.; Spreitzer, H.; Kreuder, W.; Kluge, E.; Schenk, H.; Parker, I.; Cao, Y. *Adv. Mater.* **2000**, *12*, 42. (c) Roex, H.; Adriaensens, P.; Vanderzande, D.; Gelan, J. *Macromolecules* **2003**, *36*, 5613. (d) Xing, K. Z.; Johansson, N.; Beamson, G.; Clark, T. D.; Brédas, J.-L.; Salaneck, W. R. *Adv. Mater.* **1997**, *9*, 1027.

18. Roncali, J. *Chem. Rev.* **1992**, *92*, 711.

19. (a) McCullough, R. D.; Lowe, R. D. *J. Chem. Soc. Chem. Commun.* **1992**, 70. (b) McCullough, R. D.; Lowe, R. D.; Jayaraman, M.; Anderson, D. L. *J. Org. Chem.* **1993**, *58*, 904. (c) Loewe, R. S.; Khersonsky, S. M.; McCullough, R. D. *Adv. Mater.* **1999**, *11*, 250. (d) Loewe, R. S.; Ewbank, P. C.; Liu, J. S.; Zhai, L.; McCullough, R. D. *Macromolecules* **2001**, *34*, 4324.

20. (a) Hiorns, R. C.; Khoukh, A.; Gourdet, B.; Dagron-Lartigau, C. *Polym. Int.* **2006**, *55*, 608. (b) Ouhib, F.; Hiorns, R. C.; Bailly, S.; de Bettignies, R.; Khoukh, A.; Preud'homme. H.; Desbrières. J.; Dagron-Lartigau, C. *Eur. Phys. J. Appl. Phys.* **2007**, *37*, 343. (c) Sheina, E. E.; Khersonsky, S. M.; Jones, E. G.; McCullough, R. D. *Chem.*

Mater. **2005**, *17*, 3317. (d) Adachi, I.; Miyakoshi, R.; Yokoyama, A.; Yokozawa, T. *Macromolecules* **2006**, *39*, 7793. (e) Vallat, P.; Lamps, J. P.; Schosseler, F.; Rawiso, M.; Catala, J. N. *Macromolecules* **2007**, *40*, 2600.

21. Yokozawa, T.; Yokoyama, A. *Chem*. *Rev*. **2009**, *109*, 5595.
22. Boaen, N. K.; Hillmyer, M. A. *Chem*. *Soc*. *Rev*. **2005**, *34*, 267.
23. (a) F. Reinitzer, *Monatsch Chem*. **1888**, *9*, 421. (b) O. Lehmann, Z. *Physikal*. *Chem*. **1889**, *4*, 462.
24. Figueiredo Neto, A. M.; Salinas, S. R. A. In *The Physics of Lyotropic Liquid Crystals;* Oxford University: Oxford, **2005**.
25. Hamilton, C. J.; Tighe, B. J. In *Comprehensive Polymer Science;* Allen, G., Bevington, J. C., Eds.; Pergamon: Oxford; **1989**; Vol. 3, p 261.
26. (a) Xu, Y.; Bolisetty, S.; Drechsler, M.; Fang, B.; Yuan, J.; Ballauff, M.; Müller, A. H. E. *Polymer* **2008**, *49*, 3957. (b) Kotzev, A.; Laschewsky, A.; Rakotoaly, R. H. *Macromol*. *Chem*. *Phys*. **2001**, *202*, 3257. (c) Garnier, S.; Laschewsky, A. *Macromolecules* **2005**, *38*, 7580. (d) Baussard, J.-F.; Habib-Jiwan, J.-L.; Laschewsky, A.; Mertoglu, M.; Storsberg, J. *Polymer* **2004**, *45*, 3615.
27. (a) Baussard, J.-F.; Habib-Jiwan, J.-L.; Laschewsky, A. *Langmuir* **2003**, *19*, 7963. (b) Kubowicz, S.; Baussard, J.-F.; Lutz, J.-F.; Thünemann, A. F.; von Berlepsch, H.; Laschewsky, A. *Angew*. *Chem*. *Int*. *Ed*. **2005**, *44*, 5262.
28. (a) Pu, K. Y.; Liu, B. *Biosens*. *Bioelectron*. **2009**, *24*, 1067. (b) Feng, F.; Wang, H.; Han, L.; Wang, S. *J. Am*. *Chem*. *Soc*. **2008**, *130*, 11338. (c) Fang, H.; Tang, Y.; Wang, S.; Li, Y.; Zhu, D. *J. Am*. *Chem*. *Soc*. **2005**, *127*, 12343. (d) Ho, H.-A.; Boissinot, M.; Beigeron, M. G.; Corbeil, G.; Dore´, K.; Boudreau, D.; Leclerc, M. *Angew*. *Chem*. *Int*.

Ed. **2002**, *41*, 1548. (e) Tang, Y. L.; Teng, F.; Yu, M. H.; An, L. L.; He, F.; Wang, S.; Li, Y. L.; Zhu, D. B.; Bazan, G. C. *Adv. Mater*. **2008**, *20*, 703. (a) Ho, H. A.; Doré, K.; Boissnoit, M.; Bergeron, M. G.; Tanguay, R. M.; Boudreau, D.; Leclerc, M. *J. Am. Chem. Soc*. **2005**, *127*, 12673. (b) Chen, Y.; Pu, K.-Y.; Fan, Q.-L.; Qi, X.-Y.; Huang, Y.-Q.; Lu, X.-M.; Huang, W. *J. Polym. Sci. Part A: Polym. Chem*. **2009**, *47*, 5057. (c) Balamurugan, A.; Reddy, M. L. P.; Jayakannan, M. *J. Polym. Sci. Part A: Polym. Chem*. **2009**, *47*, 5144.

29. Thomas, S. W.; Joly, G. D.; Swager, T. M. *Chem. Rev*. **2007**, *107*, 1339.
30. Cagnoli, R.; Kanzi, M.; Libertini, E.; Mucci, A.; Paganin, L.; Parenti, F.; Preti, L.; Schenetti, L. *Macromolecules* **2008**, *41*, 3785.
31. Zhai, L.; McCullough, D. *Adv. Mater*. **2002**, *14*, 901.
32. Chong, H.; Duan, X.; Yang, Q.; Liu, L.; Wang, S. *Macromolecules* **2010**, *43*, 10196.
33. Wang, J.; Wang, D.; Miller, E. K.; Moses, D.; Bazan, G. C.; Heeger, A. J. *Macromolecules* **2000**, *33*, 5153.
34. (a) Akahoshi, H.; Toshima, S.; Itaya, K. *J. Phys. Chem*. **1981**, *85*, 818. (b) Moore, J. S.; Stupp, S. I. *Macromolecules* **1986**, *19*, 1815.
35. Bird, L. C.; Kuhn, A. T. *Chem. Soc. Rev*. **1981**, *10*, 49.
36. (a) Lin, F.; Cheng, S. Z. D.; Harris, F. W. *Polymer* **2002**, *43*, 3421. (b) Bhowmik, P. K.; Burchett, R. A.; Han , H.; Cebe, J. J. *Macromolecules* **2001**, *34*, 7579.
37. Bhowmik, P. K.; Han, H.; Nedeltchev, A. K.; Mandal, H. D.; Jimenez-Hernandez, J. A.; McGannon, P. M. *Polymer* **2009**, *50*, 3128.
38. Jo, T. S.; Nedeltchev, A. K.; Biswas, B.; Han, H.; Bhowmik, P. K. *Polymer* **2012**, *53*, 1063.

39. (a) Bhowmik, P. K.; Han, H.; Nedeltchev, A. K. *J. Polym. Sci. Part A: Polym. Chem.* **2006**, *44*, 1028. (b) Bhowmik, P. K.; Han, H.; Nedeltchev, A. K.; Mandal, H. D.; Jimenez-Hernandez, J. A.; Mcgannon, P. M. *J. Appl. Polym. Sci.* **2010**, *116*, 1197.
40. Bhowmik, P. K.; Molla, A. H.; Han, H.; Gangoda, M. E.; Bose, R. N. *Macromolecules* **1998**, *31*, 621.
41. Preston, J. *Angew. Makromol. Chem.* **1982**, *109/110*, 1.
42. Nedeltchev, A. K.; Han, H.; Bhowmik, P. K. *J. Polym. Sci. Part A: Polym. Chem.* **2010**, *48*, 4408.
43. (a) Nedeltchev, A. K.; Han, H.; Bhowmik, P. K. *J. Polym. Sci. Part A: Polym. Chem.* **2010**, *48*, 4611. (b) Greaves, T. L.; Drummond, C. J. *Chem. Rev.* **2008**, *108*, 206.
44. (a) Palacios, R.; Formentin, P.; Martinez-Ferrero, E.; Pallarès, J.; Marsal, L. F. *Nanoscale Res. Lett.* **2011**, *6*, 35. (b) Inbasekaran, M.; Woo, E.; Wu, W.; Bernius, M.; WujkowskiXia, L. *Synth. Met.* **2000**, *111−112*, 397.
45. Harris, F. W.; Chuang, K. C.; Huang, S. A. X.; Janimak, J. J.; Cheng, S. Z. D. *Polymer* **1994**, *35*, 4940.
46. Huang, S. A. X.; Chuang, K. C.; Cheng, S. Z. D.; Harris, F. W. *Polymer* **2000**, *41*, 5001.
47. Bhowmik, P. K.; Han, H.; Cebe, J. J.; Nedeltchev, I. K.; Kang, S.-W.; Kumar, S. *Macromolecules* **2004**, *37*, 2688.
48. Mitschke, U.; Bäuerle, P. *J. Mater. Chem.* **2000**, *10*, 1471.
49. Liao, L.; Pang, Y.; Ding, L.; Karasz, F. E. *Macromolecules* **1999**, *32*, 7409.
50. (a) Sarker, A. M.; Strehmel, B.; Neckers, D. C. *Macromolecules* **1999**, *32*, 7409. (b) Gettinger, C.; Heeger, A. J.; Drake, J.; Pine, D. *J. Chem. Phys.* **1994**, *101*, 1673.

Chapter 2 (1−56)

1. (a) Radushkevich, L. V.; Lukyanovich, V. M. *Zurn. Fisic. Chim.* **1952**, *26*, 88. (b) Ajayan, P. M. *Chem. Rev.* **1999**, *99*, 1787. (c) Niyogi, S.; Hamon, M. A.; Fu, H.; Zhao, B.; Bhowmik, P.; Sen, R.; Itkis, M. E.; Haddon, R. C. *Acc. Chem. Res.* **2002**, *35*, 1105.

2. Iijima, S. *Nature* **1991**, *354*, 56.

3. Wildöer, J. W. G.; Venema, L. C.; Rinzler, A. G.; Smalley, R. E.; Dekker, C. *Nature* **1998**, *391*, 59.

4. Fischer, J. E.; Dai, H.; Thess, A.; Lee, R.; Hanjani, N. M.; Dehaas, D. L.; Smalley, R. E. *Phy. Rev. B* **1997**, *55*, R4921.

5. Salvetat, J.-P.; Bonard, J.-M.; Thomson, N. H.; Kulik, A. J.; Forró, L.; Benoit, W.; Zuppiroli, L. *Appl. Phys. A* **1999**, *69*, 255.

6. Yakobson, B. I.; Avouris, Phaedon. *Top. Appl. Phys.* **2001**, *80*, 287.

7. Berber, S.; Kwon, Y.-K.; Tománek, D. *Phys. Rev. Lett.* **2000**, *84*, 4613.

8. Hirsch, A.; Vostrowsky, O. *Top. Curr. Chem.* **2005**, *245*, 193.

9. Ausman, K. D.; Piner, R.; Lourie, O.; Ruoff, R. S.; Korobov, M. *J. Phys. Chem. B* **2000**, *104*, 8911.

10. Furtado, C. A.; Kim, U. J.; Gutierrez, H. R.; Pan, L.; Dickey, E. C.; Eklund, P. C. *J. Am. Chem. Soc.* **2004**, *126*, 6095.

11. Giordani, S.; Bergin, S. D.; Nicolosi, V.; Lebedkin, S.; Kappes, M. M.; Blau, W. J.; Coleman, J. N. *J. Phys. Chem. B* **2006**, *110*, 15708.

12. Landi, B. J.; Ruf, H. J.; Worman, J. J.; Raffaelle, R. P. *J. Phys. Chem. B* **2004**, *108*, 17089.

13. (a) Bahr, J. L.; Mickelson, E. T.; Bronikowski, M. J.; Smalley, R. E.; Tour, J. M. *Chem. Commun.* **2001**, 193. (b) Kim, D. S.; Nepal, D.; Geckeler, K. E. *Small* **2005**, *1*, 1117.

14. Niyogi, S.; Hamon, M. A.; Perea, D. E.; Kang, C. B.; Zhao, B.; Pal, S.K.; Wyant, A. E.; Itkis, M. E.; Haddon, R. C. *J. Phys. Chem. B* **2003,** *107,* 8799.

15. Fagan, S. B.; Souza, A. G.; Lima, J. O. G.; Mendes, J.; Ferreira, O. P.; Mazali, I. O.; Alves, O. L.; Dresselhaus, M. S. *Nano Lett.* **2004**, *4*, 1285.

16. (a) Chen, J.; Hamon, M. A.; Hu, H.; Chen, Y. S.; Rao, A. M.; Eklund, P. C.; Haddon, R. C. *Science* **1998**, *282*, 95. (b) Sun, Y. P.; Fu, K. F.; Lin, Y.; Huang, W. J. *Acc. Chem. Res.* **2002**, *35*, 1096. (c) Sano, M.; Kamino, A.; Okamura, J.; Shinkai, S. *Langmuir* **2001**, *17*, 5125. (d) Pompeo, F.; Resasco, D. E. *Nano Lett.* **2002**, *2*, 369.

17. Mickelson, E. T.; Huffman, C. B.; Rinzler, A. G.; Smalley, R. E.; Hauge, R. H.; Margrave, J. L. *Chem. Phys. Lett.* **1998**, *296*, 188.

18. Dyke, C. A.; Tour, J. M. *J. Am. Chem. Soc.* **2003**, *125*, 1156.

19. Pekker, S.; Salvetat, J. P.; Jakab, E.; Bonard, J. M.; Forro, L. *J. Phys. Chem. B* **2001**, *105*, 7938.

20. Holzinger, M.; Vostrowsky, O.; Hirsch, A.; Hennrich, F.; Kappes, M.; Weiss, R.; Jellen, F. *Angew. Chem. Int. Ed.* **2001**, *40*, 4002.

21. Chen, Y.; Haddon, R. C.; Fang, S.; Rao, A. M.; Lee, W. H.; Dickey, E. C.; Grulke, E. A.; Pendergrass, J. C.; Chavan, A.; Haley, B. E.; Smalley, R. E. *J. Mater. Res.* **1998**, *13*, 2423.

22. Ying, Y. M.; Saini, R. K.; Liang, F.; Sadana, A. K.; Billups, W. E. *Org. Lett.* **2003**, *5*, 1471.

23. Georgakilas, V.; Kordatos, K.; Prato, M.; Guldi, D. M.; Holzinger, M.; Hirsch, A. *J. Am. Chem. Soc.* **2002,** *124,* 760.

24. Lou, X. D.; Detrembleur, C.; Sciannamea, V.; Pagnoulle, C.; Jerome, R. *Polymer* **2004**, *45*, 6097.

25. (a) Qin, S.; Qin, D.; Ford, W. T.; Resasco, D. E.; Herrera, J. E. *Macromolecules* **2004**, *37*, 752. (b) Tasis, D.; Tagmatarchis, N.; Bianco, A.; Prato, M. *Chem. Rev.* **2006**, *106*, 1105.

26. Spitalsky, Z.; Tasis, D.; Papagelis, K.; Galiotis, C. *Prog. Polym. Sci.* **2010**, *35*, 357.

27. Ajayan, P. M.; Schadler, L. S.; Giannaris, C.; Rubio, A. *Adv. Mater.* **2000**, *12*, 750.

28. Sandler, J.; Shaffer, M. S. P.; Prasse, T.; Bauhofer, W.; Schulte, K.; Windle, A. H. *Polymer* **1999**, *40*, 5967.

29. Moore, V. C.; Strano, M. S.; Haroz, E. H.; Hauge, R. H.; Smalley, R. E.; Schmidt, J.; Talmon, Y. *Nano Lett.* **2003**, *3*, 1379.

30. Nish, A.; Nicholas, R. J. *Phys. Chem. Chem. Phys.* **2006,** *8,* 3547.

31. Haggenmuller, R.; Rahatekar, S. S.; Fagan, J. A.; Chun, J.; Becker, M. L.; Naik, R. R.; Krauss, T.; Carlson, L.; Kadla, J. F.; Trulove, P. C.; Fox, D. F.; DeLong, H. C.; Fang, Z.; Kelley, S. O.; Gilman, J. W. *Langmuir* **2008**, *24*, 5070.

32. Park, S.; Yang, H.-S.; Kim, D.; Jo, K.; Jon, S. *Chem. Commun.* **2008**, 276.

33. Yi, W.; Malkovskiy, A.; Chu, Q.; Sokolov, A. P.; Colon, M. L.; Meador M.; Pang, Y. *J. Phys. Chem. B* **2008**, *112*, 12263.

34. (a) Star, A.; Stoddart, J. F.; Steuerman, D.; Diehl, M.; Boukai, A.; Wong, E. W.; Yang, X.; Chung, S.-W.; Choi, H.; Heath, J. R. *Angew. Chem. Int. Ed.* **2001**, *40*, 1721. (b) Ago, H.; Petritsch, K.; Shaffer, M. S. P.; Windle, A. H.; Friend, R. H. *Adv. Mater.* **1999**, *11*, 1281. (c) Dalton, A. B.; Stephan, C.; Coleman, J. N.; McCarthy, B.; Ajayan, P. M.; Lefrant, S.; Bernier, P.; Blau, W. J.; Byrne, H. J. *J. Phys. Chem. B* **2000**, *104*, 10012. (d) Coleman, J. N.; Dalton, A. B.; Curran, S.; Rubio, A.; Davey, A. P.; Drury, A.; McCarthy, B.; Lahr, B.; Ajayan, P. M.; Roth, S.; Barklie, R. C.; Blau, W. J. *Adv. Mater.* **2000**, *12*, 213. (e) Steuerman, D. W.; Star, A.; Narizzano, R.; Choi, H.; Ries, R. S.; Nicolini, C.; Stoddart, J. F.; Heath, J. R. *J. Phys. Chem. B* **2002**, *106*, 3124.

35. Yuan, W. Z.; Sun, J. Z.; Dong, Y.; Halussler, M.; Yang, F.; Xu, H. P.; Qin, A.; Lam, J. W. Y.; Zheng, Q.; Tang, B. Z. *Macromolecules* **2006**, *39*, 8011.

36. (a) Chen, J.; Liu, H. Y.; Weimer, W. A.; Halls, M. D.; Waldec, D. H.; Walker, G. C. *J. Am. Chem. Soc.* **2002**, *124*, 9034. (b) Chen, J.; Ramasubramaniam, R.; Xue, C.; Liu, H. *Adv. Funct. Mater.* **2006**, *16*, 114.

37. (a) Rice, N. A.; Soper, K.; Zhow, N.; Erschrod, E.; Zhao, Y. *Chem. Commun.* **2006**, 4937. (b) Cheng, F.; Adronov, A. *Chem. Eur. J.* **2006**, *12*, 5053.

38. Satishkumar, B. C.; Brown, L. O.; Gao, Y.; Wang, C.-C.; Wang, H.-L.; Doorn, S. K. *Nat. Nanotechnol.* **2007**, *2*, 560.

39. Kostarelos, K.; Bianco, A.; Prato, M. *Nat. Nanotechnol.* **2009**, *4*, 627.

40. Kam, N. W. S.; O'Connell, M.; Wisdom, J. A.; Dai, H. *Proc. Natl. Acad. Sci. U. S. A.* **2005**, *102*, 11600.

41. Tang, B. Z.; Xu, H. Y. *Macromolecules* **1999**, *32*, 2569.

42. (a) O'Connell, M. J.; Boul, P.; Ericson, L. M.; Huffman, C.; Wang, Y.; Haroz, E.; Kuper, C.; Tour, J.; Ausman, K. D.; Smalley, R. E. *Chem. Phys. Lett.* **2001**, *342*, 265. (b) Sinani, V. A.; Gheith, M. K.; Yaroslavov, A. A.; Rakhnyanskaya, A. A.; Sun, K.; Mamedov, A. A.; Wicksted, J. P.; Kotov, N. A. *J. Am. Chem. Soc.* **2005**, *127*, 3463. (c) Rouse, J. H.; Lillehei, P. T. *Nano Lett.* **2003**, *3*, 59.

43. Cheng, F.; Imin, P.; Lazar, S.; Botton, G. A.; de Silveira, D.; Marinov, O.; Deen, J.; Adronov, A. *Macromolecules* **2008**, *41*, 9869.

44. (a) Okano, K.; Noguchi, I.; Yamashita, T. *Macromolecules* **2010**, *43*, 5496. (b) Li, N.; Zhang, F.; Wang, J.; Li, S.; Zhang, S. *Polymer* **2009**, *50*, 3600. (c) Loos, M. R.; Abetz, V.; Schulte, K. *J. Polym. Sci. Part A: Polym. Chem.* **2010**, *48*, 5172.

45. (a) Song, W.; Windle, A. H. *Adv. Mater.* **2008**, *20*, 3149. (b) Dierking, I.; Scalia, G.; Morales, P. *J. Appl. Phys.* **2005**, *97*, 044309. (c) Kumar, S.; Bisoyi, H. K. *Angew. Chem. Int. Ed.* **2007**, *46*, 1501. (d) Bisoyi, H. K.; Kumar, S. *J. Mater. Chem.* **2008**, *18*, 3032. (e) Kimura, M.; Miki, N.; Adachi, N.; Tatewaki, Y.; Ohta, K.; Shirai, H. *J. Mater. Chem.* **2009**, *19*, 1086.

46. (a) Song, W.; Kinloch, I. A.; Windle, A. H. *Science* **2003**, *302*, 1363. (b) Davis, V. A.; Ericson, L. M.; Nicholas, A.; Parra-Vasquez, G.; Fam, H.; Wang, Y.; Prieto, V.; Longoira, J. A.; Ramesh, S.; Saini, R. K.; Kittrell, C.; Billups, W. E.; Wade, W.; Adams, R. H.; Hauge, H.; Smalley, R. E.; Pasquali, M. *Macromolecules* **2004**, *37*,

154. (c) Kumar, S.; Dang, T. D.; Arnold, F. E.; Bhattacharyya, A. R.; Min, B. G.; Zhang, X.; Vaia, R. A.; Park, C.; Adams, W. W.; Hauge, R. H.; Smalley, R. E.; Ramesh, S.; Willis, P. A. *Macromolecules* **2002**, *35*, 9039.

47. (a) Baur, J. W.; Kim, S.; Balanda, P. B.; Reynolds, J. R.; Rubner, M. F. *Adv. Mater.* **1998**, 10, 1452. (b) Taranekar, P.; Qiao, Q.; Jiang, H.; Ghiviriga, I.; Schanze, K. S.; Reynolds, J. R. *J. Am. Chem. Soc.* **2007**, *129*, 8958.

48. Lin, F.; Cheng, S. Z. D.; Harris, F. W. *Polymer* **2002**, *43*, 3421.

49. (a) Du, F.; Fischer, J. E.; Winey, K. I. *J. Polym. Sci. Part B: Polym. Phys.* **2003**, *41*, 3333. (b) Sabba, Y.; Thomas, E. L. *Macromolecules* **2004**, *37*, 4815.

50. (a) Shaffer, M. S. P.; Windle, A. H. *Macromolecules* **1999**, *32*, 6864. (b) Kovtyukhova, N. I.; Mallouk, T. E.; Pan, L.; Dickey, E. C. *J. Am. Chem. Soc.* **2003**, *125*, 9761.

51. (a) Ziegler, K. J.; Gu, Z. N.; Peng, H. Q.; Flor, E. L.; Hauge, R. H.; Smalley, R. E. *J. Am. Chem. Soc.* **2005**, *127*, 1541. (b) Lagerwall, J.; Scalia, G.; Haluska, M.; Dettlaf-Weglikowska, U.; Roth, S.; Fiesselmann, F. *Adv. Mater.* **2007**, *19*, 359. (c) Haddon, R. C. *Nature* **1995**, *378*, 249. (d) Zou, J.; Liu, L.; Chen, H.; Khondaker, S. I.; McCullough, R. D.; Huo, Q.; Zhai, L. *Adv. Mater.* **2008**, *20*, 2055.

52. (a) Kulia, B. K.; Malik, S.; Batabyal, S. K.; Nandi, A. K. *Macromolecules* **2007**, *40*, 278. (b) Koizhaiganova, R.; Kim, H. J.; Vasudevan, T.; Kudaibergenov, S.; Lee, M. S. *J. Appl. Polym. Sci.* **2010**, *115*, 2448.

53. Rosevear, F. B. *J. Am. Oil Chem. Soc.* **1954**, *31*, 628.

54. (a) Paloniemi, H.; Ääritalo, T.; Laiho, T.; Liuke, H.; Kocharova, N.; Haapakka, K.; Terzi, F.; Seeber, R.; Lukkari, J. *J. Phys. Chem. B* **2005**, *109*, 8634. (b) Balasubramanian, K.; Friedrich, M.; Jiang, C.; Mews, A.; Burghard, M.; Kern. K. *Adv. Mater.* **2003**, *15*, 1515. (c) Bahr, J. L.; Yang, J.; Kosynkin, D. V.; Bronikowski, M. J.; Smalley, R. E.; Tour, J. M. *J. Am. Chem. Soc.* **2001**, *123*, 6536.

55. Nedeltchev, A. K.; Han, H.; Bhowmik, P. K. *J. Polym. Sci. Pat A: Polym. Chem.* **2010**, *48*, 4408.

56. (a) Bhowmik, P. K.; Han, H.; Nedeltchev, A. K. *Polymer* **2006**, *47*, 8281. (b) Rabjohns, M. A.; Hodge, P.; Lovell, P. A. *Polymer* **1997**, *38*, 3395. (c) Nardello, V.; Aubry, J. M. *Tetrahedron Lett.* **1997**, *38*, 7361.

Chapter 3 (1−58)

1. Welton, T. *Chem. Rev.* **1999**, *99*, 2071.

2. Sugden, S.; Wilkins, H. *J. Chem. Soc.* **1929**, 1291.

3. Wilkes, J. S.; Levisky, J. A.; Wilson, R. A.; Hussey, C. L. *Inorg. Chem.* **1982**, *21*, 1263.

4. Fannin, A. A.; Floreani, D. A.; King, L. A.; Landers, J. S.; Piersma, B. J.; Stech, D. J.; Vaughn, R. L.; Wilkes, J. S.; Williams, J. L. *J. Phys. Chem.* **1984**, *88*, 2614.

5. Dupont, J. *J. Braz. Chem. Soc.* **2004**, *15*, 341.

6. Huddleston, J. G.; Visser, A. E.; Reichert, W. M.; Willauer, H. D.; Broker, G. A.; Rogers, R. D. *Green Chem.* **2001**, *3*, 156.

7. Shariati, A.; Peters, C. J. *J. Supercrit. Fluids* **2005**, *34*, 171.

8. Brennecke, J. F.; Maginn, E. J. *AIChE J.* **2001**, *47*, 2384.

9. Chiappe, C.; Pieraccini, D. *J. Phys. Org. Chem.* **2005**, *18*, 275.

10. (a) Poole, S. K.; Shetty, P. H.; Poole, C. F. *Anal. Chim. Acta* **1989**, *218*, 241. (b) Wilkes, J. S.; Zaworotko, M. J. *J. Chem. Soc. Chem. Commun.* **1992**, 965. (c) Holbrey, J. D.; Reichert, W. M.; Swatloski, R. P.; Broker, G. A.; Pitner, W. R.; Seddon, K. R.; Rogers, R. D. *Green Chem.* **2002,** *4,* 407. (d) Mirzaei, Y. R.; Twamley, B.; Shreeve, J. M. *J. Org. Chem.* **2002,** *67,* 9340. (e) Bao, W. L.; Wang, Z. M.; Li, Y. X. *J. Org. Chem.* **2003,** *68,* 591.

11. Endres, F.; Abedin, S. Z. E. *Phy. Chem. Chem. Phys.* **2006**, *8*, 2101.

12.Suarez, P. A. Z.; Einloft, S.; Dullius, J. E. L.; De Souza, R. F.; Dupont, J. *J. Chim. Phys.* **1998**, *95*, 1626.

13. Mantz, R. A.; Trulove, P. C. In *Ionic Liquids in Synthesis;* Wasserscheid, P., Welton, T., Eds.; Wiley-VCH: Weinheim, 2003; p. 56.

14. Wasserscheid, P.; Keim, W. *Agnew. Chem. Int. Ed.* **2000**, *39*, 3772.

15. Holbrey, J. D.; Rogers, R. D. In *Ionic Liquids in Synthesis;* Wasserscheid, P., Welton, T., Eds.; Wiley-VCH: Weinheim, 2003; p. 41.

16. Visser, A. E.; Swatloski, R. P.; Reichert, W. M.; Griffin, S. T.; Rogers, R. D. *Ind. Eng. Chem. Res.* **2000**, *39*, 3596.

17. Dai, S.; Ju, Y. H.; Barnes, C. E. *J. Chem. Soc. Dalton Trans.* **1999**, *8*, 1201.

18. Visser, A. E.; Swatloski, R. P.; Griffin, S. T.; Hartman, D. H.; Rogers, R. D. *Sep. Sci. Technol.* **2001**, *36*, 785.

19. Chauvin, Y.; Gilbert, B.; Guibard, I. *Chem. Commun.* **1990**, 1715.

20. Carlin, R. T.; Osteryoung, R. A. *J. Mol. Catal.* **1990**, *63*, 125.

21. (a) Chauvin, Y.; Mussmann, L.; Olivier, H. *Angew. Chem. Int. Ed. Engl.* **1995**, *34*, 2698. (b) Suarez, P. A. Z.; Dullius, J. E. L.; Einloft, S.; de Souza, R. F.; Dupont, J. *Polyhedron* **1996**, *15*, 1217.

22. Shirota, H.; Mandai, T.; Fukazawa, H.; Kato, T. *J. Chem. Eng. Data* **2011**, *56*, 2453.

23. Daguenet, C.; Dyson, P. J. *Organometallics* **2004**, *23*, 6080.

24. Liang, C.; Yurn, C. Y.; Warmack, R. J.; Barnes, C. E.; Dai, S. *Anal. Chem.* **2002**, *74*, 2172.

25. Zhang, Q.; Zhang, S.; Liu, S. Ma, X.; Lu, L.; Deng, Y. *Analyst* **2011**, *136*, 1302.

26. (a) Bonhôte, P.; Dias, A.-P.; Armand, M.; Papageorgiou, N.; Kalyanasundaram, K.; Grätzel, M. *Inorg. Chem.* **1996**, *35*, 1168. (b) Hagiwara, R.; Ito, Y. *J. Fluorine Chem.* **2000**, *105*, 221. (c) McEwen, A. B.; Ngo, H. L.; LeCompte, K.; Goldman, J. L. *J. Electrochem. Soc.* **1999**, *146*, 1987.

27. Doyle, M.; Choi, S. K.; Prolux, G. *J. Electrochem. Soc.* **2000**, *147*, 34.

28. (a) Yoshizawa, M.; Xu, W.; Angell, C. A. *J. Am. Chem. Soc.* **2003**, *125*, 15411. (b) Noda, A.; Susan, M. A. B. H.; Kudo, K.; Mitsushima, S.; Hayamizu, K.; Watanabe, M. *J. Phys. Chem. B* **2003**, *107*, 4024. (c) Yamada, M.; Honma, I. *Electrochim. Acta* **2003**, *48*, 2411. (d) Sun, J.; Jordan, L. R.; Forsyth, M.; MacFarlane, D. R. *Electrochim. Acta* **2001**, *46*, 1703.

29. Engel, R.; Cohen, J. I. *Curr. Org. Chem.* **2002**, *6*, 1453.

30. La, S.; Behaj, V.; Mancheno, D.; Casiano, R.; Thomas, M.; Rikon, A.; Gaillard, J.; Raju, R.; Scumpia, S.; Castro, S.; Engel, R.; Cohen, J. L. I. *Synthesis* **2002**, 1530.

31. Wishart, J. F.; Lall-Ramnarine, S. I.; Raju, R.; Scumpia, A.; Belleue, S.; Ragbir, R.; Engel, R. *Radiat. Phys. Chem.* **2005**, *72*, 99.

32. Ito, K.; Nishina, N.; Ohno, H. *Electrochim*. *Acta* **2000**, *45*, 1295.

33. Yoshizawa, M.; Ito-Akita, K.; Ohno, H. *Electrochim*. *Acta* **2000**, *45*, 1617.

34. Anderson, J. L.; Ding, R.; Ellern, A.; Armstrong, D. W. *J. Am*. *Chem*. *Soc*. **2005**, *127*, 593.

35. Payagala, T.; Zhang, Y.; Wanigasekara, E.; Huang, K.; Bretibach, Z. S.; Sharma, P. S.; Sidisky, L. M.; Armstrong, D. W. *Anal*. *Chem*. **2009**, *81*, 160.

36. Trilla, M.; Pleixats, R.; Parella, T.; Blanc, C.; Dieudonné, P.; Guari, Y.; Man, M. W. C. *Langmuir* **2008**, *24*, 259.

37. Nakagawa, M.; Ichimura, K. *Mol*. *Cryst*. *Liq*. *Cryst*. **2000**, *345*, 275.

38. Pérez, L.; Pinazo, A.; Vinardell, P.; Clapés, P.; Angelet, M.; Infante, M. R. *New J*. *Chem*. **2002**, *26*, 1221.

39. Bhowmik, P. K.; Han, H.; Cebe, J. J.; Burchett, R. A.; Acharya, B.; Kumar, S. *Liq*. *Cryst*. **2003**, *30*, 1433.

40. Bhowmik, P. K.; Han, H.; Nedeltchev, I. K.; Cebe, J. J. *Mol*. *Cryst*. *Liq*. *Cryst*. **2004**, *419*, 27.

41. Li, X.; Bruce, D. W.; Shreeve, J. M. *J. Mater*. *Chem*. **2009**, *19*, 8232.

42. Dechambenoit, P.; Ferlay, S.; Donnio, B.; Guillon, D.; Hosseini, M. W. *Chem*. *Commun*. **2011**, *47*, 734.

43. Nedeltchev, A. K.; Han, H.; Bhowmik, P. K. *J. Mater*. *Chem*. **2011**, *21*, 12717.

44. Luo, S.-C.; Sun, S.; Deorukhkar, A. R.; Lu, J.-T.; Bhattacharyya, A.; Lin, I. J. B. *J. Mater. Chem.* **2011**, *21*, 1866.

45. Ye, Y.; Elabd, Y. A. *Polymer* **2011**, *52*, 1309.

46. Dobbs, W.; Douce, L.; Allouche, L.; Louati, A.; Malbosc, F.; Welter, R. *New J. Chem.* **2006**, *30*, 528.

47. Jo, T. S.; McCurdy, W. L.; Tanthmanatham, O.; Kim, T. K.; Han, H.; Bhowmik, P. K.; Heinrich, B.; Donnio, B. *J. Mol. Struc.* **2012**, *1019*, 174.

48. Tonzola, C. J.; Kulkarni, A. P.; Gifford, A. P.; Kaminsky, W.; Jenekhe, S. A. *Adv. Funct. Mater.* **2007**, *17*, 863.

49. Hancock, J. M.; Gifford, A. P.; Zhu, Y.; Lou, Y.; Jenekhe, S. A. *Chem Mater.* **2006**, *18*, 4924.

50. Jo, T. S.; Nedeltchev, A. K.; Biswas, B.; Han, H.; Bhowmik, P. K. *Polymer* **2012**, *53*, 1063.

51. Swallen, S. F.; Kearns, K. L.; Mapes, M. K.; Kim, Y. S.; McMahon, R. J.; Ediger, M. D.; Wu, T.; Yu, L.; Satija, S. *Science* **2007**, *315*, 353.

52. Cardinaels, T.; Lava, K.; Goossens, K.; Eliseeva, S. V.; Binnemans, K. *Langmuir* **2011**, *27*, 2036.

53. Bhowmik, P. K.; Han, H.; Nedeltchev, I. K.; Cebe, J. J.; Kang, S.-W.; Kumar, S. *Liq. Cryst.* **2006**, *33*, 891.

54. Herstedt, M.; Henderson, W. A.; Smirnov, M.; Ducasse, L.; Servant, L.; Talaga, D.; Lassègues, J. C. *J. Mol. Struc.* **2006**, *783*, 145.

55. Roche, J. D.; Gordon, C. M.; Imrie, C. T.; Ingram, M. D.; Kennedy, A. R.; Celso, F. L.; Trilo, A. *Chem. Mater.* **2003**, *15*, 3089.

56. Chiappe, C.; Pieraccini, D. *J. Phys. Org. Chem.* **2005**, *18*, 275.

57. Suppan, P.; Ghoneim, H. *In Solvatochromism*, Royal Society of Chemistry: Cambridge, UK, 1997; Chapter 4, p. 96.

58. Lakowicz, J. R. *In Principles in Fluorescence Spectroscopy*, 3rd ed., Springer: New York, 2006, Chapter 3, p. 63.

VITA

Graduate College
University of Nevada, Las Vegas
Tae Soo Jo

Degrees:

Bachelor of Science, Chemical Engineering, 2004
Kwangwoon University
Master of Science, Chemical Engineering, 2006
Yonsei University

Special Honors and Awards:

1. Graduate & Professional Student Association
2. Graduate & Professional Student Association Scholarship
3. Excellence In Graduate Polymer Research
4. UNLV Access Grant Graduate Scholarship
5. Graduate & Professional Student Association and Graduate College Award
6. Graduate Student Renewable Energy Scholarship
7. Alumni Association Faculty Scholarship
8. Strategic Plan Graduate Research Assistantship
9. Graduate Access Scholarship Award
10. Nowak-Notre Dame Award
11. Graduate Access Scholarship Award

Publications

Refereed Publications

1. Tae Soo Jo, Haesook Han, Jung Jae Koh, Jongwon Park, Bidyut Biswas, Pradip K. Bhowmik "Synthesis and characterization of poly(pyridinium salt)s-fluorene polymers with various organic counterions" *Polym. Chem.* 2012, *submitted.*

2. Tae Soo Jo, Jung Jae Koh, Haesook Han, Pradip K. Bhowmik "Solution, optical and thermal properties of bis(pyridinium salt)s including ionic liquids" *New J. Chem*. 2012, *accepted.*
3. Pradip K. Bhowmik, Alexi K. Nedeltchev, Haesook Han, Tae Soo Jo, Jung Jae Koh "Photoactive amorphous molecular materials based on bisquinoline diamines and their synthesis by Friedländer condensation reaction" *Tetrahedron* 2012, *submitted*.
4. Tae Soo Jo, Haesook Han, Pradip K. Bhowmik, Longzhou Ma "Dispersion of Sing-Walled Carbon Nanotubes with Poly(pyridinium salt)s Containing Various Rigid Aromatic Moieties" *Macromol. Chem. Phys.* **2012,** *213*, 1378-1384.
5. Tae Soo Jo, William L. McCurdy, Ontida Tanthmanatham, Haesook Ham, Pradip K. Bhowmik, Benoît Heinrich, Bertrand Donnio "Synthesis and characterization of luminescent tricationic salts of mesitylene and stilbazolium moieties" *J. Mol. Struc*. **2012,** *1017*, 174-182.
6. Tae Soo Jo, Alexi K. Nedeltchev, Bidyut Biswas, Haesook Han, Pradip K. Bhowmik "Synthesis and characterization of poly(pyridinium salt)s derived from various aromatic diamines" *Polymer* **2012,** *53*, 1063−1071.
7. Tae Soo Jo, Haesook Han, Longzhou Ma, Pradip K. Bhowmik "Dispersion of Sing-Walled Carbon Nanotubes with Poly(pyridinium salt)s" *Polym*. *Chem*. **2011,** *2*, 1953−1955.
8. Tae Soo Jo, Se Hye Kim, Jihoon Shin, Chulsung Bae, "Highly Efficient Incorporation of Functional Groups into Aromatic Main-Chain Polymer Using Iridium-Catalyzed C–H Activation and Suzuki-Miyaura Reaction" *J. Am. Chem. Soc*. **2009,** *131*, 1656–1657.
9. Tae Soo Jo, Coreen H. Ozawa, Bryce Eagar, Lacie V. Brownell, Daehyun Han, Chulsung Bae, "Synthesis of Sulfonated Aromatic Poly(ether amide)s and Their Application to Proton Exchange Membrane Fuel Cells" *J. Polym. Sci. Part A*: *Polym*. *Chem*. **2009,** *47*, 485–496.
10. Tae Soo Jo, Meilong Yang, Lacie V. Brownell, Chulsung Bae, "Synthesis of Quaternary Ammonium Ion-Grafted Polyolefin via Combination of Activation of Inert C–H bond and Nitroxide Mediated Radical Polymerization" *J. Polym. Sci. Part A: Polym. Chem.* **2009,** *47,* 4519–4531.

Refereed Conference Proceedings:

1. Ying Chang, Hanniel H. Lee, Se Hye Kim, Tae Soo Jo, Chulsung Bae "Controlled C−H functionalization of aromatic polysulfone" *Polym*. *Prepr. Am. Chem. Soc. Div. Polym. Chem.* **2012,** *53(2)*, 226−227.
2. Tae Soo Jo, Alexi K. Nedeltchev, Bidyut Biswas, Haesook Han, Pradip K. Bhowmik "Solution and optical properties of poly(pyridinium salt)s derived from

various aromatic diamines" *Polym. Prepr., Am. Chem. Soc. Div. Polym. Chem.* **2011,** *52(1)*, 115−116.

3. Tae Soo Jo, Haesook Han, Longzhou Ma, Pradip K. Bhowmik "High-concentration dispersions of single-walled carbon nanotubes with poly(pyridinium salt)s" *Polym. Prepr., Am. Chem. Soc. Div. Polym. Chem.* **2011,** *52(1)*, 305−306.
4. Tae Soo Jo, Joseph K. Wray, Ontida Tanthmanatham, Haesook Han, Pradip K. Bhowmik "Thermotropic Hexacationic Liquid Crystals Based on Tripodal Viologen Salts" *Polym. Prepr., Am. Chem. Soc. Div. Polym. Chem.* **2011,** *52(2)*, 387−388.
5. Tae Soo Jo, Jungjae Koh, Haesook Han, Pradip K. Bhowmik "Synthesis and Characterization of Water-Soluble Poly(pyridinium salt)s Derived from Aromatic Diamines" *Polym. Prepr., Am. Chem. Soc. Div. Polym. Chem.* **2011,** *52(2)*, 351−352.
6. Tae Soo Jo, Ontida Tanthmanatham, Jun-Wen Lin, Haesook Han, Pradip K. Bhowmik "Luminescent Dicationic Liquid Crystals Based on Stilbazolium Moieties" *Polym. Prepr., Am. Chem. Soc. Div. Polym. Chem.* **2011,** *52(2)*, 276−277.
7. Tae Soo Jo, Jungjae Koh, Haesook Han, Pradip K. Bhowmik, Longzhou Ma "Dispersions of Single Walled Carbon Nanotubes with Rigid-Rod Poly(pyridinium salt)s" *Polym. Prepr., Am. Chem. Soc. Div. Polym. Chem.* **2011,** *52(2)*, 250−251.
8. Tae Soo Jo, William L. McCurdy, Ontida Tanthmanatham, Tae K. Kim, Haesook Han, Pradip K. Bhowmik "Luminescent Tricationic Liquid Crystals Based on Stilbazolium Moieties" *Polym. Prepr., Am. Chem. Soc. Div. Polym. Chem.* **2011,** *52(2)*, 278−279.
9. Ying Chang, Lacie V. Brownell, Tae Soo Jo, Chulsung Bae "Polystyrene-based superacidic fluoroalkyl sulfonated ionomers for fuel cell applications" *Proc. SPIE — Int. Soc. Opt. Eng.* **2010,** *55*, 233−234.
10. Park Il-Seok, Chulsung Bae, Tae Soo Jo, Justina Troung, Sang-Mun Kim, Kwang J. Kim, Woosoon Lim, Joon-Soo Lee, "Sulfonated Polyamide Based IPMCs" *Proc. SPIE. — Int. Soc. Opt. Eng.* **2009,** *7287,* 72870X/1–72870X/8.

Presentations:

1. Ying Chang, Hanniel H. Lee, Se Hye Kim, Tae Soo Jo, Chulsung Bae "Controlled C−H functionalization of aromatic polysulfone" 243rd ACS National Meeting & Exposition, Philadelphia, PA, United States, Aug. 19−23, 2012.
2. Tae Soo Jo, Jungjae Koh, Haesook Han, and Pradip K. Bhowmik "Synthesis and Characterization of Water-soluble Poly(pyridinium salt)s Derived from Aromatic Diamines" 242nd ACS National Meeting & Exposition , Denver, CO, United States, Aug. 29−Sep.1, 2011.

3. Tae Soo Jo, Jungjae Koh, Haesook Han, Longzhou Ma and Pradip K. Bhowmik "Dispersions of Single-Walled Carbon Nanotubes with Rigid-Rod Poly(pyridinium salt)s" 242nd ACS National Meeting & Exposition , Denver, CO, United States, Aug. 29−Sep.1, 2011.
4. Tae Soo Jo, William McCurdy, Ontida Tanthmanatham, Tae K. Kim, Haesook Han, and Pradip K. Bhowmik "Luminescent Tricationic Ionic Liquid Crystals Based on Stilbazolium Moieties" 242nd ACS National Meeting & Exposition , Denver, CO, United States, Aug. 29−Sep.1, 2011.
5. Tae Soo Jo, Joseph K. Wray, Ontida Tanthmanatham, Haesook Han, and Pradip K. Bhowmik "Thermotropic Hexacationic Liquid Crystals Base on Tripodal Viologen Salts" 242nd ACS National Meeting & Exposition , Denver, CO, United States, Aug. 29−Sep.1, 2011.
6. Tae Soo Jo, Ontida Tanthmanatham, Jun-Wen Lin, Haesook Han, and Pradip K. Bhowmik "Luminescent Dicationic Liquid Crystals Based on Stilbazolium Moieties" 242nd ACS National Meeting & Exposition , Denver, CO, United States, Aug. 29−Sep.1, 2011.
7. Tae Soo Jo, Alexi K. Nedeltchev, Bidyut Biswas, Haesook Han, and Pradip K. Bhowmik "Solution and Optical Properties of Poly(pyridinium salt)s Derived from Various Aromatic Diamines" 241st ACS National Meeting & Exposition , Anaheim, CA, United States, March 27−31, 2011.
8. Tae Soo Jo, Haesook Han, Longzhou Ma, and Pradip K. Bhowmik "High-Concentration Dispersions of Single-Walled Carbon Nanotubes with Poly(pyridinium salt)s" 241st ACS National Meeting & Exposition , Anaheim, CA, United States, March 27−31, 2011.
9. Ying Chang, Lacie V. Brownell, Tae Soo Jo, and Chulsung Bae, "Polystyrene-based superacidic fluoroalkyl sulfonated ionomers for fuel cell applications" 240th ACS National Meeting & Exposition, Boston, MA, United States, August 22-26, 2010, Fuel-152.
10. Joseph K. Wray, Tae Soo Jo, and Pradip K. Bhowmik "Synthesis of Bis-styrylbenzene Derivatives via Wittig-Horner Reaction" NIH INBRE UROP, June 16, 2010, Las Vegas, NV
11. Bradley Davey, Tae Soo Jo, and Pradip K. Bhowmik "Synthesis of Several Heteroaromatic Quinols for Colon and Renal Cancers" NIH INBRE UROP, June 16, 2010, Las Vegas, NV
12. Kwang J. Kim, Chulsung Bae, Il-Seok Park, Tae Soo Jo, Wonsoon Yim, and Joon-Soo Lee, "Newly developed PFSA or TRIPA based IPMCs for microwave-driven systems" Electroactive Polymer Actuators and Devices (EAPAD) XI, San Diego, CA, United States, 2009.
13. Tae Soo Jo, Meilong Yang, and Chulsung Bae, "Chemical Modification of a Crystalline Isotactic Poly(butene) via Combination of Activation of Inert C–H

Bonds and Nitrooxide Mediating Radical Polymerization" 42^{nd} Western Regional Meeting 2008 American Chemical Society , Las Vegas, NV, United States, 2008.

14. Tae Soo Jo and Chulsung Bae, "Synthesis of Ionic Conducting Polymers for Fuel Cell Applications and Biodiesel Productions" 42^{nd} Western Regional Meeting 2008 American Chemical Society, Las Vegas, NV, United States, 2008.
15. Tae Soo Jo, Bryce Eagar, Jack Yang, Julian Reese and Chulsung Bae, "Synthesis and Characterization of Sulfonated polyamides for Fuel Cell Membrane" Energy Symposium, Las Vegas, NV, United States, 2007.

Dissertations Title: Synthesis and Characterizations of Pyridinium Salts Including Poly(pyridinium salt)s and Their Applications

Dissertation Examinatino Committee:

Chairperson, Pradip K. Bhowmik, Ph. D.
Committee Member, Vernon F. Hodge, Ph. D.
Committee Member, Kathleen A. Robins, Ph. D.
Graduate Faculty Representative, Laxmi P. Gewali, Ph. D.